Nika Mahne, BSc

Oxide Coated Europium Activated Silicon Nitride Phosphors for Use in Chip-On-Board Technology

MASTERTHESIS

In partial fulfillment of the requirements for the academic degree

Diplom-Ingenieurin

in the field of study of Technical Chemistry

submitted at

Graz University of Technology

Supervisor

Assoc.Prof. Dr.techn.Dipl.-Ing. Roland Fischer

Institute of Inorganic Chemistry
Graz University of Technology
in cooperation with TRIDONIC Jennersdorf GmbH

Graz, October 2014

AFFIDAVIT

I declare that I have authored this thesis independently, that I have not used other than the declared sources/resources, and that I have explicitly indicated all material which has been quoted either literally or by content from the sources used. The text document uploaded to TUGRAZonline is identical to the present master‘s thesis.

Date	Signature

There were clouds in the sky on the way home,
so I couldn't see the Milky Way.

·•○•·

Mark Haddon

·•○•·

'*The curious incident of the dog in the night-time*'

ABSTRACT

In this study europium activated silicon nitride phosphors of formula $Ba_2Si_5N_8$ and $CaAlSiN_3$ were coated with inorganic layers. The coating procedure was carried out in order to improve the stability of silicon nitride phosphors against moisture and oxidation at elevated temperatures for use in Chip-On-Board Technology. The inorganic layers were formed *via* a solution-coating process. The structure of the obtained inorganic layer on phosphor particles as well as the luminescence behavior of coated phosphor particles was characterized by several characterization methods. XRD, ATR-IR, SEM, EDX and Fluorescence Spectroscopy of uncoated and coated phosphor particles were carried out at Graz University of Technology, whereby FEM and EDX measurements were carried out at Materials Center Leoben (MCL). Luminescence measurements of the scaled up experiments were performed at TRIDONIC Jennersdorf GmbH.

The synthesis of coating on $Ba_2Si_5N_8$ particles of a SiO_2 layer by a modified Stöber synthesis caused a shift of the emission maxima shift of CIE color coordinates and a decrease in quantum efficiency. This was caused by hydrolysis of particles during the catalyzed solution-coating process. Inorganic layers of Al_2O_3 as well as MgO were obtained via a 2-Step-Synthesis-Route: $Al(OH)_3$ and $Mg(OH)_2$, the products of a Brønsted precipitation reaction were further annealed at appropriate temperatures under inert gas atmosphere. The formed layer of Al_2O_3 on phosphor particles is of amorphous structure.

Attempts at Al_2O_3 coated $CaAlSiN_3$ phosphor particles on a larger scale mainly resulted in agglomeration of $Al(OH)_3$. The coating and the annealing process itself influenced the luminescence behavior of the phosphor in a negligible degree. Just, a negligible shift of emission maxima and CIE color coordinates of the phosphor occurred. Furthermore, a slight reduction of the quantum efficiency of all coated phosphor materials compared to untreated phosphor occurred. Probably this is caused by diffuse scattering of light at the Al_2O_3 layer. A color shift due to oxidation of Eu^{2+} to Eu^{3+} could not be observed. The thermal stability of Al_2O_3 triple coated $CaAlSiN_3$ phosphor particles was proved by TG-DSC-MS analysis. No decomposition of the coated phosphor particles and of the glass encapsulant ZASNP11C below temperatures of 680°C occurred compared to uncoated phosphor. Therefore an encapsulation into ZASNP11C is possible due to the improved thermal stability of the coated phosphor.

TABLE OF CONTENT

ACKNOWLEDGMENT

Very special thanks to my supervisor Assoc.Prof. Dipl.-Ing. Dr.techn. Fischer who enabled me to work on that forward-looking topic for my Master Thesis at Graz University of Technology. Thanks to Tridonic Jennersdorf GmbH, especially to Dr. Franz Schrank and Dr. Martin Pfeiler-Deutschmann who showed me how luminescence measurements are carried out in Industry. This work was supported by a grant from the Austrian Research Promotion Agency (FFG), Projekt Nr. 842562.

A big thanks to Dr. Sergey Borisov and Dipl.-Ing. Christoph Staudinger from the Institute of Analytical Chemistry and Food Chemistry at Graz University of Technology for providing me the spectrofluorometer and their patience while helping me with luminescence measurements. Thanks to everyone involved in the characterization of phosphor particles and encapsulation glass, especially to Oberrätin Dipl.-Ing. Dr.techn. Brigitte Bitschnau, Ao.Univ.-Prof. Dipl.-Ing. Dr.techn. Klaus Reichmann, Dipl.-Ing. Dr.techn. Angelika Reichmann and Dipl.Ing. Theresa Kainz. Thanks to Ao.Univ.-Prof. Dipl.-Ing. Dr.techn. Gatterer for providing me literature of phosphor materials.

I would also like to thank the members of the Institute of Inorganic Chemistry of Graz University of Technology for all the helpful conversation regarding my master thesis, especially to Dr. Ana Torvisco Gomez and Dipl.Ing. Pierre Baumann. Special thanks goes to my office colleagues Angela, Johanna and Mel: I had a great time with you in the 'teahouse'.

Rada bi se zahvalila svojima staršema Marini in Petru, ki sta me med študijem vseskozi podpirala in mi omogočila pridobiti čudovite izkušnje s študija v tujini.

1 INTRODUCTION

1.1 Light-Emitting Diode

A light-emitting diode (LED) is an electronic semiconductor device that emits light when an electric current passes through it.[1,2] A LED resembles a basic p-n-junction diode which can be ascribed to semiconductor light sources.[2,3] When a proper voltage is applied to the leads, electrons are able to recombine with electron holes within the device, releasing energy in the form of photons (see Figure 1). The photon emission of a material subsequent energy supply is generally called luminescence, in case of a LED this effect is called electroluminescence.[4]

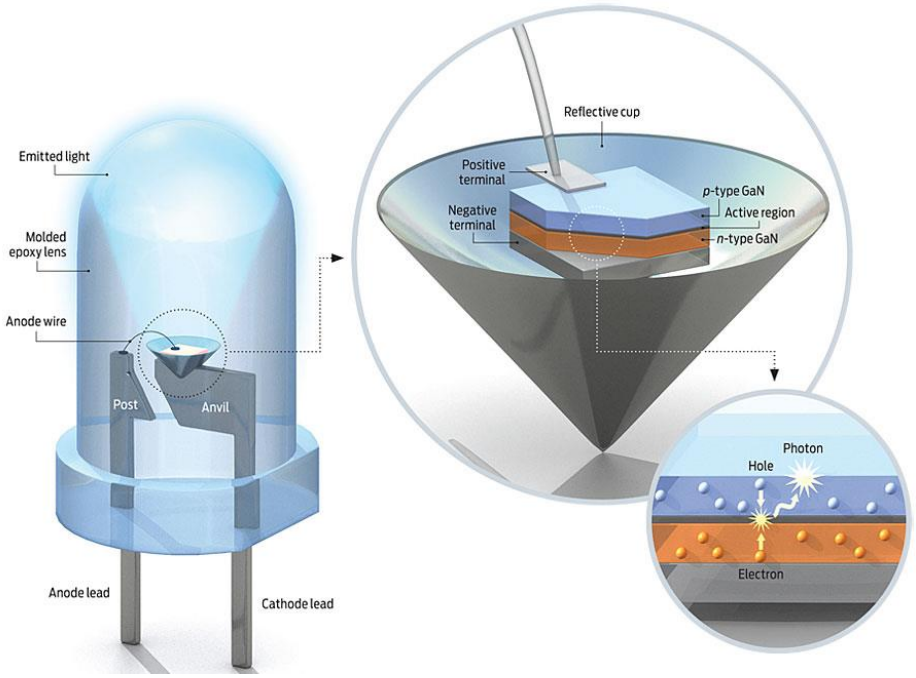

Figure 1: LED Architecture: The semiconductor chip is traditionally positioned on top of the cathode lead.

Conventional LEDs can be made from a variety of inorganic semiconductor materials as listed in Table 1 (see emitting colors and materials).[5] Modern LEDs are available from the visible, ultraviolet and to the infrared region and are therefore used in everyday objects like interior lighting, automobile headlights or rear lights, indicator lamps, display backlighting, advertising, traffic signals, sensors and many more beside that.[2,6,7] LEDs have numerous advantages over incandescent light sources including lower energy consumption, longer lifetime, improved physical robustness, barely UV percentage, a smaller size and faster switching.[7,8]

Table 1: Variety of inorganic semiconductor materials.[5]

Emitted Color	Semiconductor Material	Voltage Drop [ΔV]	Wavelength λ [nm]
IR	GaAs	x< 1.63	x> 760
Red	AlGaAs	1.63 < x< 2.03	610 <x< 760
Orange	GaP	2.03 < x< 2.10	590 <x< 610
Yellow	GaAsP	2.10 < x< 2.18	570 <x< 590
Green	GaN	1.9 < x< 4.0	500 <x< 570
Blue	ZnSe	2.48 < x< 3.7	450 <x< 500
Violet	InGaN	2.76 < x< 4.0	400 <x< 450
UV	AlN	3.1 < x< 4.4	x< 400

1.2 Physics of a LED

Figure 1 shows the conventional mounting form of LEDs. Figure 2 is the basis for the following description of the physics of a LED: The LED consists of a chip of semiconducting material doped with dopants to create a p-n-junction.[5,6] The p-n-junction is a boundary between two types of semiconductor materials, where the electronic process of the device takes place. Characteristic for a p-n-junction is the formation of a so called depletion region (depleted of charge carriers), and is hence non-conductive, depending on the relative voltages of the two semiconductor regions.[5] Thus the current flows from the p-side to the n-side (anode → cathode) but not in the reverse direction. The charge carriers, electrons (e^-) and holes (h^+), flow into the junction from electrodes with different voltages. When an electron recombines with a hole, it falls into a lower energy level and releases energy in form of a photon. This recombination can also be non-radiative and thus a thermal transition. The wavelength of the emitted photon, and thus its color, depends on the band gap energy ΔE_g of the materials forming the p-n-junction.

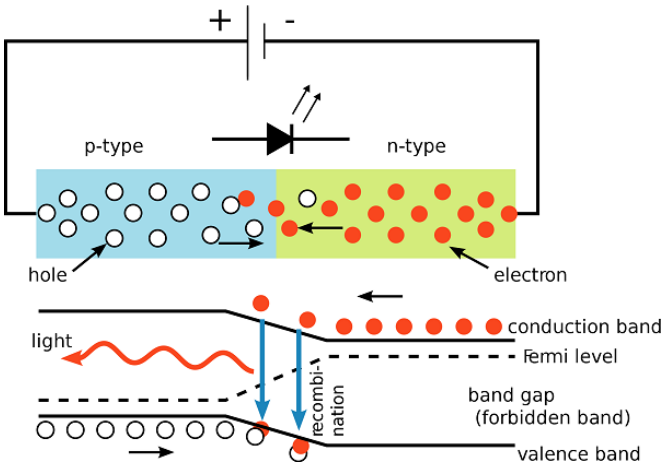

Figure 2: Graphical symbol of a photodiode, circuit of an LED (above) and its band diagram (below).

Materials used for LEDs have direct band gaps (see Figure 3, left) with energies corresponding to near-IR, VIS and near-UV light. However, in a germanium diode, electrons and holes recombine by a non-radiative transition, which produces no optical emission, as germanium is an indirect band gap material. Figure 3 (left) shows a simplified diagram of the electronic band structure of a direct semiconductor in which the maximum of the valence band is precisely below the minimum of the conduction band (conservation of momentum without need of a phonon). Whereby in an indirect semiconductor (see Figure 3, right) the maximum of the valence band is not located below the minimum of the conduction band: A momentum transfer is necessary in from of a phonon.

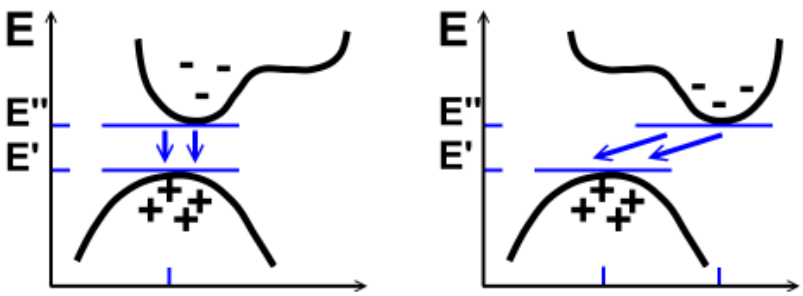

Figure 3: Band structure of a direct (left: GaAs) and an indirect semiconductor (right: Si).

1.3 Generation of White Light: Color Conversion

In 2009 the European Union decided to ban traditional incandescent lamp, because of their bad efficiency, high power consumption and short lifetime.[7,9] Despite the high efficiency of fluorescent lamps a big disadvantage is that they contain toxic mercury. Due to rising fuel prices, increasing consumption of energy and economic difficulties light bulbs should be replaced by other types of electric lighting. Therefore white light emitting diodes have been considered as a promising next generation light source also for interior lighting. As incandescent lamps generate heat radiation (IR) besides visible radiation, LEDs are considered as an alternative especially for use in food presentation in showcases, medicine and microscopy, where a defined temperature is needed. White light emitting diodes featuring the advantages of high light efficiency, low energy consumption, and long service lifetime, have drawn much attention.[8] There are three basic principles of white light generation *via* LED technology:[10]

- Additive composition of the fundamental colors red, green and blue; so called RGB-LEDs (see Figure 4, left)
- UV-LED with at least 3 phosphors in the colors red, green and blue (see Figure 4, mid)
- Blue LED chip with color conversion (see Figure 4, right)

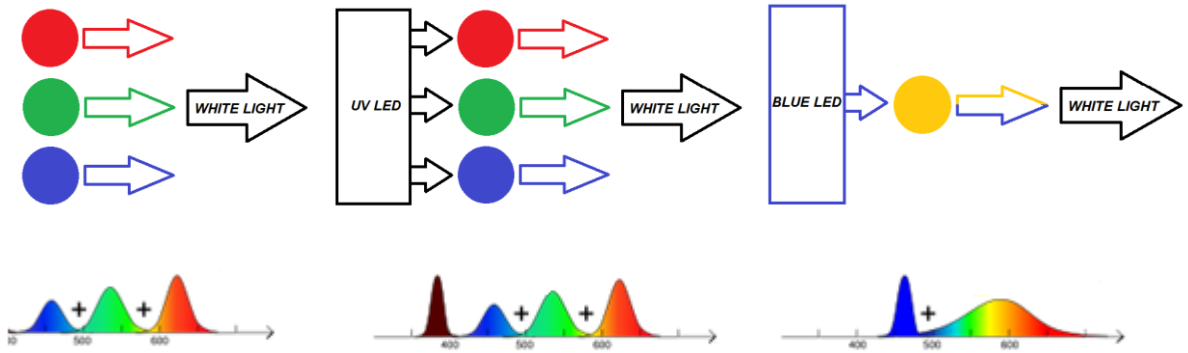

Figure 4: The three basic principles of white light generation: RGB LEDs (left), UV-LED (mid) + RGB phosphors and blue LED + yellow phosphor (right) (legend: red, green and blue LED).

The three basic principles do not only differ in their composition set-up, but also in their emitted color temperature of white light. Figure 4 shows the emission spectra of a RGB-LED, a UV-LED with RGB phosphors and a blue-LED with a yellow phosphor. The white light generated by a RGB LED results from the emission spectra of the blue, green and red LED (3 peaks), in case of a UV-LED with 3 phosphors it results from the emission spectrum of the UV-LED, of the blue, green and red phosphor. Whereby white light generated by a blue-LED with a yellow phosphor results from combination of the blue LED with the yellow light emitted by the yellow phosphor caused by color conversion. The spectrum in Figure 4 (right) shows a sharp dominant peak at around 450nm caused by the blue LED and a lower broader peak in the area around 500-800nm. Their emission bands differ in shape (several peaks) and in their intensities. But they have one following in common: The emission band ranges from around 380nm to 780nm (VIS), in other words they aim to cover the spectrum of visible light generated by the earth's sun (without UV radiation). The emission band of the solar radiation covers the electromagnetic spectrum from the UV-region, over the VIS and the IR-region with an emission maximum at 560nm, which is located in the green-yellow area of the visible

spectrum (see Figure 5, right). The human's eye spectral sensitivity peaks at around 560nm and therefore very sensitive to blue and yellow light. Humans *ipso facto* the consumer prefer light with a spectrum based on solar radiation. Therefore a consumer-friendly light can be realized *via* a warm light LED for interior lighting based on COB Technology with a blue LED combined with a phosphor. Figure 5 (left) shows the emission spectra of the earth's sun, of a halogen lamp and a fluorescence lamp. Figure 5 (right) shows the emission spectra of the earth's sun compared to a halogen lamp and fluorescent lamp. LEDs show the clear advantage of generating emission in the VIS area (tuned properties) and not in IR area of the electromagnetic spectrum compared to other light sources (thermal radiation).[11]

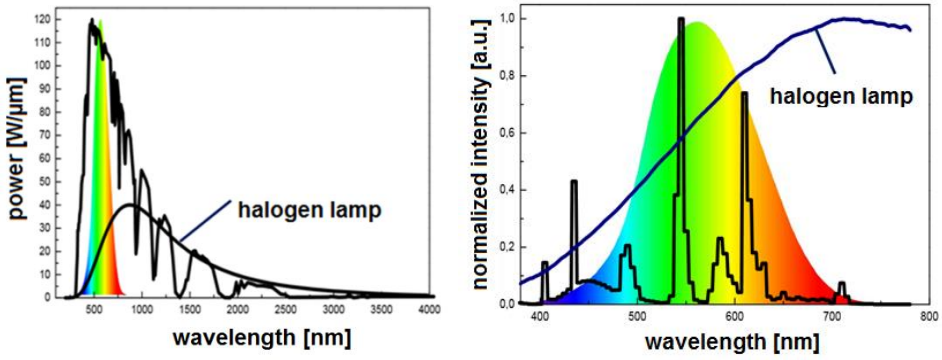

Figure 5: Emission spectra of the earth's sun compared to a common halogen lamp (left) and a fluorescence lamp compared to a halogen lamp (right).

1.4 The CIE System of Colorimetrie

Besides the quantum yield, the quality of a phosphor material is further characterized for example by its color point.[4] The color point is derived from the spectral energy distribution of the emission and is defined according to the Comission Internationale de L'Eclairage abbreviated as CIE in a normalized two-dimensional coordinate system (see Figure 6, right and see References 12 and 13 for detailed information).[4,12,13] The color coordinates are like coordinates on a map. A color plots as a point in an [x,y] chromaticity diagram. Figure 6 (left) shows the important CIE [x,y] chart features, which lie on or below and to the left of the line y=1-x. The spectral locus is a horseshoe-shaped path swept by a monochromatic source as it is tuned from 400-700nm. All colors lie within the horseshoe-shaped region: Points outside this region are not colors and black has no place in a chromaticity diagram. There is no unique physical definition of white. White plots in the central area of the chromaticity diagram with following CIE [X,Y,Z] values of about [1,1,1] and [x,y] coordinates of [⅓,⅓]. The system was developed to allow accurate color measurements by standardization of the various factors (standardized for a hypothetical standard observer) which influence the perceived color of a material.[12,13] It shall support color measurements and a worldwide specification for instance between manufacturers of lightning systems as white light emitting diodes. Many important sources of illumination are blackbody radiators, whose chromaticity coordinates, lie on the black body locus (Planckian locus). A blackbody is an idealized body that absorbs all incident electromagnetic radiation, regardless from frequency or angle of incident also referred to as idealized radiation source. Light sources can be classified in thermal emitters and non-thermal emitters: Thermal emitters provide continuous radiation (radiation maximum shifts with increasing temperature to shorter wavelengths from IR to UV according Wien's

displacement law). Incandescent lamps are an example for thermal emitters. Whereby LEDs are defined as non-thermal emitters due to their lack of thermal radiation.

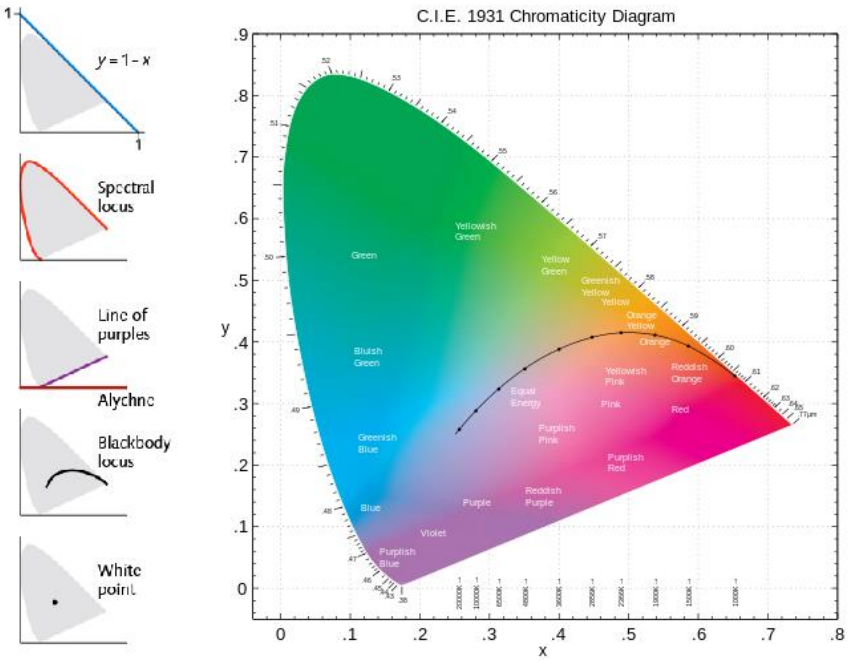

Figure 6: The CIE 1931 color space chromaticity diagram (right) and CIE [x,y] chart features (left).

2 PHOSPHOR FOR COLOR CONVERSION

A luminescent material, a so called phosphor, is a solid which converts a certain type of energy into electromagnetic radiation.[4,14] Besides that, thermal radiation is generated. Classical inorganic phosphors are usually crystals of 1-10µm in size and consist of a host lattice with an activator ion doped, in small concentrations of a few mole percent or less, into it.[4] Activator ions like lanthanides Ln^{n+} possess energy levels that can be excited by direct excitation or indirectly by energy transfer and are responsible for the luminescence. There are two types of activators which have to be distinguished: The energy levels of the activator ion like lanthanide ions Ln^{3+} involved in the emission process show only weak interactions with the host lattice. Optical transitions take place between 4f terms that are well shielded from their chemical environment by outer electrons. As a consequence characteristic line emission spectra can be observed (see Figure 7, emission spectrum of a Eu^{3+} activated Y_2O_2S phosphor).[11]

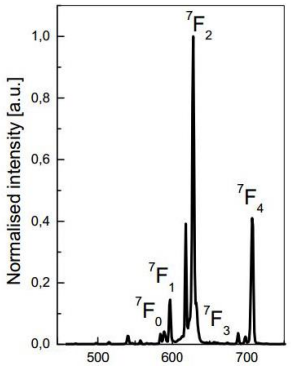

Figure 7: Emission spectrum of an Eu^{3+} activated Y_2O_2S red emitting phosphor with line emissions.

The second type strongly interacts with the host lattice, where d-electrons are involved, for example Mn^{2+}, Eu^{2+} and Ce^{2+}, as well as for s^2 ions like Pb^{2+}, Sb^{3+}.[4] The strong coupling of the electronic states with vibrational modes of the host lattice, mainly leads to broad bands in the spectrum. Especially, Eu^{2+} is the best-known and most widely used rare earth ion, due to its impressive luminescence properties.[14] Eu^{2+} doped phosphors emit long-wavelength light with a broad band owing to the 4f→5d transition, which is energetically allowed and therefore very fast.

Phosphors can be synthesized by several solid-state-reaction methods like gas pressure sintering, normal pressure sintering, self-propagating high-temperature synthesis, sol-gel-processes, solution-combustion or carbothermal reaction.[8,14,15] They can be found in a broad range of every-day applications such as cathode ray tubes, fluorescent tubes and light emitting diodes.[4]

Since traditional incandescent and fluorescent lamps have many weaknesses white light-emitting diodes (w-LEDs) have been considered as the next generation light source, due their high efficiency and long lifetime.[7,16] A conventional white LED composed of a blue InGaN LED and a yellow-emitting Ce^{3+} doped yttrium aluminum garnet phosphor (like $Y_3Al_5O_{12}:Ce^{3+}$) has a low color rendering index (CRI), because of its lack of a red fraction in their emission spectra.[8,16] To compensate the red color deficiency and thus increase the CRI and therefore develop warm-white LEDs many investigations have been carried out to develop red-emitting phosphors, which can be excited by blue LEDs.[8,16]

2.1 Eu^{2+} Activated Silicon Nitride Phosphors

Recently, Eu^{2+} activated silicon nitride phosphors like $CaAlSiN_3:Eu^{2+}$ have drawn much interest because of their favorable photoluminescence properties.[8] Among Eu^{2+} doped red nitride phosphors used in Solid State Lighting, $CaAlSiN_3:Eu^{2+}$ was found to show excellent optical properties due to its adequate thermal stability, lack of environmental hazard, non-toxicity, high quantum efficiency, high quenching temperature (T_{MAX}=180°C) and low thermal quenching.[8,15,17] Thermal quenching is expressed by a quick drop of photoluminescence efficiency of a phosphor as the temperature increases, due to non-radiative transitions.[18] It is precisely for this reason why an improvement of red emitting phosphors due to their photoluminescence efficiency at elevated temperatures (limited to x<150°C) and thermal quenching resistance is desired in LED lighting applications. Despite these advantages, these materials are hygroscopic and have the potential to be degraded by atmospheric moisture at high temperatures under operation.[16] For example, in some cases it is quite difficult to stabilize Eu^{2+} because of its lower oxidation stability compared to Eu^{3+}.[19] Trivalent lanthanide ions feature an electron configuration of $[Xe]4f^n$ with n=0-14, when Ln^{3+} ions are incorporated in a host lattice (for example silicon nitride) their energy levels are hardly affected because of the shielding effect caused by 5s and 5p orbitals. Lanthanide doped phosphors show extremely high resistance to photobleaching and photochemical degradation as 4f electrons are not involved into chemical bonding.

2.2 Problems Related to Silicon Nitride Phosphors

The generation of light from LEDs typically causes heat as a byproduct.[20] Phosphors exposed to higher temperatures may have decreased quantum efficiencies, as a result the emitted light may dim or the color may shift as the device enters steady state operation. Furthermore some phosphors undergo hydrolysis reactions under elevated temperatures and humidity. That is the reason why there is a continued demand for color stable phosphors. A search for new materials with very high stability which is invariable to operating conditions is briskly performed, by industry and university laboratories.[4]

3 CHIP-ON-BOARD TECHNOLOGY

Currently, the most common approach to produce white light in these devices is to combine a blue LED chip with a red and yellow phosphor, which is also used in Chip-On-Board technology (COB).[10,16] The Chip-On-Board technology is a microelectronic production technology in which the LED-chip is applied directly to the circuit board (*Die Bonding*) and afterwards electrical connected to the circuit board by thin gold wires (*Wire Bonding*).[10,21] Finally, the LED-chip is encapsulated *via* a *Dispens-Process* with a potting compound (*Resin*) which is referred to as *Glob Top* (see Figure 8). One of the purposes of LED chip encapsulation is to provide a physical housing to protect the LED chip and bonding wires from external influences, especially real working conditions like moisture, dust, vibration, mechanical and thermal shock. [21,22] The COB Technology enables high chip packing density (minimum space requirements and flat design), individual LED design and at the same time high luminous flux [lm/mm²] values.[21,22]

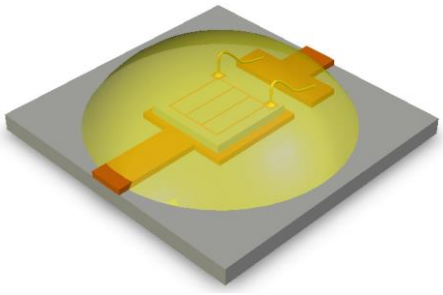

Figure 8: LED with COB-Technology view from above.

As already mentioned the generation of white light is based on the additive mixing of the emission of the blue LED-chip and a blend of phosphors. Phosphors on light emitting diodes (COB-Technology) are excited by near UV or blue light (for example GaP or GaN).[8,15,16,20] The phosphor absorbs the primary light of the LED (UV or blue LED) completely or partly and emits light in another region of the visible spectrum (phosphor for color conversion).

3.1 State of the Art: Coating of Phosphor Particles and Following Encapsulation

One of the most effective methods to improve the stability of moisture-resistance and handleability of phosphor particles is to create a coating layer on the surface of each individual phosphor particle.[23] The use of coatings is known to improve the adhesion strength between phosphors and for example glass substrates (COB-Technology), allowing excellent stability of phosphors when exposed to moisture and other atmospheric

components.[23,24] The coating should be optically transparent, and a precise quantity of it must homogeneously cover the surface of the individual phosphor particle so as to minimize reduction in photoluminescence intensity.[24] Although organic coatings could prevent the phosphor from hydrolyzing in water to a great extent, the encapsulation may not be stable at high temperatures. Therefore, inorganic materials such as SiO_2 or Al_2O_3 are usually chosen to act as the coating layer on the surface of phosphors. The conditioning of the surface of the phosphor grains is a major research topic these days to obtain luminescent materials with improved performance.[4] This conditioning is mainly achieved by a chemical refinement step after synthesis or by an additional coating on the phosphors particle surface (see Figure 9). The search for new materials with very high stabilities is briskly performed, by industry and university laboratories.

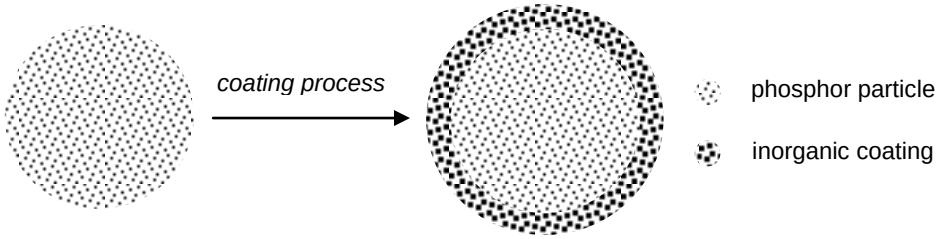

Figure 9: Sketch of a chemical refinement step in order to coat phosphor particles.

Stöber et al.[25] reported about controlled growth of monodisperse spherical silica particles of uniform size in 1968. By hydrolysis of alkyl silicates with ammonia as morphological catalyst and following subsequent condensation of silicic acid in alcoholic solutions silica particles are synthesized as followed (see Equation 1):

$$Si(OEt)_4 + 4H_2O \xrightarrow{EtOH,\,NH_3} Si(OH)_4 + 4EtOH$$

$$Si(OH)_4 \rightarrow H_2SiO_3 + H_2O$$

$$H_2SiO_3 \rightarrow SiO_2 + H_2O$$

Equation 1: Hydrolysis of TEOS and further formation to SiO_2.

It is state of the art to coat phosphor particles with a SiO_2 layer *via* a sol-gel process based on the process proposed by Stöber et al.[23,24,26] with alkyl silicates like tetraethylorthosilicate (TEOS) chosen as a precursor. Sun et al.[23] demonstrated a simple, rapid and low temperature method to coat $SrSO_4:Sm^{3+}$ phosphors with a uniform and continuous SiO_2 coating in a modified Stöber process, in reverse microemulsion conditions. According to them, a SiO_2 coating is obtained *via* a sonochemical synthesis, which means that the chemical process occurs in liquids under the effect of power ultrasound using TEOS as silicon coating reagent. Apart from the successful synthesis of a SiO_2 coating layer, no loss of photoluminescence intensity and a much slower degradation in contact with atmospheric humidity was recorded. In contrast, Zhuang et al. [24] reported that the thickness of SiO_2 coating to $Ca_3SiO_4Cl_2:Eu^{2+}$ phosphor has an effect on the luminescence intensity of the phosphor.

In 2011 Murphy et al.[20] published a patent application for color stable phosphors for use in phosphor converted LEDs. The phosphor should be used with a lighting apparatus as shown in Figure 10 which includes a semiconductor light source and a phosphor composition

radiationally coupled to the light source and containing a coated phosphor. The color stable phosphor may be blended with other blue, yellow, orange or red phosphor to yield white light phosphor blends. Only parts which are relevant for this work are explained below (see Figure 10), more details according the assembly may be derived from Murphy et al.[20]

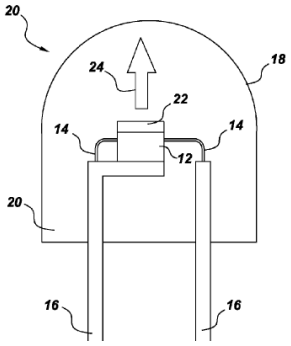

(12) *light emitting diode chip*
(14) *leads*
(16) *lead frames*
(18) *shell*
(20) *encapsulant*
(22) *phosphor*
(24) *emitted white light*

Figure 10: Schematic cross-section of parts of a light emitting assembly according to Murphy et al.[18]

The LED chip (12) should be encapsulated within a shell (18) made out of glass or plastic, which encloses the LED chip and an encapsulant material (20. As an encapsulant material epoxy resin, low temperature glass, spin-on glass, polymer, thermoplastic or thermoset material should be used preferably. Both, the shell and the encapsulant, are preferably transparent or substantially optically transmissive with respect to wavelength of light produced by the LED chip and phosphor composition (22). Murphy et al. have carried out their coating experiments with a phosphor with the chemical formula $(Sr_{1-z}M_z)_{1-(x+w)}A_wCe_x)_3(Al_{1-y}Si_y)O_{4+y+3(x-w)}F_{1-y-3}$ with A is Li, Na, K or Rb, or a combination thereof with M=Ca, Ba, Mg, Zn, or a combination thereof and $0<x<0.10$, $0<y<0.5$, $0<z<0.5$ and $0<w<x$.[18,20] The synthesis of $(Sr_{0.895}Ca_{0.1}Ce_{0.005})_3Al_{0.6}Si_{0.4}O_{4.415}F_{0.585}$ is described in detail in Murphy et al.[20]

In contrast to Sun et al.[23] and Zhuang et al.[24] Murphy et al.[20] used coating compositions including materials made out of oxides, hydroxides and phosphates of the II. and XIII. main group elements. For example aluminum oxide, magnesium oxide, calcium oxide, barium oxide, strontium oxide, zinc oxide, boron oxide, aluminum hydroxide, magnesium hydroxide, phosphates of aluminum, magnesium calcium, barium and strontium and boron nitride BN. Their methods include contacting the above mentioned phosphor in particulate form with a coating precursor at an acidic or basic pH in a solvent comprising water.[18] The coating precursors are tetraethylorthosilicates, fumed silica, alkali metal silicates, phosphates of formula $R_n(PO_4)_m$ and a combinations thereof (R=H, NH_4, Li, Na, Rb). The contacting is performed at a pH less than or equal to about 5 or greater than or equal to about pH 9, except for fumed silica where a pH of less than or equal 3 is required. For example having TEOS as a precursor, H_2O and either an acid or base catalyst are required. The reaction has to be proceeded in such a way that 2moles of H_2O react with 1mole of TEOS to form SiO_2 as shown in Equation 1. Therefore the solvent should comprise H_2O, and may additionally include at least one alcoholic solvent like methanol, ethanol, propanol, ethylene glycol, propylene glycol and combinations thereof. Furthermore the coating precursor should be present in an amount corresponding to 1-15 percent by weight, based on the weight of the phosphor. Besides that, the temperature at which the phosphor is

contacted with the coating precursors may vary from room temperature to less than 60°C. The coated phosphor composition is then deposited (by coating and drying) on the LED by any appropriate method. For example, a silicone-slurry in which the coated phosphor particles are randomly suspended (with an average particle size of 1-25µm, better 15-20µm), is placed over the LED chip (COB-Technology).

3.2 Problems Related to Silicone as Potting Compound in the COB-Technology

In the COB-Technology preferable silicones with methyl groups are used as gel-like potting compound material, which are cross linked *via* a platinum catalyzed hydrosilylation.[27] For heat dissipation aluminum plates are used due to temperature of more than 120°C generated by the LED.[18] Silicones show following material properties: They are resistant against oxidation and weather influences, are water repellent and electrically non-conductive.[27] Despite the advantages of mechanical protection and transparency (i.e. no light emitted by the LED or the phosphor gets absorbed by the potting compound) unfortunately silicones show signs of aging with increasing number of working hours: The silicone gets degraded by heat and humid environment which leads to weight loss and yellowing of the silicone.[28] At the same time the important protection layer for phosphor particles gets lost and hydrolysis and degradation of phosphor particles can occur as well. Therefore silicones are only partly suitable for use in applications with temperatures above 150°C, thus other potting compound materials are desired.

4 AIM OF THIS WORK

In this study a silicon nitride phosphor shall be improved in terms of its stability against external influences, as they tend to be degraded by atmospheric moisture and elevated temperatures under operation. In order to prevent the phosphor from hydrolysis and losses of luminescence behavior, like decreased quantum efficiency, a shift of CIE color coordinates or a shift of the emission maximum, it is covered by an inorganic layer. The stability of the uncoated phosphor against acids and bases should be determined by tests and further investigated by several characterization methods and also due to its luminescence properties. Several types of inorganic layers like SiO_2, Al_2O_3 and MgO shall serve as coating on phosphor particles. These coating needs to be optically transparent and has to cover the surface of the individual phosphor particles homogeneously. The coating and the annealing process itself must not influence the luminescence behavior of the phosphor. Moreover, an oxidation of the activator ion Eu^{2+} to Eu^{3+} shall not occur. A SiO_2 coating should be obtained by a modified Stöber synthesis, whereby a layer of Al_2O_3 or MgO should be obtained by a Brønsted precipitation reaction from a mixture of aluminum nitrates or aluminum halides with a base, as proposed by Murphy et al. Consequently, further temperature treatment is performed in order to form metal oxides from metal hydroxides.

As silicon nitride phosphors are used in Chip-On-Board technology for the generation of white light *via* color conversion, they have to be encapsulated in a matrix. Due to several disadvantages related to silicone, an alternative encapsulation material is aspired for these purposes. The coated phosphor particles shall be encapsulated into glass with low melting temperature. In addition it should be lead-free glass, because of health concerns due to the fact that the heavy metal lead and its compounds like PbO, which is often used in the glass industry, are harmful to humans.[29] Maximum 5wt% of coated phosphor shall be encapsulated into the low melting glass. It should be examined if an encapsulation into low melting glass is possible. Several characterization methods will be used in order to determine whether the encapsulation process does affect the coated phosphors luminescence behavior and further if it affects the structural properties of the glass.

5 EXPERIMENTAL SECTION

5.1 Materials and Laboratory Equipment

All reagents used in this work are of analytical grade. The ammonia solution (32% extra pure, CAS:7664-41-7) sodium hydroxide (platelets, CAS:1310-73-2) and zirconium dioxide (Art.8914, CAS:1314-23-4) were purchased from Merck. Sodium hydrogen carbonate (GPR RECTAPUR, CAS:144-55-8), chloroform (AnalaR Normapur, CAS:67-66-3) and hydrochloric acid (37%, CAS:32862-91-2) were purchased from VWR. Aluminum nitrate nonahydrate (99+%, CAS:7784-27-2) and polystyrene (average M.W. 250.000, CAS:9003-53-6) were purchased from Acros Organics. Magnesium chloride (anhydrous 99%, CAS:7786-30-3) and tetrasodium pyrophosphate decahydrate (>97%, CAS:13472-36-1) were purchased from Alfa Aesar. Urea (p.A., CAS:57-13-6) was purchased from Loba Feinchemie, 1-octanol (99,5%, CAS:111-87-5) from Riedel-de Haen, isopropanol (VLSI PURANAL® CAS:67-63-0) from Honeywell and tetraethyl orthosilicate from Fluka (98%, CAS:78-10-4). Deionized water was obtained from own production. Melinex® ST506 (double sided adhesive coated PET-foil of 125µm thickness) for luminescence measurements at the ACFC was purchased from DuPont Teijin Films.

For the synthesis procedure an ultrasonic bath from Elma (Elmasonic S30, 50/60Hz), a stirrer from IKA Labortechnik (RW20, level 3, modus II, 50/60Hz, 600rpm), an automatic syringe device from KD Scientific (LDS-200-CE, 50/60HZ), a microliter needle (1100TLL, 1000ml, without piston stop) and syringe needle tubes from Hamilton (PTFE, 2x1mm,1000mm) were used. Filters were purchased from Schleicher & Schnell (5893 blue ribbon, ashless, Ø110mm) and MSI (WESTBORO, Lot.No. 95785, MicronSep, cellulosic, white plain, for hydrophilic solutions, $Ø_{pore}$ 0.45µm, $Ø_{filter}$ 47mm). Further a pH meter from Mettler Toledo (Education Line EL20) and a drying closet from Binder were used.

For the sample preparation for luminescence measurements at TRIDONIC Jennersdorf GmbH Silicon A and silicon B were purchased from Momentive Performance Materials (XE14-C0035BY A MAT.#109046 and XE14-C0035BY B, MAT.#109046) and orthosilicic acid (HDK H18) was purchased from Wacker Chemie AG.

5.2 Characterization of Red emitting Silicon Nitride Phosphors

To obtain more information about the starting material beyond the data sheet, and to point out differences before and after the coating process as well as the encapsulation process, several characterization methods were carried out. The uncoated phosphor particles were characterized by Attenuated Total Reflection Infrared Spectroscopy (ATR-IR), Scanning Electron Microscopy (SEM), Energy-dispersive X-ray Spectroscopy (EDX) and X-ray Diffraction (XRD) to obtain information about shape, morphology, composition, elemental distribution, crystal structure as well as lattice parameters. The luminescence behavior was analyzed by Fluorescence Spectroscopy. Detailed measurement parameters and used equipment are described as followed: ATR-IR spectra were recorded on a Bruker spectrometer (Alpha-P, ATR Platinum Diamond). The measurements were carried out with mid-wavelength infrared (MIR) radiation in the range of 4000-375cm^{-1}. The spectrum of air

was used as background. A baseline correction was carried out with the concave elastic band method (64points). To look at the morphology of uncoated particles SEM investigations using secondary electrons were recorded. For that reason the sample had to be coated with a thin electrically conductive layer using Au (film thickness 2-5nm) for the topography images as well as for the chemical analysis. Images were taken with several magnifications with the program VegaTC. SEM measurements were carried out in a Tescan Performance Nanospace (topography images of the particles with SE and BSE) and INCA from Oxford Instruments equipped with a TESCAN LUSTD Detector for Energy Dispersive X-ray Spectroscopy. The phase compositions of uncoated phosphors were analyzed by powder diffraction using CuK_{α} radiation (Bruker, D8 Advance, LYNXEYE Detector, Bragg Brentano Geometry). The phase purity was evaluated by Rietveld refinement of the XRD patterns using the program X-PertHighScorePlus (PANalytical). Luminescence measurements were carried out at the Institute of Analytical Chemistry and Food Chemistry (ACFC) at Graz University of Technology. The photoluminescence properties of the uncoated phosphor particles were determined using a spectrofluorometer (Horiba Scientific, Jobin Yvon, Fluorolog-3) at room temperature equipped with a 450W xenon CW lamp. Excitation spectra and emission spectra were measured in a range of 455-475nm and 500-800nm with an excitation wavelength of 465nm (front-face modus). The samples were made from a slurry-mixture consisting of 200mg phosphor, 200mg polystyrene in 1000mg chloroform, which was stirred for 1h. The slurry was knife-coated on a PET-foil with a wet film thickness of 25µm. Quantum efficiencies were measured *via* an absolute method with an extra modular integrating sphere unit (Quanta-φ) using a filter in non-reflecting PTFE sample holders. The used reference material ZrO_2, features a similar refraction index, shows a similar particle size distribution and no emission occurs after excitation with visible light as compared to the phosphor. Quantum efficiency and CIE color coordinates were calculated with the program FluorEssence.

5.2.1 Characterization of LP-N620

An europium-activated barium silicon nitride with the name LP-N620 (Lot:M-14131-1) with unknown chemical formula was purchased from Leuchtstoffwerk Breitungen (LWB). Since no data sheet was available, information about the starting material LP-N620 had to be obtained.

SEM of uncoated phosphor LP-N620

A SEM analysis was carried out to obtain information about the shape of particles, its particle size and their distribution. Figure 11 shows the secondary electron images of LP-N620. The particles are irregular shaped, more like platelets. Figure 11 reveals a large particle size distribution with particles of grain sizes smaller than 15µm up to nanometer range.

EDX of uncoated phosphor LP-N620

Via EDX a qualitative analysis was carried out to get information about the chemical composition of the particles. N, Al, Si, Sr, Ba, and Eu were found as shown in Figure 11 (right). N, Si and Ba are part of the phosphors host lattice in which Eu^{2+} is doped instead of Ba (known from LWB). The signals for Al result from the sample holder.

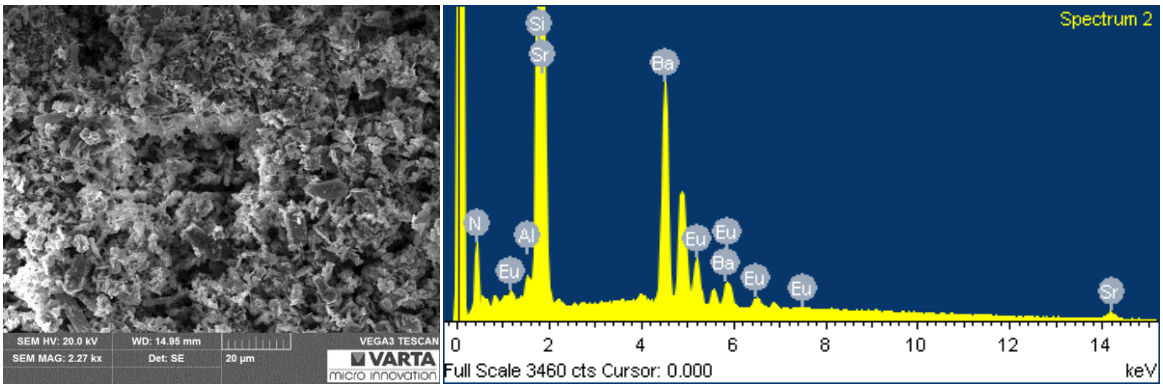

Figure 11: SEM (SE) image of LP-N620 (left) and EDX spectrum of qualitative analysis via mapping mode (right).

Sr shows interference with Si and *vice versa*. From this point it is not sure if Sr is part of the phosphors host lattice or if it is simply an interference signal from Si. A quantitative analysis could not be carried out, because of the poor electrical conductivity of the material. According to latest publications barium silicon nitride phosphors with the chemical formula like $MSiN_2:Eu^{2+}$ and $M_2Si_5N_8:Eu^{2+}$ (M=Ca, Sr, Ba) are known.[8,30]

XRD of uncoated phosphor LP-N620

XRD measurements and further evaluation were carried out in order to investigate the composition of the phosphors host lattice as well as its crystal structure. Figure 12 shows the result of the Rietveld refinement of powder X-ray data of uncoated phosphor LP-N620. The corresponding sharp peaks are in good agreement (ICSD 401501 $Ba_2Si_5N_8$). The material is nearly pure phase europium-activated barium silicon nitride with the chemical formula $Ba_2Si_5N_8$. Figure 12 shows also a not identified phase at 29.2°2θ of 1% per volume. SiO_2 in crystalline form as quartz can be excluded.

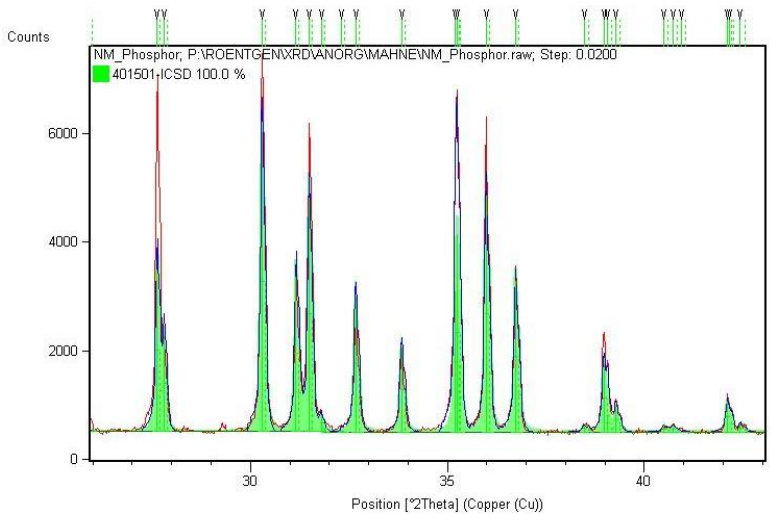

Figure 12: XRD pattern of uncoated phosphor LP-N620.

Figure 13 shows the crystal structure of uncoated phosphor. LP-N620 has an orthorhombic crystal system with the space group P m n 2_1. The lattice parameters of the europium (II) doped crystal are as follows: a=5.7406[Å], b=6.8791[Å], c=9.3575[Å] and with an unit cell volume of 369.5292 [$Å^3$] (see Table 2).

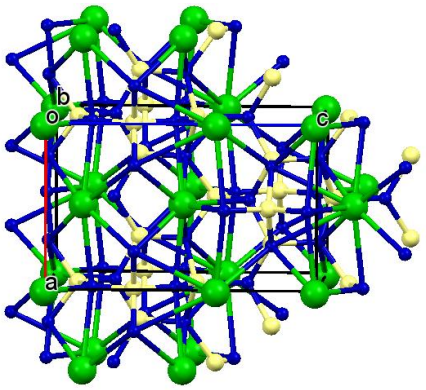

Lattice Parameters	LP-N620
α	90°
β	90°
γ	90°
a	5.7406[Å]
b	6.8791[Å]
c	9.3575[Å]
Cell Volume	369.5292[Å^3]

Figure 13 and Table 2: Crystal structure of LP-N620 with Ba (green), N (blue) and Si (yellow) and lattice parameters of uncoated phosphor before coating process (see right).

Figure 14 shows the crystal structure only build up by nitrogen and silicon: Silicon tetrahedrons are linked with planar nitrogen atoms. From view along the c-axis hexagons and from view along a-axis octagons are visible made up from linked silicon and nitrogen atoms.

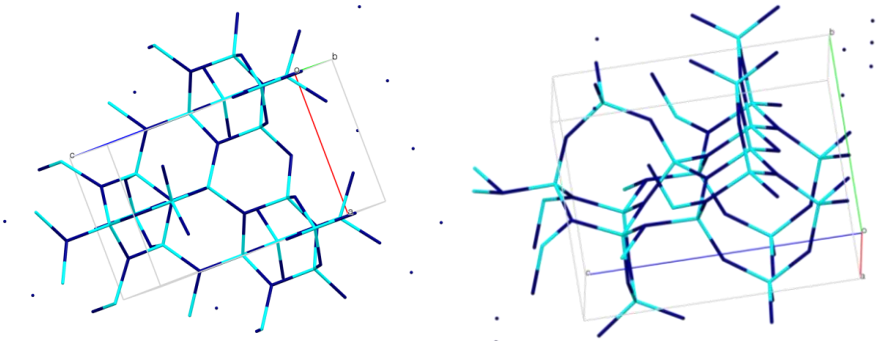

Figure 14: Crystal structure of LP-N620 with N (dark blue) and Si (turquoise), hexagons (left) and octagons (right).

The lattice parameters of LP-N620 are smaller than values from literature for pure $Ba_2Si_5N_8$ which can be ascribed to the doping of Ba through Eu or Sr.[31] The radius of the divalent barium ion is 1.17Å and respectively 1.18Å larger than the divalent Eu and Sr ions. Table 3 shows the ion radii of the divalent ions of strontium, barium and europium.

Table 3: Ion radii of divalent ions of barium, strontium and europium (coordination number of 6).[31]

Divalent Ion	Ion Radius r[Å]
Ba^{2+}	1.49
Eu^{2+}	1.32
Sr^{2+}	1.31

Due to the results of EDX analysis and Rietveld refinement of powder X-ray data of uncoated phosphor LP-N620 calculations according lattice parameter were carried out (see Table 4). Table 4 shows the lattice parameters for a, b and c of LP-N620 and the ICSD standards for $Ba_2Si_5N_8$, $Sr_2Si_5N_8$ and $Eu_2Si_5N_8$. The lattice parameters a, b and c were plotted versus the subscript x of Ba in the chemical formula of $Ba_xSi_5N_8$, whereby x is the number of contained atoms of the compound. The calculated value of x is equal 0.55 provides the best match with the obtained lattice parameters of LP-N620. According to this calculation $Ba_xSi_5N_8$ is doped with 45% europium (100-x) and 55% barium. However, this result cannot be correct and has to be questioned, due to the fact that phosphors are usually doped with an activator ion in a small percentage of a few mole percent or less in the phosphors host lattice.[4] Therefore a distinction between strontium and europium is difficult due to their similar ion radii, which

differ in size only for 0.01Å (1%). The educts used in phosphor synthesis could give information about the actual elements of the host lattice and its dopants. Therefore the assumption can be made that the phosphors host lattice consists out of N, Si, Sr, Ba, and Eu as activator ion.

Table 4: Lattice parameters a, b and c of ICSD standards for $Ba_2Si_5N_8$, $Sr_2Si_5N_8$ and $Eu_2Si_5N_8$ plotted against x in $Ba_xSi_5N_8$.

Compound	$Ba_2Si_5N_8$	$Sr_2Si_5N_8$	$Eu_2Si_5N_8$	$Ba_xSi_5N_8$
ICSD Standard	ICSD 401501	ICSD 401500	ICSD 59257	LP-N620
a [Å]	5.783	5.710	5.709	5.741
b [Å]	6.959	6.822	6.821	6.879
c [Å]	9.391	9.341	9.320	9.358

ATR-IR of uncoated phosphor LP-N620

Because an exact assignment of the vibrational modes of the europium-activated barium silicon nitride phosphor is not possible, the obtained ATR-IR spectrum (see Figure 15, left) should serve as a reference spectrum for the following coating experiments. Therefore special emphasis is given to new bands and increasing or decreasing peak intensities after the coating process.

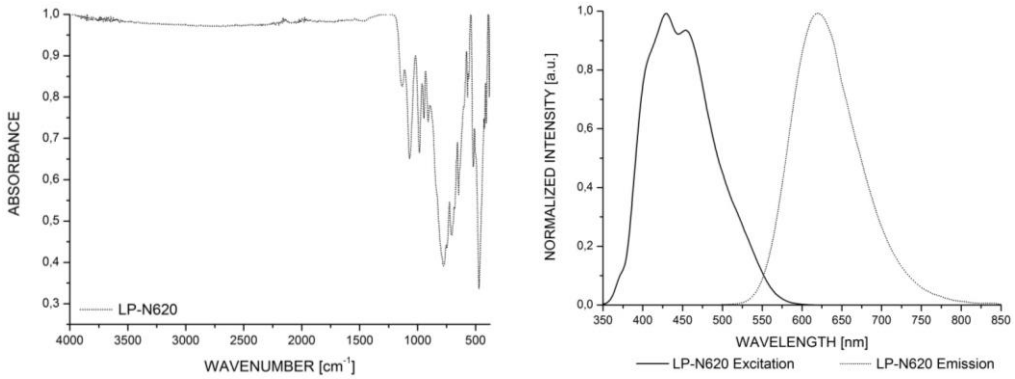

Figure 15: ATR-IR spectrum of LP-N620 (left) and excitation and emission spectra of LP-N620 (right).

Fluorescence Spectroscopy of uncoated phosphor LP-N620

Figure 15 (right) shows the excitation and emission spectra of LP-N620 in a range between 350nm and 850nm. The excitation spectrum shows a broad peak with a maximum at 430nm and a small shoulder at 450nm. On this account the phosphor can be excited by a conventional LED and is therefore suitable for use in COB technology. The $Ba_2Si_5N_8:Eu^{2+}$ phosphor shows a broad symmetric single band in a range of 530-800nm with an emission maximum at 621nm. The determined CIE color coordinates are shown in Table 5.

Table 5: CIE color coordinates (1931) properties of uncoated Phosphor (result of measurement at ACFC).

	CIE Color Coordinate x	CIE Color Coordinate y
ACFC	0.630	0.369

5.2.2 Characterization of BR-101H

In this study we used a red nitride phosphor with the identification Fluorescent Material BR-101H purchased from Mitsubishi Chemical Corporation. The fine powdery orange colored fluorescent material is an europium-activated calcium aluminum silicon nitride phosphor with the chemical formula $CaAlSiN_3:Eu^{2+}$. According to the material safety data sheet, the

chemical content of the starting material contains 30-40% of Ca_3N_2, 25-35% of AlN and 30-40% of Si_3N_4 doped with 0-5% Eu_2O_3. However, it is nonflammable, considered to be of low toxicity in usual handling and due to its water, acid and moisture sensitivity, ammonia gas may be generated by contact with the before mentioned reactants.

SEM of uncoated phosphor BR-101H

The morphological analysis of uncoated phosphor is shown in Figure 16 (left). It exhibits single particles of spherical to oval structures of different particle size and besides that the particles do not agglomerate. The average particle distribution of 5-15µm was obtained from a multiple measurement with a snipping tool included in the program Vega TC.

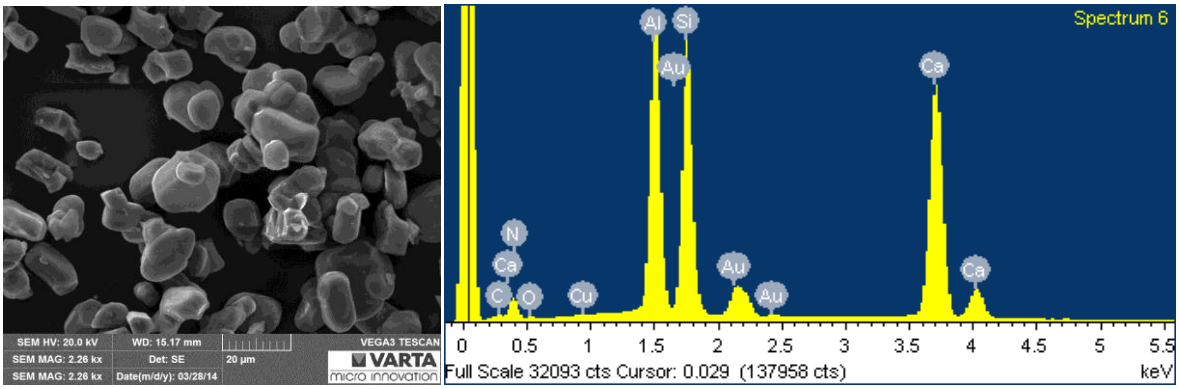

Figure 16: SEM (SE) image of uncoated BR-101H (left) and EDX spectrum of Point and ID mode (right).

EDX of uncoated phosphor BR-101H

Figure 16 (right) shows the EDX spectrum obtained by Point and ID mode recorded with 100.000 counts. Signals of Au result from the coating process for SEM analysis (Au layer of 2-5nm) as explained in Chapter 5.2. Peaks of Cu, O and C can be assigned to the sample foil, which was attached to the sample holder *via* a double-sided adhesive tape. The phosphors host lattice elements N, Al, Si and Ca show significant and high peaks. Eu was not found. After the coating process with inorganic layers of SiO_2, MgO and Al_2O_3 peaks for O, Al and Si should increase and a new peak for Mg should appear, which is not an element of the phosphors host lattice. To obtain the atomic ratio of the host lattice, the atomic percentage of N, Al, Si and Ca was calculated by subtraction of the elements C, O, Cu and Au. The XRD analysis led to a chemical formula of $CaAlSiN_3$ and could be confirmed by EDX analysis. The calculation results in Ca:Al:Si:N=16:15:20:49=1:1:1:3 with a total number of 6 atoms with 100%. Table 6 shows the processed results of EDX analysis of uncoated BR-101H.

Table 6: Results of EDX analysis of uncoated BR-101H in Point and ID mode.

Element	Atomic Percent [%]	Number of Atoms
N	49	3
Al	15	1
Si	20	1
Ca	16	1
Total	100	6

XRD of uncoated phosphor BR-101H

Figure 17 shows the result of the Rietveld refinement of powder X-ray data of uncoated phosphor. The corresponding sharp peaks are in good agreement (ICSD 161796 $CaAl_{0.54}Si_{1.38}N_3$). The material is pure phase europium-activated calcium aluminum silicon nitride with the chemical formula $CaAlSiN_3$[8,15,16] and are fully consistent with the results of EDX analysis.

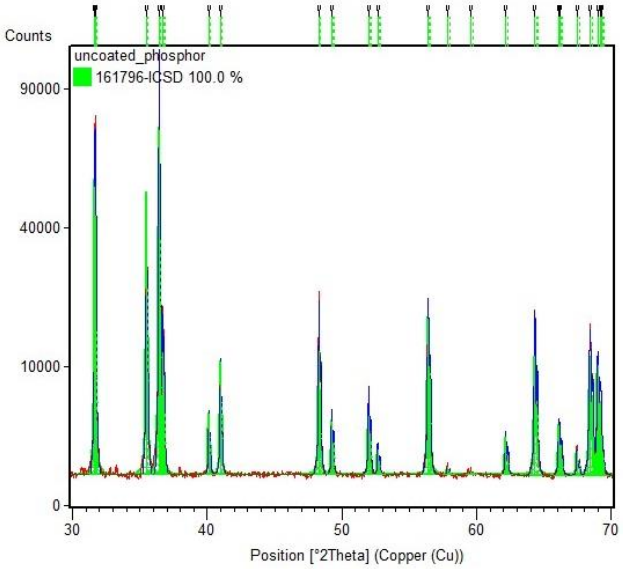

Figure 17: XRD pattern of uncoated phosphor BR-101H.

Figure 18 shows the crystal structure of uncoated phosphor. BR-101H has an orthorhombic crystal system with the space group C m c 2_1. The lattice parameters of the europium (II) doped crystal are as follows: a=9.7917[Å], b=5.6461[Å], c=5.0579[Å] and an unit cell volume of 279.62050[$Å^3$] (see Table 7).

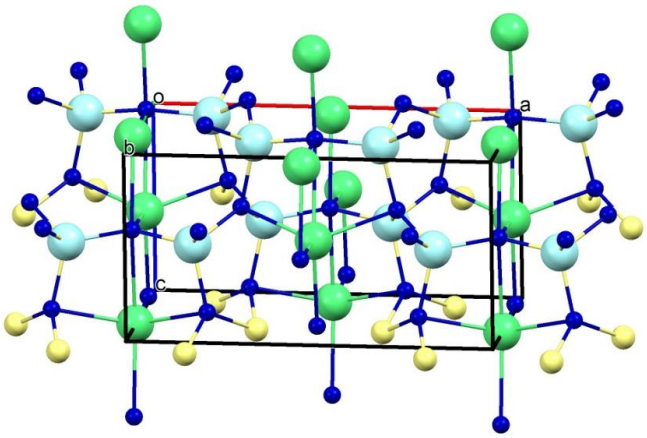

Lattice Parameters	BR-101H
α	90°
β	90°
γ	90°
a	9.7917[Å]
b	5.6461[Å]
c	5.0579[Å]
Cell Volume	279.62050[$Å^3$]

Figure 18 and Table 7: Crystal structure(left) of nitride phosphor Ca (green), N (blue), Si (yellow), Al (light blue) and lattice parameters of uncoated phosphor before coating process (right).

ATR-IR of uncoated phosphor BR-101H

Figure 19 (left) shows the obtained ATR-IR spectrum of uncoated phosphor BR-101H. The obtained ATR-IR spectrum should serve as a reference spectrum for the following coating processes, because an exact assignment of the vibrational modes of the europium-activated calcium aluminum silicon nitride phosphor is not possible. Therefore special emphasis is given to new bands and increasing or decreasing peak intensities after the coating process.

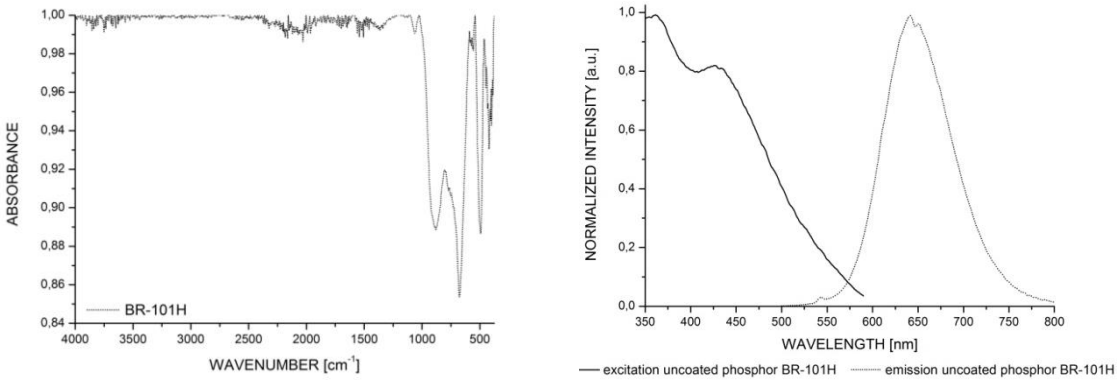

Figure 19: ATR-IR spectrum of uncoated BR-101H (left) and excitation spectrum and emission spectrum of uncoated phosphor BR-101H (right).

Fluorescence Spectroscopy of uncoated phosphor BR-101H

Figure 19 shows the excitation and emission spectra of uncoated phosphor. The excitation spectrum shows a broad peak from the NUV to the VIS area with a peak maximum at 352nm. The excitation of the host lattice and further energy transfer to the dopant Eu^{2+} can be ascribed to the peak maximum in the NUV region.[8,14,17] The excitation peak corresponding to Eu^{2+} extends towards the visible region with a maximum at 430nm. Consequently the phosphor can be excited by a conventional blue LED. The $CaAlSiN_3$:Eu^{2+} phosphor shows a broad symmetric single band in a range of 500-800nm with an emission maximum at 643nm, which is typical for a 5d-4f transition of Eu^{2+}.[8,16,17] It covers a part of the visible light in the area between 550nm and 750nm and it is therefore a well suited phosphor for use in Chip-On-Board technology. The quantum efficiency of the uncoated phosphor is 75% and should serve as a reference value for following measurement of coated also for the encapsulated phosphor. Color coordinates differ from the values given in the Certificate of Quality with 0.652 x and 0.347 y (see Table 8). The reason for that can be the used method of quantum efficiency determination. For the measurement we used a direct method with ZrO_2 as reference material Mitsubishi Chemical Corporation used BR-101A. Ideally the reference material should be the phosphors host lattice $CaAlSiN_3$ not doped with Eu^{2+}, thus without the activator ion responsible for luminescence. Furthermore it should have a similar particle size distribution and a similar refractive index.

Table 8: CIE color coordinates properties of uncoated phosphor (results ACFC and MSDS).

	CIE Color Coordinate x	CIE Color Coordinate y
ACFC	0.663	0.337
MSDS	0.652	0.347

Acid-base study of uncoated phosphor BR-101H

Due to results from SiO_2 coating experiments in Chapter 6.1.1 regarding effects of acids and base catalyzed reactions, pretest were carried out. According to the Material Safety Data Sheet BR-101H may generate ammonia gas by contact with water, acid or moisture as mentioned before. In order to investigate the hydrolytic stability, 0.2g of uncoated phosphor was stirred by means of a magnetic stirrer with 600rpm in 2ml of 0.1M HCl and in 2ml of 0.1M NaOH in a vial at room temperature for 14 days. After that the treated phosphor was dried for 1 day at 100°C. In order to get information about the obtained dried product, ATR-IR measurements and luminescence measurements were carried out according to Chapter 5.2.

The acid-base study of the material showed that the uncoated phosphor is conditionally stable in acids and bases. After a few days first visually changes could have been observed. A bright layer of whitish color was formed on top of the diluted acid and base like shown in Figure 20 (left and mid). The color of unexcited and of excited phosphor changed and a color gradient is shown from bottom of the vial to the top of the liquid. Figure 20 (right) shows the ATR-IT spectra of uncoated treated phosphor after acid and base treatment compared to untreated phosphor BR-101H for 14 days. Spectrum of 0.1M HCl total product shows a new small absorption peak at around 3400cm^{-1} which can be assigned to the symmetric and asymmetric stretch modes of water and 1620cm^{-1} to the stretching and bending mode of water respectively.[32] Significant differences in peak intensities (strong decrease of signal) are observable in the upper whitish phase of acid and base treated phosphor in the range of 1600-375cm^{-1} (see Figure 20, right).

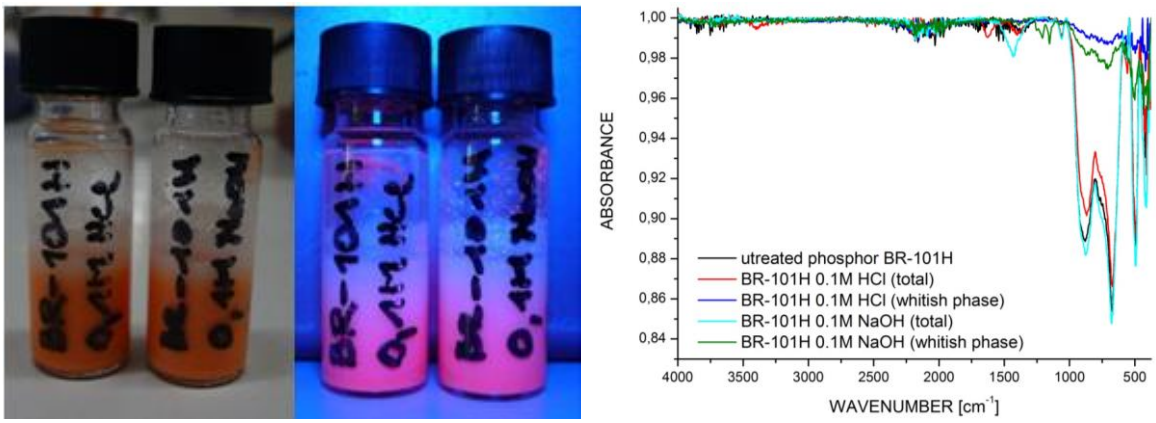

Figure 20: Unexcited (left) and excited (mid) uncoated phosphor BR-101H after acid-base study (14 days) and ATR-IR spectra of BR-101H untreated and treated with 0.1M acid and 0.1M base (right).

Figure 21 shows the ATR-IR spectra of uncoated and acid (left) or base (right) treated phosphor BR-101H in the range of 1800-375cm^{-1}. New absorption peaks are observed in 1405cm^{-1} and 555cm^{-1} in Figure 21 (see arrows; acid catalyzed, left) and 1430cm^{-1}, 1210cm^{-1} and 1150cm^{-1} in Figure 21 (see arrows; base catalyzed, right) due to formation of hydrolysis products of the phosphor like $Al(OH)_3$ (characteristic absorption bands).[32]

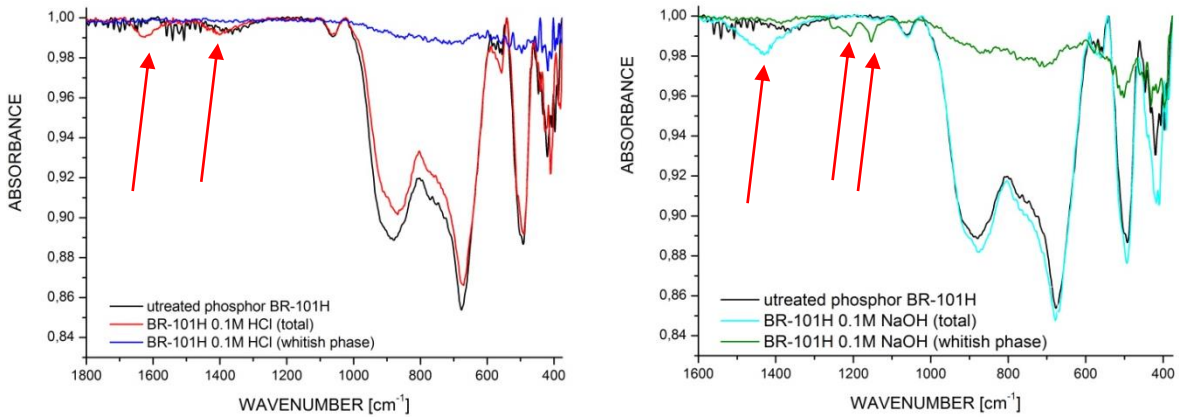

Figure 21: ATR-IR Spectra of untreated and treated phosphor 0.1M HCl (left) and 0.1M NaOH (right).

Figure 22 shows the emission spectra of uncoated phosphor treated with 0.1M acid and 0.1M base compared to the not treated phosphor. The emission maxima of the acid and as well of the base treated phosphor shifted to smaller wavelengths from 643nm to 638nm.

The acid-base study showed that the phosphor is conditionally stable in acids and bases. Only the surface of phosphor particles reacted with the acids and bases *via* hydrolysis reaction. Unfortunately a synthesis without use of water as a solvent is limited to the used educts and cannot be replaced by another solvent easily.

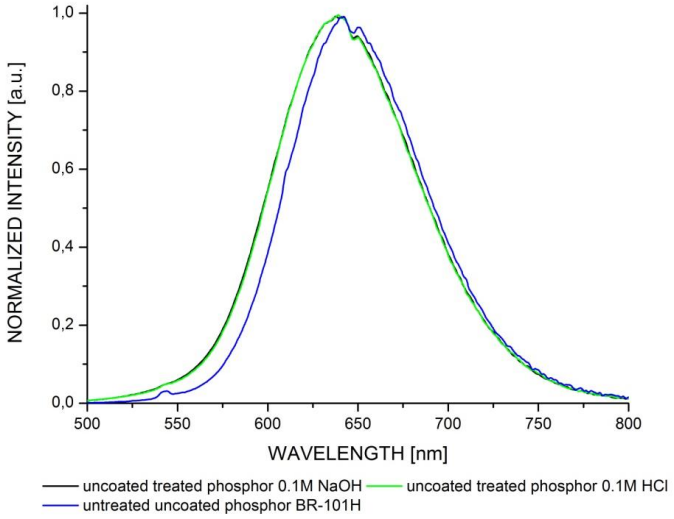

Figure 22: Emission spectra of uncoated phosphor before and after acid (left) and base (right) treatment.

5.3 Synthesis of Inorganic Coating

Suitable synthesis routes were selected to be carried out to create an inorganic layer of SiO_2, Al_2O_3 and MgO on phosphor particles, which are hereinafter explained in detail. It is recommended for all syntheses routes, to use in addition to ultrasonic dispersion a dispersing agent like Dispex® from BASF a polyacrylate based on water, to maximize dispersion of the phosphor particles in the suspension.[20] In order to prevent H_2O as the solvent of choice, due to the possibility of hydrolysis, educts for synthesis were tried to be dissolved in isopropyl alcohol, octanol and butanol (see Table 9). According to Murphy et al.[20] the most uniform coating layer on phosphor particles is formed when the educts solutions were added slowly (timeframe of 5min<x) to the phosphor suspension. Murphy et al.[20] reported that in the event of a too rapid addition of educts solutions, preferred nuclei of metal hydroxide were formed, instead of just coating the phosphor.

Table 9: Solubility of educts in different solvents like H_2O, isopropyl alcohol, butanol and octanol.

Educt	H_2O	Isopropyl Alcohol	Butanol	Octanol
$NaHCO_3$	yes	no	no	no
$MgCl_2$	yes	no	no	no
$Al(NO_3)_3 \cdot 9H_2O$	yes	yes	yes	no
Urea	yes	yes	-	-

A coating of SiO_2 should be synthesized by a modified Stöber synthesis like already mentioned in Chapter 3.1. To form Al_2O_3 and MgO, metal nitrates or metal halides are used as a cation source and a water soluble material such as $NaHCO_3$ or urea is used as the hydroxide source like proposed by Murphy et al.[20] *via* a precipitation reaction. A precipitation reaction occurs when the attraction between particular charged ions in solution outweigh, which leads to the formation of an insoluble product i.e. with lower solubility. The other product remains in the solution. The precipitate-free liquid remaining above the solid is called the supernatant.

5.3.1 SiO_2 Coating Procedure

Several experiments based on a modified Stöber synthesis[25] were carried out according to Azuma et al.[26], Murphy et al.[20] and Sun et al.[23] to synthesize an SiO_2 layer on phosphor particles (see Equation 1), which are explained in detail in this chapter. Specific conditions like concentration of educts, molar ratio, drip rate, ultrasonic dispersion, dispersant, reaction time, water-bath temperature and the work up procedure of the product were varied (see Appendix Chapter 9.3 Table 34, 35 and 36). In addition the coating procedure was carried out without phosphor, to investigate the nature of the precipitate. Phosphor LP-N620 was used for SiO_2 coating experiments. At first a coating procedure according to Azuma et al.[26] synthesis will be described below using the example of NM001-1 synthesis (see Appendix Chapter 9.3 Table 34 synthesis NM001-1/-2). 0.150g of uncoated phosphor were added to a mixture of 2.73ml EtOH, 12.1ml of 1M NH_3 and 0.36ml H_2O, which was sonicated for 10 minutes. Next a solution containing 5ml EtOH and 0.53ml TEOS was added dropwise manually *via* a syringe to the suspension while it was stirred vigorously *via* a metallic flatblade stirrer, suitable for reaction solutions with dynamic viscosities below 0.5Pa·s.[25] The mixture was stirred for further 3h to continue the reaction. The coated particles were filtered *via* a blue ribbon filter, rinsed twice with 20ml ethanol and dried at 80°C over night.

Other test trials were carried out according to following procedure (see Appendix Chapter 9.3 Table 34 synthesis NM002-1/-2, NM003-1/-2 and NM004-1/-3). After the suspension of phosphor particles was dispersed sufficiently a solution containing 0.7ml TEOS in 50ml EtOH was added dropwise manually *via* a syringe to the suspension while it was stirred vigorously *via* a metallic flatblade stirrer. After 90 minutes an additional solution containing 0.3ml TEOS in 5ml EtOH was added to the suspension. The mixture was stirred for further 55 minutes to continue the reaction. The coated particles were centrifuged at 2000rpm for 15 minutes, the supernatant was decanted and the particles were dried at 80°C over night.

According to Murphy et al.[20] synthesis test trials were carried out (see Appendix Chapter 9.3 Table 35 synthesis NM005-1/-2/-3). Here a detailed procedure for synthesis NM005-3 is explained as follows. 0.5ml H_2O, 2.74ml EtOH and 0.27ml TEOS were dispersed *via* ultrasonic treatment (no stirring) in a vial for 10 minutes. The pH-value was adjusted to pH 3 *via* a 0.1M H_2SO_4, and again after addition of 0.5g phosphor. The reaction was stopped after 90 minutes. The coated particles were centrifuged at 2000rpm for 15 minutes, the supernatant was decanted and the particles were dried at 80°C over night.

Experiment NM006-1 was carried out according to Sun et al.[23] and its procedure is explained as followed (see Appendix Chapter 9.3 Table 36 synthesis NM006-1/-2 and NM007-1/-2). 0.5g of phosphor were sonicated and stirred for 15 minutes in 30ml EtOH. A chilled 0.13M NH_3 solution was added dropwise to the suspension and was further sonicated for 15 minutes. After that, a chilled solution of 3ml TEOS in 23ml EtOH was added rapidly to the suspension. The hydrolysis of TEOS was stopped after further 60 minutes. The coated particles were centrifuged at 2000rpm for 15 minutes, the supernatant was decanted and the particles were dried at 80°C over night.

All coating procedures underlie the following synthesis route according to a modified Stöber synthesis [25] shown in Equation 2: Starting with the hydrolysis of TEOS to the intermediate orthosilicic acid to yield in SiO_2 *via* several condensation reactions.

$$Si(OEt)_4 + 4H_2O \xrightarrow[-4\,EtOH]{} Si(OH)_4 \xrightarrow[-H_2O]{} H_2SiO_3 \xrightarrow[-H_2O]{} SiO_2$$

Equation 2: Hydrolysis of TEOS and further condensation to SiO_2 based on a modified Stöber synthesis.[25]

5.3.2 Al_2O_3 Coating Procedure

Test series were carried out in order to obtain Al_2O_3 as a coating layer on phosphor particles. The coating procedure was carried out according to Murphy et al.[20] Specific conditions like concentration of educts, molar ratio, drip rate, ultrasonic dispersion, dispersant, reaction time, water-bath temperature, methode of separation of solvents and annealing temperature were varied (see Appendix Chapter 9.3). Two different silicon nitride phosphors were used for these test series. One of the two is a $Ba_2Si_5N_8$ based material which was used in SiO_2 coating experiments in Chapter 5.3.1 (see Chapter 5.2.1 and Appendix Chapter 9.3 Table 38 synthesis NM009-3/-4 and NM010-1/-2/-4) and the other one is a $CaAlSiN_3$ based material (see Chapter 5.2.2 and 9.3 Table 37 and 39 synthesis number NM011, NM012-1/-2/-3/-4 and NM013). In order to obtain thick Al_2O_3 layers this procedure was repeated three times with the same coated particles (see Appendix Chapter 9.3 Table 39 and 40 syntheses NM029, NM032, NM033 and NM034). Furthermore scaleup experiments were carried out to be used for luminescence measurements at Tridonic Jennersdorf (see Table 40 US01, US02 and US03). Exemplarily, the coating procedures are described at the example of NM029 as followed: 1g of uncoated phosphor and 80ml isopropyl alcohol were sonicated while stirred vigorously for 20 minutes. To obtain a good turbulence inside the reaction vessel made out of Teflon, a paddle mixer with diagonal arranged blades was used, suitable for reaction solutions with dynamic viscosities below 0.5Pa·s.[33] The precursor solutions were prepared according to Table 39 and the synthesis was carried out without a dispersing agent. 5ml of the $Al(NO_3)_3 \cdot 9H_2O$ solution were added dropwise with a constant drip rate of 1.0ml/min *via* an automatic syringe pump to the suspension. After 20ml of $Al(NO_3)_3 \cdot 9H_2O$ and 20ml of $NaHCO_3$ were simultaneously added dropwise with a constant drip rate of 0.34ml/min to the suspension and stirred for additional 30 minutes, to form $Al(OH)_3$ on phosphor particles. The coated particles were filtered *via* vacuum, rinsed twice with 20ml deionized H_2O, twice with 20ml isopropyl alcohol, dried at 100°C and annealed for 2h at 400°C in a tubular furnace under constant N_2 flow of 2bar to obtain a homogeneous coating of Al_2O_3 according to Equation 3.

$$2Al(NO_3)_3 \cdot 9H_2O + NaHCO_3 \rightarrow 2Al(OH)_3 + side\ products \xrightarrow{\Delta T} Al_2O_3 + 3H_2O \uparrow_{vap}$$

Equation 3: Chemical equation of the precipitation reaction of aluminum hydroxide and further formation of aluminum oxide after annealing.

In some cases additional solvent had to be added *via* dropping funnel, because the energy of the ultrasonic device heated up the water bath and hence the solvent evaporated in parts. Furthermore solvent was added *via* a syringe to rinse the interior walls of the reaction vessel with solvent, to guaranty that all phosphor particles take place in the reaction and thus to be coated.

5.3.3 MgO Coating Procedure

Another coating procedure was carried out according to Murphy et al.[20] to form a layer of MgO on phosphor particles. Again, the procedure was carried out once without and once with phosphor particles to compare the obtained products (see Appendix Chapter 9.3 Table 41 synthesis NM030 and NM031). Following the procedure is explained based on NM030. 0.5g of uncoated phosphor material and 75ml isopropyl alcohol were sonicated while stirred vigorously for 10 minutes. The precursors solutions were prepared as followed: 0.163g of $MgCl_2$ was dissolved in 25ml of H_2O and 0.206g urea was dissolved in 25ml H_2O (see Appendix Chapter 9.3 Table 41). 5ml of the $MgCl_2$ solution were added dropwise with a constant drip rate of 1.0ml/min *via* an automatic syringe pump to the suspension. After the remaining 20ml of $MgCl_2$ solution and 25ml of the urea solution were simultaneously added dropwise with a constant drip rate of 2ml/min, the suspension was stirred for additional 3h at a temperature of 42°C to form $Mg(OH)_2$ on phosphor particles. It was necessary to add solvent, in this case 20ml every 30 minutes. The coated particles were filtered *via* vacuum, rinsed twice with 20ml deionized H_2O, twice with 20ml isopropyl alcohol, dried at 100°C and annealed for 2h at 400°C MgO according to Equation 4. Synthesis NM035 was carried out with $NaHCO_3$ as precipitation agent according to Equation 5 and Table 41 (see Appendix Chapter 9.3). As the synthesis was carried out overnight, the reaction vessel was covered with an aluminum foil to prevent losses of solvent.

$$MgCl_2 + 2CO(NH_2)_2 \rightarrow Mg(OH)_2 + side\ products \overset{\Delta T}{\rightarrow} MgO + 2H_2O \uparrow_{vap}$$

Equation 4: Chemical equation of the precipitation reaction of magnesium hydroxide with urea as precipitation agent and further formation to magnesium oxide after annealing.

$$MgCl_2 + NaHCO_3 \rightarrow Mg(OH)_2 + side\ products \overset{\Delta T}{\rightarrow} MgO + 2H_2O \uparrow_{vap}$$

Equation 5: Chemical equation of the precipitation reaction of magnesium hydroxide with $NaHCO_3$ as precipitation agent and further formation to magnesium oxide after annealing.

5.4 Characterization of Inorganic Coating

To look at the morphology of particles and to examine the inorganic coating of SiO_2, Al_2O_3 and MgO on the phosphor particles several characterization methods were carried out. SEM (SE, BSE), SEM-Focused Ion Beam (FEM), EDX, ATR-IR, XRD and Fluorescence Spectroscopy measurements were carried out according to Chapter 5.2 for sample preparation on the same instruments, with the same settings and under the same conditions. Only SEM investigations with secondary electrons and qualitative EDX analysis on the cross section of coated phosphor particles were carried at the Institute of Electron Microscopy and Nanoanalysis (FELMI), Focused Ion Beam ablations (SEM-FIB) of the surface of coated phosphor particles were carried out at Materials Center Leoben (MCL). Luminescence measurements of Al_2O_3 coated scaleup experiments were performed at TRIDONIC Jennersdorf GmbH.

5.4.1 SEM Analysis of Cross Section at FEMLI

Only Al_2O_3 coated particles were chosen to be analyzed by SEM with SE and BSE and further *via* EDX. To look at the morphology of particles and to examine the efficiency of Al_2O_3 coating on the phosphor SEM investigations were recorded. For that reason the sample had

to be coated with a thin electrically conductive layer using gold for the topography images and carbon for the chemical analysis. The SEM measurements were carried out in a Tescan Performance Nanospace (topography images of the particles) and in an Ultra 55 from Zeiss equipped with a silicon drift detector (SDD) from EDAX for energy dispersive X-ray spectroscopy. For the examination of the Al_2O_3 coating and the chemical analysis a cross section was prepared. Therefore the powder was embedded in epoxy resin, afterwards the sample was ground on silica carbide paper finishing with 4000 grit and was polished using a 0.25µm diamond paste.

5.4.2 Focused Ion Beam at MCL

A detailed analysis of the coated phosphor particles of NM029 and NM032 was carried out by SEM-Focused Ion Beam (FEM) at Material Center Leoben. The SEM measurements were carried out in an Auriga from Zeiss SMT equipped with a SESI, CZ BSD and ESB detector from EDAX (EDX Apollo 40+) for Energy Dispersive X-ray Spectroscopy. The particles were spread on a double adhesive carbon pad and coated with a thin conductive layer of gold. The ablation of material was carried out *via* a focused ion beam (Ga as ion source) to investigate the Al_2O_3 coating.

5.4.3 Luminescence Measurement at TRIDONIC Jennersdorf GmbH

The sample preparation of a 20g paste for luminescence measurement was carried out as followed: The uncoated and coated phosphor material was sieved via a test sieve from Retsch® (for bulk material of x ≤ 100µm grain size, ISO 3310-1) to avoid agglomerates in the paste. 44.6wt% of each silicone, A and B, 5.7wt% of orthosilicic acid and 5% per weight of phosphor were added in an appropriate mixing tank in the said order (see Table 10).

Table 10: Weights of sample preparation for luminescence measurements at TRIDONIC Jennersdorf GmbH.

Component	Phosphor [g]	Orthosilicic acid[g]	Silicon A [g]	Silicon B [g]
BR-101H	1.00	1.1413	8.90	8.88
NM0US01	1.00	1.1409	8.91	8.93
NM0US02	1.01	1.1404	8.91	8.93

The mixture was dispersed in a Speed Mixer™ with 2000rpm for 1 minute to obtain a homogenous paste. The paste was evacuated for 10 minutes, transferred in a syringe and again evacuated for 5min to degas it, to avoid air entrapment (see Figure 23, left). Measurements were carried out with consideration of ESD-security on a compact array spectrometer (instrument systems CAS 140CT, Optische Messtechnik) with an integrating sphere (instrument systems, Ø50cm, Optische Messtechnik ISP500) with a potentiostat from Keithley (Keithley 2420). After a background spectrum was recorded, measurements of the blue LED module were done. The light flux [lm] referred to the radiant power [mW] of the blue LED chips were measured in the wavelength range of 380-830nm in with an excitation wavelength of 449nm, 455nm, 460nm and 464nm. Like carried out in the Chip-On-Board technology a drop of the prepared silicon paste was applied on top of the blue LED chip (see Figure 23, mid and right). This procedure was carried out 10 times (increasing globe) at each excitation wavelength of the four different blue-LEDs to obtain a x color coordinate of 0.44.

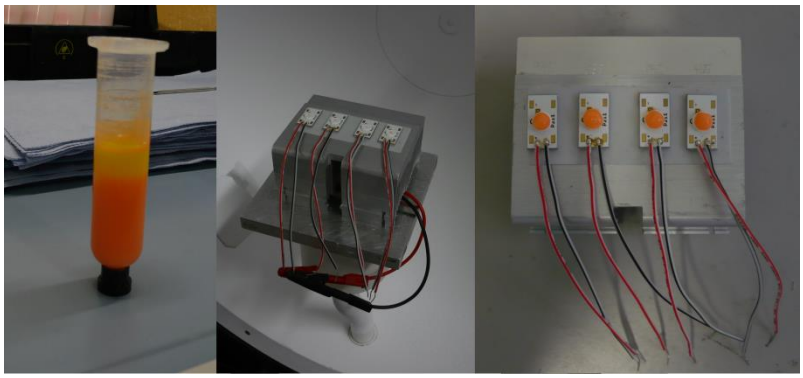

Figure 23: Prepared globe top paste (left), integrating sphere with a LED module with different blue LED chips with wavelengths of 449nm, 455nm, 460nm and 464nm (mid and right).

5.5 Grinding of BR-101H

BR-101H particles were ground wet in a Fritsch planetary mill (Pulverisette 6, milling modus) for 2h at 400rpm without a dispersant (see details in Table 11) to decrease its particle size, in order to determine if its coating behavior improves or declines with decreased particle size. During the grinding process quenching of luminescence of the phosphor may occur, due to traces of Bismuth(III/V)oxide and Titanium oxide on the grinding balls as well as on the interior wall of the grinding bowl.

Table 11: Weight of sample taken for the grinding process.

Material	Components	m [g]
Grist	BR-101H	4.99
Grinding balls	YSZ (lead free)	50.0
Grind medium	H_2O (D.I.)	21.4
Grinding bowl, lid, sealing ring	ZrO_2 (250ml capacity)	1874

The obtained milled fractions were further analyzed by several methods to determine their particle size distribution *via* SLS (Static Light Scattering), particle shape *via* SEM, luminescence behavior *via* Fluorescence Spectroscopy (emission maxima, quantum efficiency, CIE color coordinates), crystal structure and lattice parameters *via* XRD and their elemental distribution *via* EDX.

5.6 Encapsulation into Lead-free Glass

Silicone as a potting compound in the COB-Technology causes problems as already mentioned in Chapter 3.2 and should be replaced by a low melting glass as an encapsulant material, to encapsulate coated phosphor particles. Common glass types like fused silica glass, soda-lime-silica glass, sodium borosilicate glass or lead-oxide glass are not suitable for our purposes. The reason for this is that their sinter process has to be carried out at temperatures which the phosphor cannot stand without serious damages in its luminescence behavior. For example Schotts DURAN® borosilicate glass requires processing temperature of 1260°C and it is therefore no eligible candidate.[34] The global market leader for displays for electronic devices is Corning® Gorilla® glass. It is an ideal cover glass for smart phones, tablets, notebooks and computer screens. It shows following advantages: It is thin (2-4mm thickness), lightweight, damage resistant and show a high degree of chemical strengthening.[35] Therefore it was meant to be a good candidate for the encapsulation of

coated phosphor particles. Despite these clear advantages this glass type has to be annealed at temperatures far above 600°C and thus not suitable for our phosphor (see results in Chapter 6.1.2 headline ATR-IR Al_2O_3 single coating).[36]

An alternative may be a low melting glass with the description ZASNP11C investigated by Otto Schott Institute for Glasschemistry at Friedrich Schiller University of Jena.[37] According the project report from Herrmann[37] ZASNP11C is a zinc phosphate glass with the following composition shown in Table 12.

Table 12: Chemical composition of ZASNP11C glass.

	$NH_4H_2PO_4$	ZnO	Na_2O	$ZnSO_4$	Al_2O_3
ZASNP11C [mol%]	50.0	26.0	16.0	8.0	0.5

It is a low melting glass which can be sintered *via* a hot pressing process.[37] The encapsulation process can be carried out at its transition temperature of 380°C, with 120N and for 10-15 minutes.

5.6.1 Characterization of ZASNP11C

In order to obtain more information about ZASNP11C as reported in the project report from Herrmann[37] following Characterization methods were use: SEM and EDX were carried out according to Chapter 5.2. X-ray Fluorescence Spectroscopy (XRF) measurements were performed on a FISCHERSCOPE® X-RAY XAN-FD from Helmut Fischer GmbH & Co KG (V_{ANODE}=50keV, without primary filter, collimator Ø of 2mm). The evaluation was carried out with the program WinFTM. Two thermoanalytical techniques were used as followed: Thermogravimetry (TG) and Differential Scanning Calorimetry (DSC) coupled with Mass Spectroscopy (MS) measurements were carried out in an inert gas atmosphere. In the case of TG the thermal strain in µV was recorded with increasing temperature. Whereas in the case of DSC-MS mass changes in mg were recorded with increasing temperature. The obtained data can give information about commonly processes like thermal stability, decomposition, dehydration, oxidation, determination of volatile components and moreover physical transformations like phase transitions (exothermic or endothermic) and glass transition. The measurements were carried out at the Institute for Chemistry and Technology of Materials (ICTM) of Graz University of Technology by Dipl.Ing. Theresa Kainz. The TG and DSC analysis was simultaneously carried out on a NETZSCH STA 409 Cell coupled with a mass spectrometer from NETZSCH QMS 403C (see details in Table 13).

Table 13: Measurement parameters and settings of TG-DSC-MS.

Parameter	Setting
Amount of Sample	~15mg
Crucible	Pt
Flow rate N_2	50ml/min
Heating Program	Dynamic
T_{START}	35°C
T_{END}	720°C
$T_{EMERGENCY\ STOPP}$	730°C
Reference Material	MgO
Thermal Strain	± 250µV
Mass Change	± 250mg

After successful equilibration of the equipment the reference and the sample crucibles were baked out over a temperature range of 700°C with a heating rate of 10K/min, which served as baseline. A sample of ZASNP11C was measured as loose powder. The obtained data was evaluated with the program NEZTSCH Proteus Thermal Analysis.

5.6.2 Encapsulation of Coated Phosphor Particles into Glass

Due to the low glass transition temperature it was decided to try the encapsulation of coated phosphor particles into ZASNP11C. Unfortunately, a suitable hot press was not at hand. Test series were therefore carried out in a commercially available tubular furnace in N_2 atmosphere as well as in a Domed Hot Stage DHS 1100 (Anton Paar GmbH, Temperature Control Unit TCU 200) in Ar atmosphere.

Encapsulation in Bullseye Glass

Before the encapsulation in ZASNP11C was done, pretests with Bullseye Glass purchased from Bullseye Glass Company were performed in the Domed Hot Stage DHS 1100. Bullseye Glass Company proposes the firing schedule shown in Table 14. As an inert gas Ar was used (0.01bar) and compressed air was used for cooling with of (4bar).

Table 14: Firing schedule for the sinter process of Bullseye Glass.

Step	Description	Rate [DPH]	Temperature [°C]	Hold [min]
1	Initial Process Soak	333	691-788	10
2	Rapid Cool Down	AFAP	482	60
3	Anneal Cool	55	371	0
4	Final Cool	AFAP	RT	0

Furthermore pretest were carried out in a tubular furnace in N_2 atmosphere: The samples were heated up from a room temperature up to 400°C and further in 10°C steps until an observable change occurred.

Encapsulation in ZASNP11C and simultaneous TG-DSC-MS Analysis

After pretest further encapsulation tests and simultaneous analysis *via* TG-DSC-MS were carried out according to Chapter 5.6.1. Therefore 5wt% of uncoated and coated phosphor particles were blended with ZASNP11C. This was performed with pure ZASNP11C with 5wt% uncoated BR-101H in ZASNP11C and with 5wt% coated phosphor NM029 in ZASNP11C as loose powder samples.

6 RESULTS AND DISCUSSION

Most experiments and measurements were carried out as described in Chapter 5.2. Luminescence measurements were carried out at TRIDONIC Jennersdorf GmbH as described in Chapter 5.4.3, SEM as well as EDX analysis were carried out by Dr. Angelika Reichmann at the Institute of Electron Microscopy and Nanoanalysis (FELMI) as described in Chapter 5.4.1 and a surface analysis *via* FIB was carried out by the Materials Center Leoben (MCL) as described in Chapter 5.4.2.

6.1 Characterization of Inorganic Coating

6.1.1 Results: SiO_2 Coating

ATR-IR SiO_2 coating

In order to prove the complete reaction of TEOS to the desired end product SiO_2 the interpretation of ATR-IR spectra should give information. Absorption bands which can be ascribed to water, the educt TEOS or intermediate products indicate a not complete reaction. Rubio et al. [38] published a detailed FT-IR study of the hydrolysis of TEOS in 1998. According these results Table 15 shows the detailed assignments of all possible absorption bands of the successful hydrolysis of TEOS and the stepwise condensation of orthosilicic acid $Si(OH)_4$ over H_2SiO_3 to yield in SiO_2.[38]

Table 15: Infrared absorption bands of the hydrolysis of TEOS to orthosilicic acid and condensation to SiO_2.[38]

$\tilde{\upsilon}$ Wavenumber [cm^{-1}]	Assignment	Educts
3500-3000	O-H stretching	H_2O, Si-OH
2974	Asymmetric C-H stretching	CH_3 in TEOS
2930	Asymmetric C-H stretching	CH_2 in TEOS
2892	Asymmetric C-H stretching	TEOS
1446	Asymmetric C-H bending	CH_3 in TEOS
1381	Symmetric C-H bending	CH_3 in TEOS
1416,1324	O-H bending and C-H wagging	CH_2 in TEOS
1275	C-H twist/wagging	C-H in TEOS
1200	Si-O-Si asymmetric stretching	Cyclic structures of Si-O-Si
1168	C-H rocking	CH_3 in TEOS
1147	Si-O-Si asymmetric stretching	Linear structures of Si-O-Si
1100	Si-O-Si symmetric stretching	Linear structures of Si-O-Si
1100	C-O asymmetric stretching	TEOS
1086	Si-O-Si symmetric stretching	Cyclic structures of Si-O-Si
960	C-H rocking	CH_3 in TEOS
920	Si-O non bridging free broken	$Si\text{-}O^-$
812	CH_2 rock	TEOS
793	SiO_4 asymmetric	TEOS
793	Si-O-Si bend	SiO_2
473	O-C-C	TEOS
473	O-Si-O bend	SiO_2

Figure 24 shows the FT-IR spectrum of TEOS.[39] Rubio et al. reported that absorption bands located at 1168cm^{-1} and 812cm^{-1} confirm the hydrolysis of TEOS since they disappear after completed hydrolysis reaction.[38] Moreover bands located at 1200cm^{-1} and 1147cm^{-1} can be assigned to the condensation of $\tilde{\upsilon}$[Si–OH] groups forming $\tilde{\upsilon}$[Si–O–Si] bonds. A pH dependency has to be mentioned due to a decrease in the rate of hydrolysis in the pH range between 1.6 and 12 as well as precipitation in the range between pH 9 and 12 occurred.

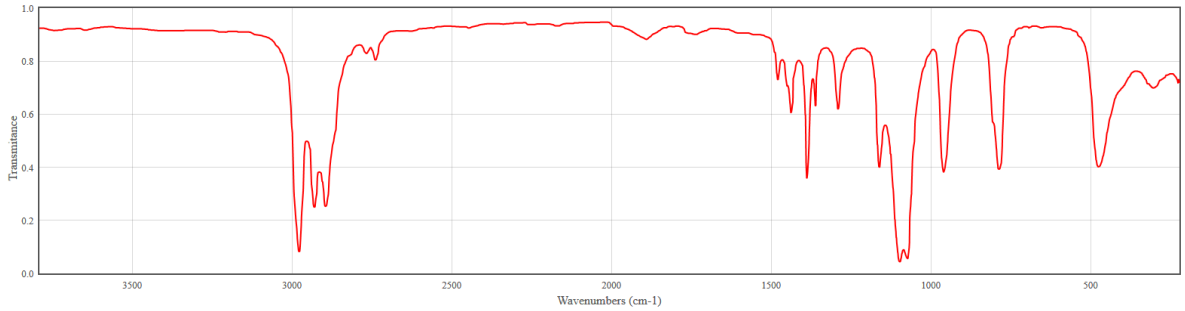

Figure 24: FT-IR spectrum of TEOS in the range of 3700-375cm^{-1}.

The results from acid-base study of uncoated phosphor in Chapter 5.2.2 already indicated that hydrolysis on the surface of phosphors particles occurred. As the SiO_2 coating procedure was always catalyzed by an acid or a base the surface of phosphor particles was again hydrolyzed during the experiment in a low extent. In general absorption peak intensities increase or decrease compared to uncoated phosphor (see Figure 25). Due to the above mentioned, a decrease of absorption peak intensities for $Ba_2Si_5N_8$ in the finger print area after the coating process can be ascribed to a hydrolyzed surface of phosphor particles. Due to the signals for uncoated (not hydrolyzed) phosphor decreased. This process caused a modification of the phosphors surface, which shall improve the coating of hydrated silica on the phosphors surface due to the increased chemical affinity. Moreover ATR-IR is not an absolute method and shall be used in addition with other characterization methods to obtain information about the layer on phosphor particles. Furthermore it has to be mentioned that the uncoated phosphor should serve as a reference spectrum in terms of absorption peaks, but not in terms of absorption peaks intensities, because the spectrum of uncoated phosphor is not normalized. Following ATR-IR spectra of uncoated phosphor LP-N620 and SiO_2 coated products of all reactions from NM001-NM007 are shown in Figure 25. After the coating process no broad absorption peaks at 3500-3000cm^{-1} (symmetric and asymmetric stretch modes of water) and a peak at 1640cm^{-1} (stretching and bending mode of water) are observed, which indicate residual water.[32]

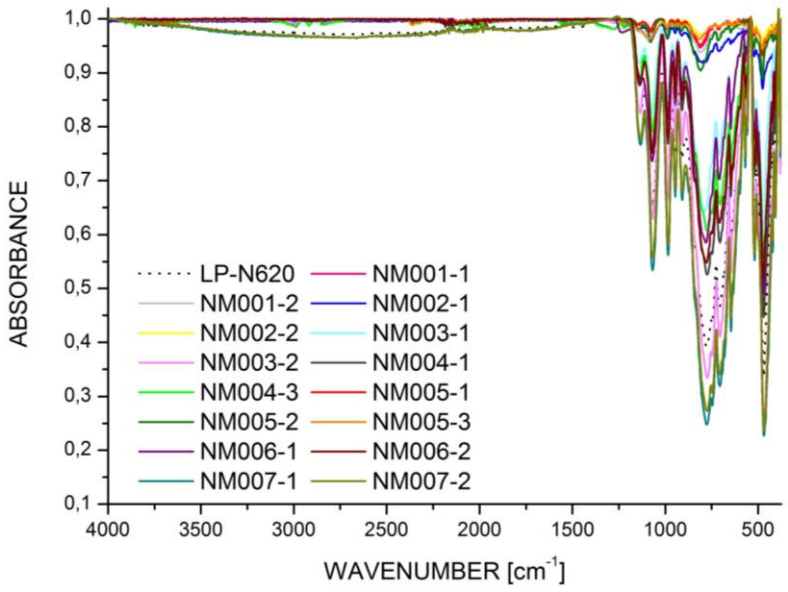

Figure 25: ATR-IR spectra of LP-N620 and NM001-NM007 in the wavenumber range of 4000-375cm^{-1}.

Figure 26 (left and right) show the ATR-IR spectra of all SiO_2 coated samples in the range of 1750-375cm^{-1} compared to uncoated phosphor LP-N620. Following the single spectra of the coated products have to be examined in detail: The spectrum of europium-activated barium silicon nitride ($Ba_2Si_5N_8$) shows no sign for TEOS, but several sharp peaks in the finger print area from 1100cm^{-1} to 380cm^{-1} (see black dotted line). In general no new bands could have been observed. The absorption peaks in spectra NM003-2, NM007-1 and NM007-2 increased, whereby the absorption peak intensities of all other samples decreased. A formation of SiO_2 cannot be confirmed. The absorption bands compared to uncoated phosphor do not change in shape they just increase slightly in intensity or decrease. Unfortunately the ATR-IR spectra do not contain the information if SiO_2 was formed or not, nor the information if a layer of SiO_2 was coated on the phosphor particles. Since coating series NM005-1, NM005-2 and NM005-3 (all acid catalyzed) show significant changes in absorption peak intensities which could stem from hydrated silica of form $SiO_{2-n}(OH)_{2n}$, those samples will be further characterized *via* SEM and EDX.

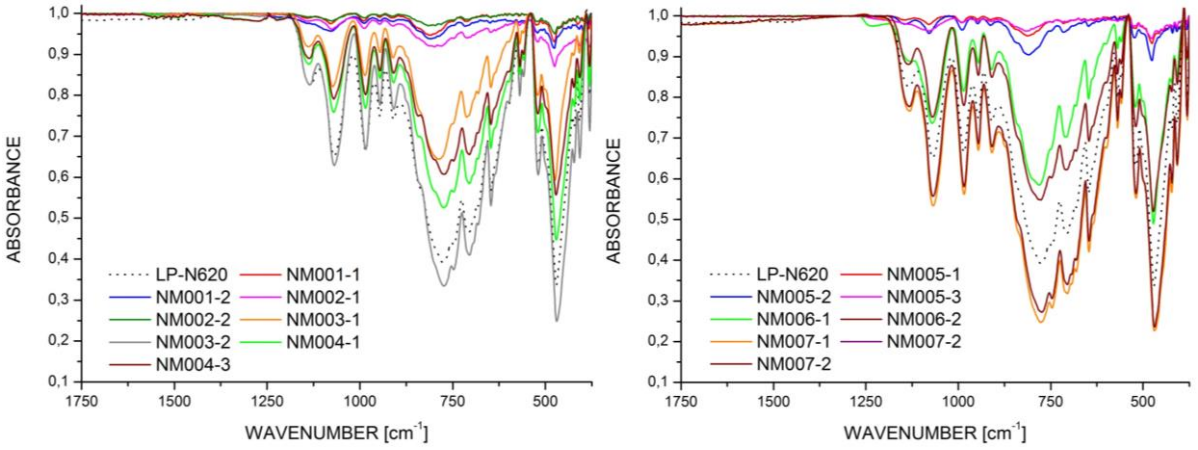

Figure 26: ATR-IR spectra of LP-N620, NM001-NM004 (left) and of LP-N620, NM005-NM007 (right).

The reason for that may be an unsuccessful synthesis: It may be that the catalyst NH_3 and HCl were used in an amount which was insufficient. Therefore the hydrolysis reaction was not catalyzed. It was thus slower than expected to be. Since the first step of the reaction was incomplete the condensation reaction of $Si(OH)_4$ to SiO_2 via hydrated silica was not possible. Furthermore the condensation reaction from orthosilicic acid $Si(OH)_4$ over hydrated silica to yield in SiO_2 was probably not successful because an insufficient reaction temperature. It may be that the used temperature between 18 and 57°C was not adequate for the calcination to drive off the combined H_2O.

SEM SiO_2 coating

Figure 27 shows the SEM images of NM005-2 and NM005-3, both acid catalyzed, but the synthesis was carried out at different temperatures. Figure 27 (left) shows NM005-2 synthesized at 18°C with no clear differences to uncoated phosphor (see Figure 11 and Appendix Chapter 9.3 Table 35), whereby Figure 27 (right) shows a low fine particle fraction, which could stem from SiO_2 particles or of hydrated silica of form $SiO_{2-n}(OH)_{2n}$.

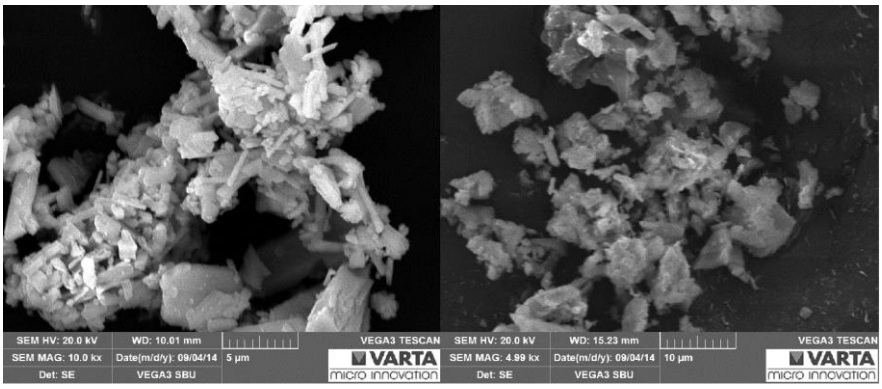

Figure 27: SEM (SE) image of NM005-2 acid catalyzed with a water bath temperature of 18°C and SEM image of NM005-3 acid catalyzed with a water bath temperature of 40°C.

EDX SiO_2 coating

The EDX spectra of NM005-2 and NM005-3 are shown in Figure 28 (left and right). Due to the components of the phosphors host lattice and the SiO_2 coating, a qualitative analysis *via* EDX should exhibit peaks for N, O, Si, Ba and Sr. The qualitative analysis revealed peaks for N, Si, Sr, Ba and Eu as part of the phosphors host lattice and O. If the coating process with SiO_2 would have been successful, peaks for O and Si should increase or be larger in NM005-3 than in NM005-2 according the fine particle fraction in NM005-3. The EDX spectra of NM005-3 show increased peaks for O and Si compared to NM005-2.

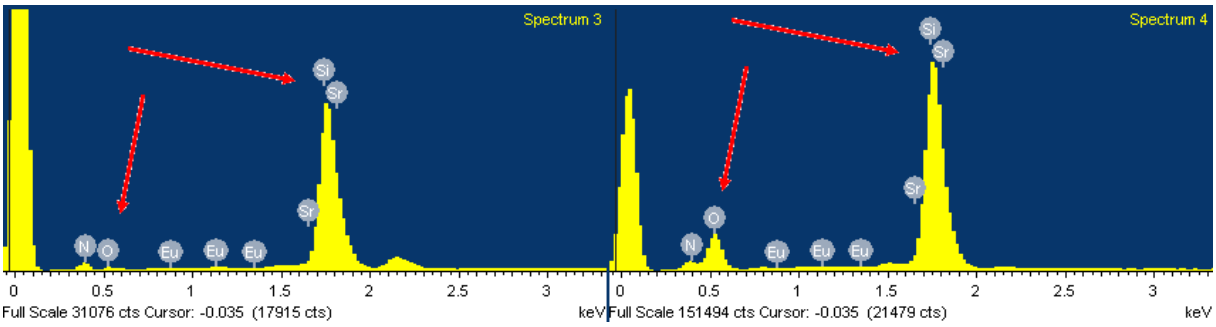

Figure 28: EDX spectrum of acid catalyzed samples NM005-2 (left) with a water bath temperature of 18°C and of NM005-3 (right) with a water bath temperature of 40°C.

Table 16 reveals the elemental distribution in atomic percentage of the coated phosphor NM005-2 and NM005-3. The value for O is larger in NM005-3 with 45% than compared to NM005-2 with 6%. The values for N, Eu, Ba, Sr and Si are smaller in NM005-3 than in NM005-2. This can be explained by the fact that NM005-3 was hydrolyzed more strongly at a temperature of 40°C or it was coated with a thicker layer of hydrated silica. Therefore an increase of signals for Si and O and a decrease of the phosphors host lattice elements occur.

Table 16: Results of EDX quantitative analysis of NM005-2 and NM005-3.

Atomic Percentage [%] of Element	N	O	Si	Sr	Ba	Eu
NM005-2	42	6	36	7	8	1
NM005-3	24	45	25	3	3	0

LUMINESCENCE SiO_2 coating

The results of luminescence measurements in form of emission spectra of coated phosphor sample NM001-NM006 are shown in Figure 29.

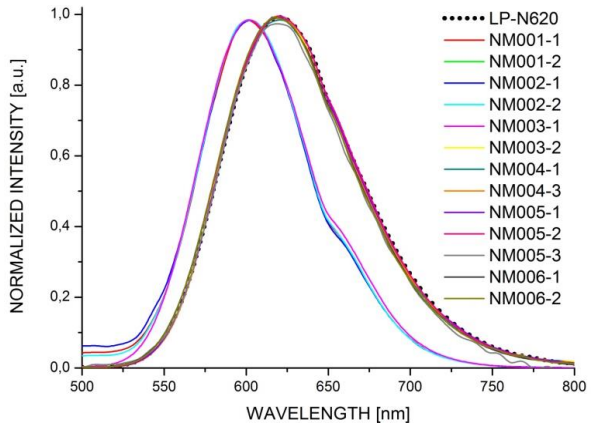

Sample	Emission Maximum [nm]	Catalyst
LP-N620	621	NH_3
NM001-1	601	NH_3
NM001-2	603	NH_3
NM002-1	599	NH_3
NM002-2	603	NH_3
NM003-1	601	NH_3
NM003-2	606	NH_3
NM004-1	622	NH_3
NM004-3	623	HCl
NM005-1	620	HCl
NM005-2	622	HCl
NM005-3	623	HCl
NM006-1	621	NH_3
NM006-2	616	NH_3

Figure 29 and Table 17: Emission spectra of all SiO_2 coated phosphors NM001-NM006 and emission maxima of SiO_2 coated samples.

Figure 30 show again the emission spectra of SiO_2 coated samples. The emission maxima of NM001-1, NM001-2, NM002-2 and NM003-1 shifted to shorter wavelengths at an average of 20nm from 621nm like shown in Table 17, other samples show a negligible shift of the emission maxima to shorter (-5nm) or to longer (+2nm) wavelength.

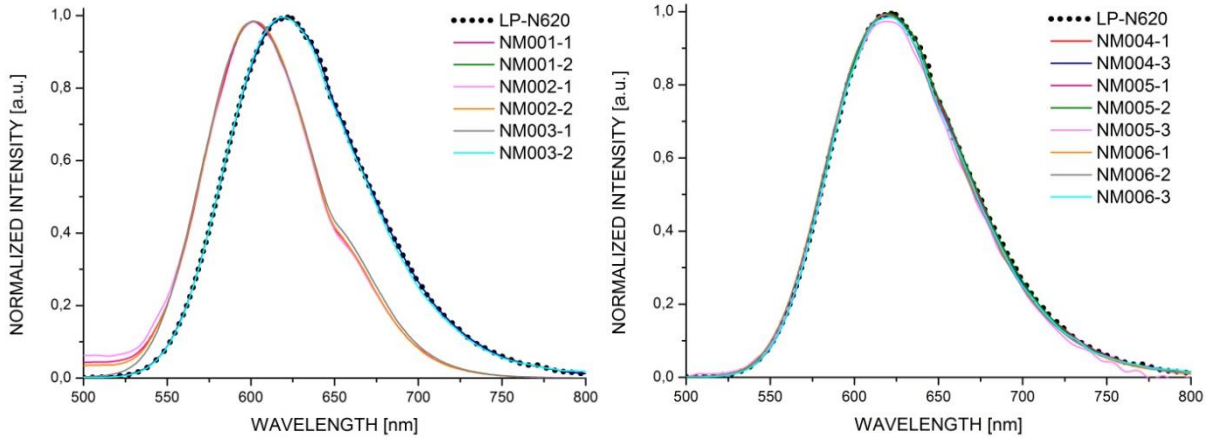

Figure 30: Emission spectra of NM001-NM003 (left) and NM004-NM006 (right).

The shift of the emission maxima tends to be caused by the used catalyst for hydrolysis of TEOS. A shift to lower wavelength is observed when HCl was used as a catalyst (see Table 17), whereby the emission maximum of NH_3 catalyzed products shifted negligible. The shift of the emission maxima of 20nm goes along with a change of the CIE color coordinates. A color shift in that extent is unusable and not acceptable for use in LED applications. As it is not clear from ATR-IR spectra if small amounts of SiO_2 or hydrated silica were formed, another synthesis route and consequently another inorganic layer should be tested. Due to the unsatisfactory results of ATR-IR, SEM, EDX and luminescence measurements further experiments on SiO_2 coating by a modified Stöber synthesis[25] were discontinued.

6.1.2 Results: Al_2O_3 Coating

According to Equation 6 the precipitation reaction of $Al(NO_3)_3 \cdot 9H_2O$ with $NaHCO_3$ as a precipitation agent leads to the formation of $Al(OH)_3$. 2mole of $Al(NO_3)_3 \cdot 9H_2O$ yield in 2mole of $Al(OH)_3$ and after the annealing procedure 1mole of Al_2O_3 is formed. Theoretically a stoichiometric ratio of 2:1 equal $Al(NO_3)_3 \cdot 9H_2O$:$NaHCO_3$ is necessary for the complete precipitation.

$$2Al(NO_3)_3 \cdot 9H_2O + NaHCO_3 \rightarrow 2Al(OH)_3 + side\ products \xrightarrow{\Delta T} Al_2O_3 + 3H_2O \uparrow_{vap}$$

Equation 6: Chemical equation of the precipitation reaction of aluminum hydroxide and further formation of aluminum oxide after annealing.

After annealing at 400°C a decrease of weight due to formation of H_2O is expected. Also an increase of weight of the obtained product (phosphor particles and layer) should be recorded after the coating process in accordance with the calculation shown in Table 18, as shown here for the synthesis of NM029.

Table 18: Sample weight of precursors for Al_2O_3 synthesis and weight of products after synthesis as well as after the annealing process based on NM029.

	Material	M [g/mol]	m [mg]	Mole Ratio	n [mmol]
	$CaAlSiN_3$	137.1651	1004	-	-
	$Al(NO_3)_3 \cdot 9H_2O$	375.1338	828	1	2.4
Educts	$NaHCO_3$	84.0066	555	2.8	6.6
Intermediate	$Al(OH)_3$	78.0036	183	-	2.4
Product	Al_2O_3	101.9613	119	-	1.2
Product	$CaAlSiN_3 + Al_2O_3$	-	1123	-	-

Work up of Al_2O_3 single coating

The suspension of coated $Ba_2Si_5N_8$ product (synthesis NM009-3 to NM0012-4) was transferred in a Schlenk flask to have a look at the process of sedimentation as shown in Figure 31 (NM010-3, A). The liquid phase was colorless, whereby the precipitated aluminum hydroxide was orange colored due to the phosphors color. The precipitate was further centrifuged to separate it from the liquid phase. Figure 31 (B) shows the product NM010-3 after centrifugation. In general all products (coated $Ba_2Si_5N_8$) showed a phase separation after centrifugation: Particles with higher density migrated outward due to their higher mass inertia. At the same time particles with lower density were forced out and stayed above the higher density particles. Here the larger and heavier phosphor particles (see Figure 31, B, dark orange) were separated from the lighter precipitated aluminum hydroxide in which the fines of phosphor particles (light orange, assumption Ø of x ≤ 1µm) were embedded. This can be explained by the large particle size distribution of LP-N620 like shown before in the SEM image in Figure 11. In consideration of the observation of centrifugation results, it was decided to try the same coating procedure on phosphor particles with more uniform particle size and narrower particle size distribution. For the above mentioned reason TRIDONIC Jennersdorf GmbH provided a new red emitting silicon nitride phosphor named BR-101H for further studies (see characterization of BR-101H in Chapter 5.2.2). Figure 31 (C) shows the centrifuged product of phosphor particles synthesis NM011 of coated $CaAlSiN_3$. The centrifugation of NM011 led to a complete separation of phosphor particles and precipitated aluminum hydroxide (see Figure 31, C).

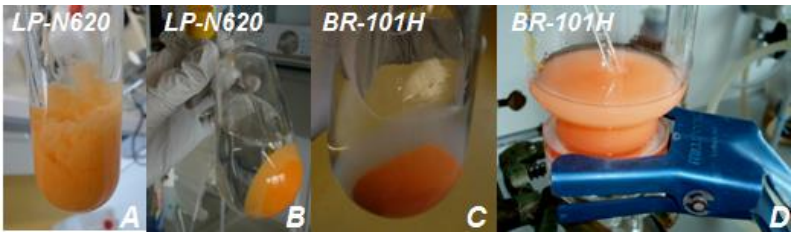

Figure 31: Product NM010-3 after sedimentation (A), NM012-2 (B), NM011 (C) after centrifugation and NM032 while filtration (D).

The result can be explained by the fact that the BR-101H phosphors particle has a more uniform particle size and a more narrow particle size distribution, but the particles size itself is bigger than in LP-N620. Unfortunately the above mentioned considerations have not achieved the desired result: Based on these results centrifugation as the separation method of choice was reconsidered, as an alternative filtration was carried out. Products from NM0029 to US03 were vacuum filtrated *via* a frit and additional with cellulosic filters for hydrophilic solutions with pore sizes of Ø 0.45µm, to be sure that particles do not pass the filter and not to lose product. The filtration was a time consuming step, sometimes taking 2h or even over night, due to blocking of filter pores. In general the working up procedure of the product after synthesis caused a few problems, due to this an accurate documentation of gain in weight was not possible. The majority of losses had to be recorded on the walls of the reaction vessel made out of Teflon, on the blades of the paddle mixer and on the filter paper. After successful annealing of $Al(OH)_3$, 3mole H_2O manifested as a percentage of theoretical 35wt% should be calcinated by temperature treatment (see calculation Table 18). After the coating process the color of unexcited particles changes from orange to brighter turbid orange, this can be ascribed to an optically not absolutely transparent layer of Al_2O_3.

ATR-IR Al_2O_3 single coating

According to Murphy et al.[20] the precipitated product aluminum hydroxide should be annealed at 400°C to form aluminum oxide. This step was verified via ATR-IR measurements in 100°C steps starting from 100°C to observe the increasing an decreasing of absorption bands and the formation of new bands. After an annealing temperature of 700°C the phosphors changed its color noticeable (see color faint in Figure 32, left) from orange over dark yellow to mossy green. By excitation with a conventional blue LED its luminescence behavior was inspected. The dark yellow powders showed decreased luminescence behavior, whereby the mossy green powder did not show any (Figure 32, right).

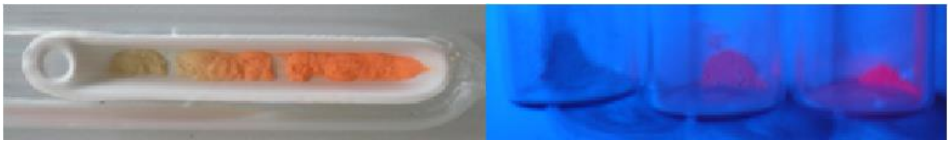

Figure 32: NM013 after annealing at 700°C unexcited (left) and after excitation via conventional blue LED (right).

Based on these results from temperature treatment a temperature above 700°C caused serious damage in terms of the phosphors luminescence behavior: The coated phosphor is limited to temperatures below 700°C. Due to these results it can be assumed that the activator ion Eu^{2+} was oxidized to Eu^{3+} or the phosphors host lattice was oxidized. The phosphors luminescence behavior is not only reliant on the activator ion but also from

the host lattice. Figure 33 (left) shows the obtained ATR-IR spectra of NM013 after temperature treatment from 100°C up to 700°C in the range of 4000-375cm^{-1}. No new absorption bands are observed only a decrease and increase of absorption bands of the coated phosphor compared to uncoated phosphor are indicated.

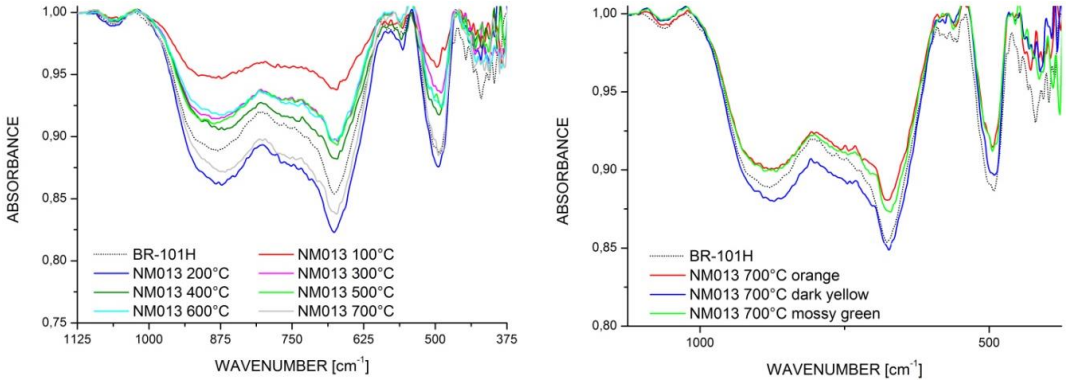

Figure 33: ATR-IR spectra of NM013 annealed at temperatures from 100°C up to 700°C and ATR-IR spectra of orange, dark yellow and mossy green samples in the range of 1125-375cm^{-1} (right).

Figure 33 (right) shows the ATR-IR spectra of NM013 annealed at 700°C of the orange, the dark yellow and the mossy green sample. The spectra show no serious changes in absorption peaks. Due to this result it can be said that the phosphors host lattice did not suffer from the temperature treatment and decomposition did not occur in a great extent, only the surface was affected. The mossy green sample showed no luminescence compared to uncoated phosphor. On the basis of the results from ATR-IR measurements and as described in literature an annealing temperature of 400°C for further annealing experiments was selected. Al_2O_3 (γ-modificiation) is formed by carefully heating of $Al(OH)_3$ (γ-modification known as hydrargillite) up to 400°C according as shown in Equation 7: [40]

$$2\,\gamma - Al(OH)_3 \xrightarrow[\gamma - AlO(OH)]{400°C} \gamma - Al_2O_3 + H_2O$$

Equation 7: Formation of γ-Al_2O_3 by carefully heating of γ-$Al(OH)_3$ up to 400°C.[40]

SEM Al_2O_3 single coating

Figure 34 shows SEM images of uncoated BR-101H (left), NM011 (mid) and NM013 (right). In general the shape of particles did not change, but the image indicates that the particles in NM011 as well as NM013 are surrounded in parts by a fine particle fraction. Besides that the electrical conductivity of the coated phosphor particles decreased due to the coating process indicated by blurry images. In Figure 34 (mid) agglomerates of NM011 particles are shown (see red circle).

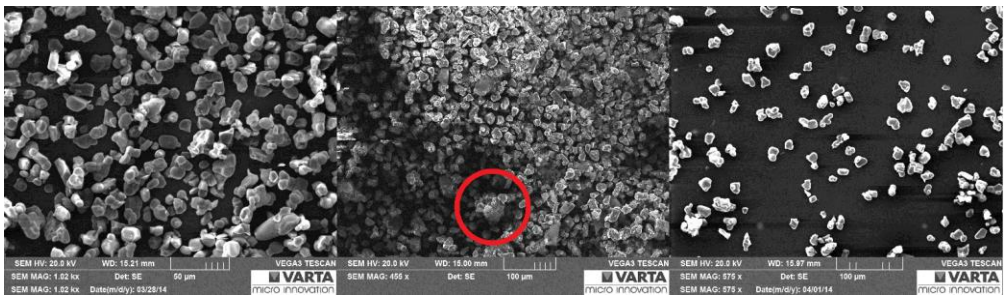

Figure 34: SEM image of uncoated BR-101H (left), NM011 (mid) and NM013 (right).

EDX Al_2O_3 single coating

Figure 35 shows the SEM image of the selected area for EDX analysis of sample NM011 in the left upper corner. The EDX analysis revealed following elemental distribution for the elements C, N, O, Al, Si, Ca, Cu and Au (highlighted in color). The upper row shows the elements of the sample holders foil and glue (C, O) and the conductivity additive (Au). It has to be mentioned that no signal for O stems from the glue on the sample foil, because the highlighted color is congruent with the particles. In the lower row elements of the phosphors host lattice and the coating layer are shown. The images suggest that the precipitation of Al_2O_3 was successful due to the observed elemental distribution for O and Al, which are unambiguously on the phosphors particles (see electron image in Figure 35, left corner).

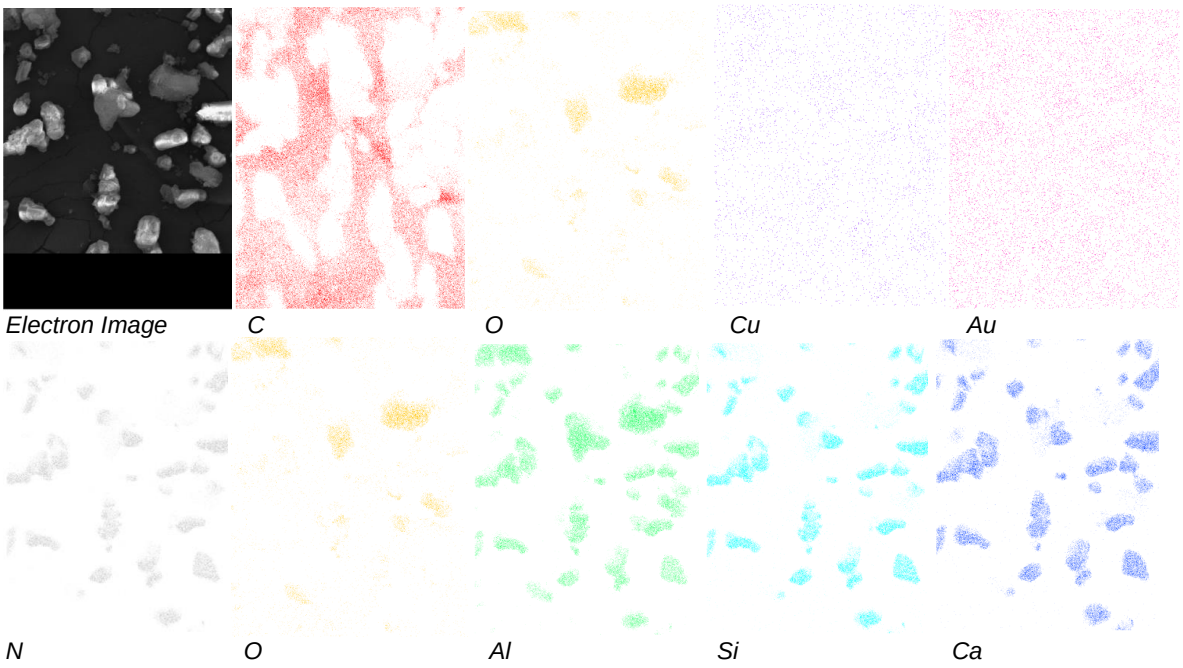

Figure 35: SEM (BSE) image of NM011 in mapping mode (EDX) with the elements C, N, O, Al, Si, Ca, Cu and Au (highlighted in color).

The EDX spectrum of NM013 (left) and the corresponding results of the elemental distribution on the coated particles are shown in Figure 36 (see Table 19, right). The EDX spectrum of a chosen particle from sample NM013 (excluded C, Cu and Au, signals stem from glue and sample preparation) show the usual signals for the host lattice of N, Al, Si and Ca, but also peaks for Na, O and P (see Table19). This can be explained by the fact that tetrasodium pyrophosphate decahydrate was used as a dispersing agent. Its task is to maximize dispersion of phosphor particles in the suspension during synthesis to avoid the formation of agglomerates. This suggests that the interaction between particles and dispersing agent was stronger than the interaction of particles and precipitated aluminum hydroxide. In case of NM011, where 1–octanol was used a dispersant, a qualitative EDX analysis is not convincing due to the fact that signals for C and O are also coming from the sample preparation. This does not exclude the possibility that 1-octanol was bound on the particles and (with a boiling point of 195°C) then was evaporated trough the temperature treatment at 200°C in all or part of. The chemical structural formulas of 1-octanol and tetrasodium pyrophosphate decahydrate are shown in Figure 37.

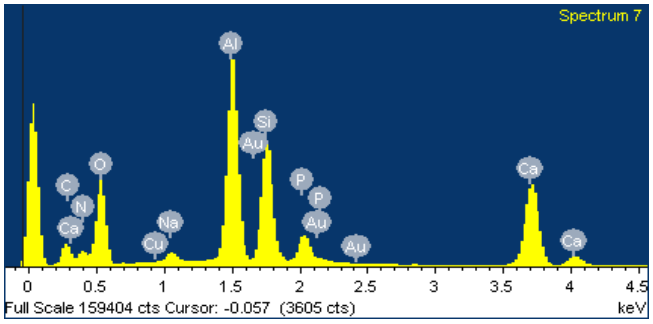

Element	Atomic Percentage [%]
C	-
N	11
O	58
Na	1
Al	13
Si	9
P	2
Ca	6
Cu	-
Au	-

Figure 36 and Table 19: EDX spectrum of NM013 (left) with the values for atomic percentages of the coated particles (right).

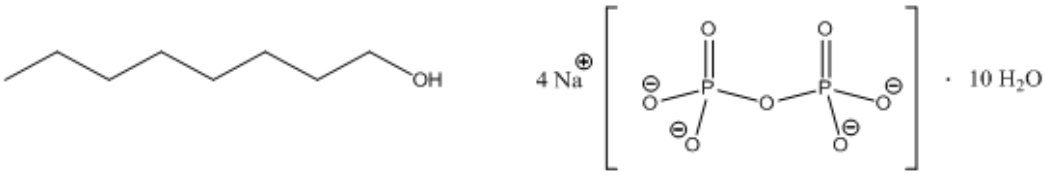

Figure 37: Structural formula of dispersing agent 1-octanol and tetrasodium pyrophosphate decahydrate.

Due to the proof of dispersing agent on phosphor particles after the coating and the annealing process through EDX analysis the use of 1-octanol and tetrasodium pyrophosphate decahydrate was stopped.

LUMINESCENCE single coating

In following Figure 38 (left) the emission spectra of uncoated BR-101H, NM011 and NM013 are shown. The shape of the emission band did not changed in general. Moreover a color shift to shorter or longer wavelengths did not occurr. The maximum of the emission wavelength of coated NM011 shifts slightly from 643nm of uncoated phosphor to 644nm. Despite the temperature treatment at 700°C the emission maximum of NM013 remains the same at 643nm.

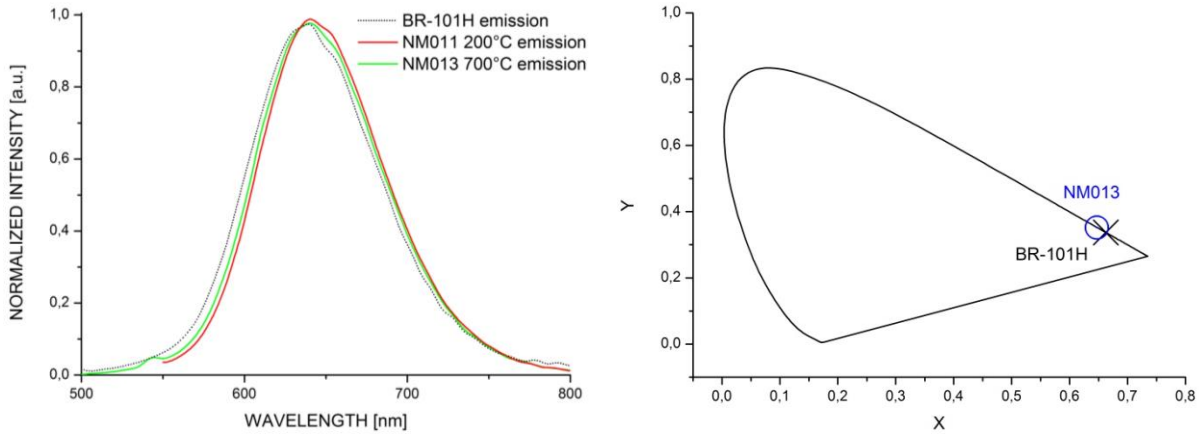

Figure 38: Emission spectra of BR-101H, NM011 and NM013 and CIE color coordinate diagram of BR-101H and NM013.

The calculation of quantum efficiencies led to following results shown in Table 20. The quantum efficiency of NM013 decreased only for 7% compared to uncoated phosphor. The CIE diagram with color coordinates for the samples is shown in Figure 38 (right). CIE color coordinates for NM013 shifted (-0.016x and -0.015y). The result for NM011 with 115%

quantum efficiency and color coordinates outside the CIE with x 0.690 and y 0.340 has to be declared as wrong, due to a not assignable measurement error.

Table 20: Results of luminescence measurements of sample NM011 and NM013

Sample	Quantum Efficiency [%]	CIE Color Coordinate x	CIE Color Coordinate y
BR-101H	75	0.663	0.337
NM013	70	0.647	0.352

ATR-IR Al_2O_3 triple coating

The ATR-IR spectra of uncoated BR-101H and coated phosphor NM029, NM032, NM033 and NM034 after coating process number 1, 2 as well as 3 after drying at 100°C (left) and after the annealing process at 400°C (right) are shown in Figure 39. The spectrum of uncoated europium-activated calcium aluminum silicon nitride shows several sharp peaks in the finger print area from 800cm^{-1} to 400cm^{-1}. One trend can be observed in this wavelength range: Compared to the uncoated phosphor the intensities are decreasing due to the hydrolysis of uncoated phosphor through water and the formation of hydrolysis products during the coating process (insignificant on phosphor particle surface). The results from acid-base study of uncoated phosphor in Chapter 5.2.2 indicated that hydrolysis on the surface of phosphors particles occurred (see and compare also Chapter 6.1.2 headline Al_2O_3 ATR-IR single coating). As the Al_2O_3 coating procedure was always carried out with aqueous educts solution particles were hydrolyzed during the experiment in a low extent. Due to the above mentioned a decrease of absorption peak intensities for Ca_3N_2, AlN and Si_3N_4 in the finger print area after the coating process can be ascribed to a hydrolyzed surface of phosphor particles. Due to this signals for uncoated (not hydrolyzed) phosphor are bigger. This process caused a modification of the phosphors surface, which shall improve the coating of $Al(OH)_3$ on the phosphors surface due to the increased chemical affinity. Moreover ATR-IR is not an absolute method and shall be used in addition with other characterization methods to obtain information about the layer on phosphor particles. Furthermore it has to be mentioned that the uncoated phosphor should serve as a reference spectrum in terms of absorption peaks, but not in terms of absorption peaks intensities, because the spectrum of uncoated phosphor is not normalized. Figure 39 (left) shows the spectra of the samples dried at 100°C, which show new absorption peaks marked with red arrows: One broad absorption peak at 3400cm^{-1} and two (overlapped) peaks at 1400cm^{-1} and 1360cm^{-1}. The broad absorption peak at 3400cm^{-1} can be assigned to the symmetric and asymmetric stretch modes of water $\tilde{\nu}$[O–H].[32] The absorption peak at 1400cm^{-1} as well as 1360cm^{-1} can be dedicated to the bending vibration of the $\tilde{\nu}$[O–H] bond in $Al(OH)_3$, not to residual moisture.[32] These absorption peaks decreases after annealing at 400°C due to the formation of Al_2O_3 from $Al(OH)_3$ (see Figure 40, right). The formation of Al_2O_3 from $Al(OH)_3$ after treatment at 400°C can be further confirmed due to the lack of signal in the area around 3400cm^{-1} (see Figure 39, left) and new signals at around 1400cm^{-1}, 1360cm^{-1}, 1200cm^{-1} and 1150cm^{-1} (see arrows in Figure 39 and Figure 40). By comparing the weight of sample NM029 after drying at 100°C and 400°C a loss of weight of around 13% was observed. This loss of weight can be ascribed to the formation of H_2O besides Al_2O_3 (calcination of H_2O).

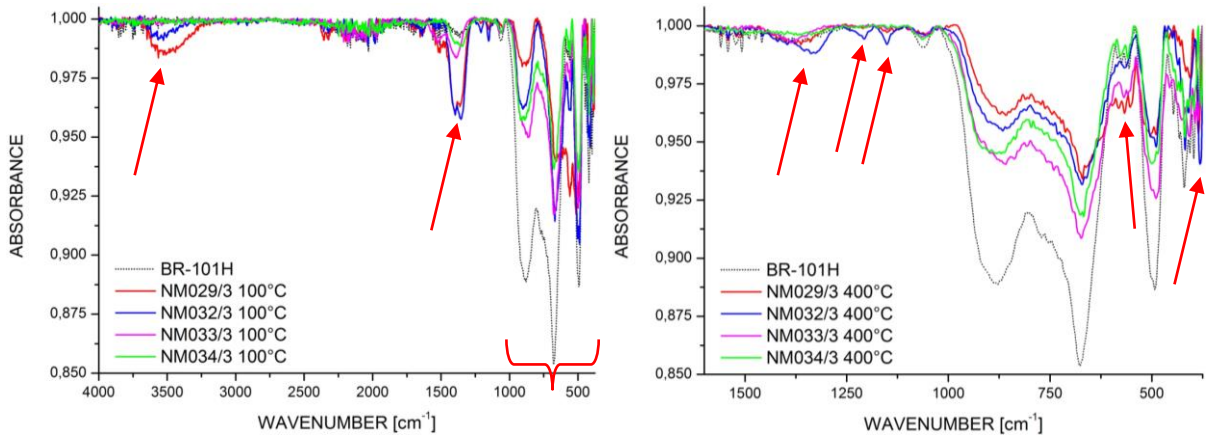

Figure 39: ATR-IR spectra of uncoated BR-101H, NM029, NM032, NM033 and NM034 coating number 3 after drying at 100°C (left) in the range of 4000-375cm^{-1} and at 400°C (right) in the range of 1600-375cm^{-1}.

The new signals at around 1350cm^{-1}, 1200cm^{-1} and 1150cm^{-1} (see arrows in Figure 39, right) are characteristic absorption bands of Al_2O_3.[32] The increase of absorption peak intensities in the area between 590cm^{-1} and 375cm^{-1} is attributed to $\tilde{\nu}$[Al–O] or $\tilde{\nu}$[Al–O–Al] stretching in Al_2O_3 at 570cm^{-1}, 460cm^{-1} and 380cm^{-1}.[32] Due to these results the formation of Al_2O_3 can be confirmed. Mayor changes in absorption peak intensities in the range of 1500-100cm^{-1} can be seen in sample NM032 dried at 100°C as well as annealed at 400°C. In conclusion can be said that samples NM033 and NM034 has been coated with Al_2O_3 in lower extent compared to NM029 and NM032, since insignificant changes of peak intensities at 1200cm^{-1} and 1150cm^{-1} occurred. All significant absorption peaks of Al_2O_3 in the range between 1600cm^{-1} and 375cm^{-1} are shown in Table 21 below.

Table 21: Ascribed absorption peaks of uncoated phosphor and coated phosphor samples NM029, NM032, NM033 and NM034 annealed at 400°C with following legend: increase (i), decrease (d), none (n), no change (n.c.) and stretching modes (s.m.) compared to uncoated phosphor (see Figure 39, left and right).

$\tilde{\nu}$ [cm^{-1}]	BR-101H	NM029	NM032	NM033	NM034	Ascribed Absorption Band of Al_2O_3
	1362	1360 (i)	1330 (i)	1385 (n.c.)	1362 (d)	$\tilde{\nu}$[Al–O] *(s.m.)*
	(n) at 1210	1206 (n.c.)	1206 (i)	(n) at 1210	(n) at 1210	$\tilde{\nu}$[Al–O] *(s.m.)*
	(n) at 1150	1150 (i)	1150 (i)	(n) at 1150	(n) at 1150	$\tilde{\nu}$[Al–O] *(s.m.)*
	555	560 (i)	570 (n.c.)	568 (i)	556 (n.c.)	$\tilde{\nu}$[Al–O] or $\tilde{\nu}$[Al–O–Al] *(s.m.)*
	387	385(i)	381(i)	385(i)	378(i)	$\tilde{\nu}$[Al–O] or $\tilde{\nu}$[Al–O–Al] *(s.m.)*

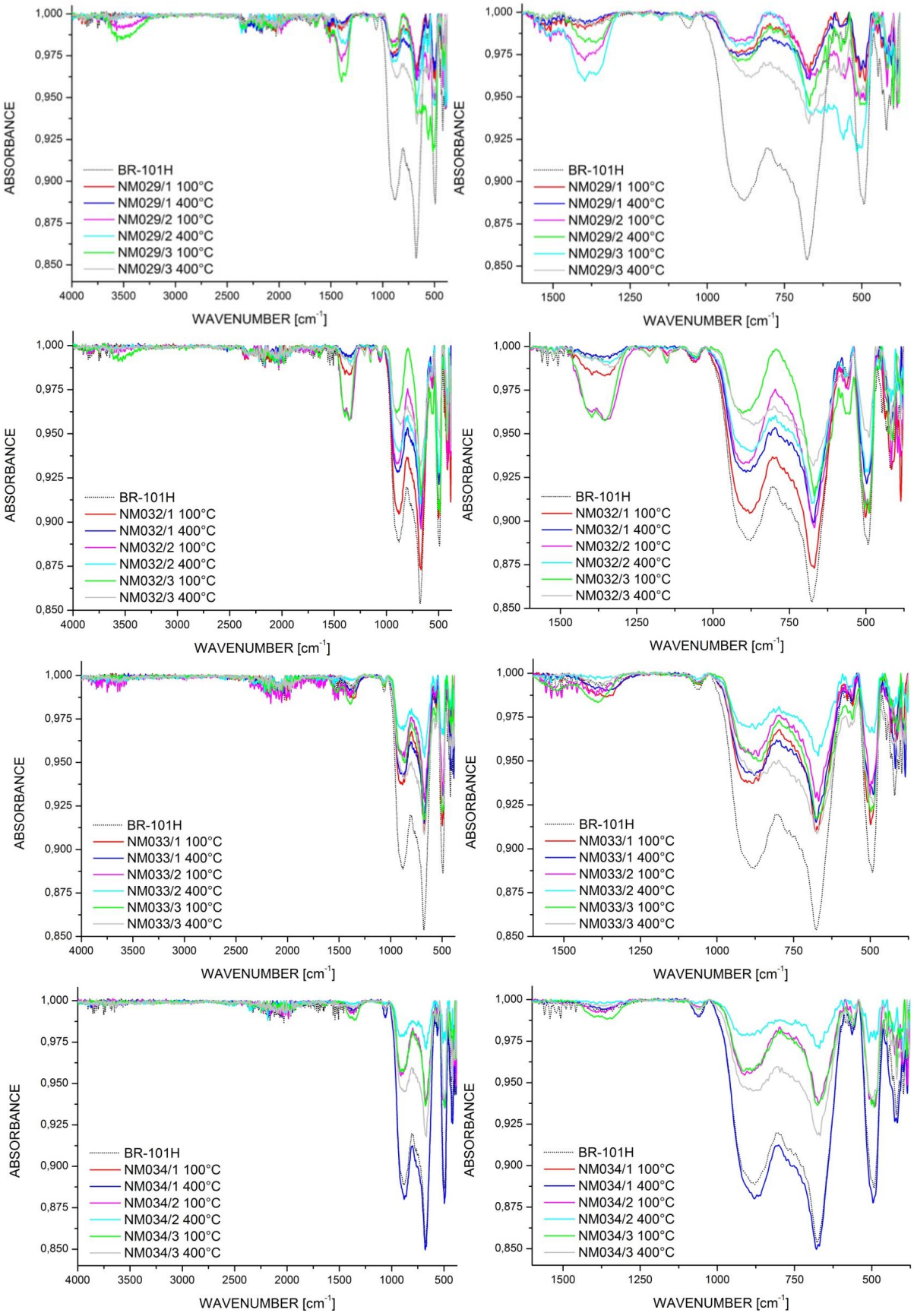

Figure 40: ATR-IR spectra of uncoated BR-101H, NM029, NM032, NM033 and NM034 coating 1, 2 and 3 after drying at 100°C (left) and after the annealing process at 400°C (right) in the range of 4000-375cm^{-1}.

XRD Al_2O_3 triple coating

The XRD pattern of NM029 annealed at 400°C (see Figure 41, right) shows no significant peak changes compared to uncoated phosphor BR-101H (see Figure 41, left).

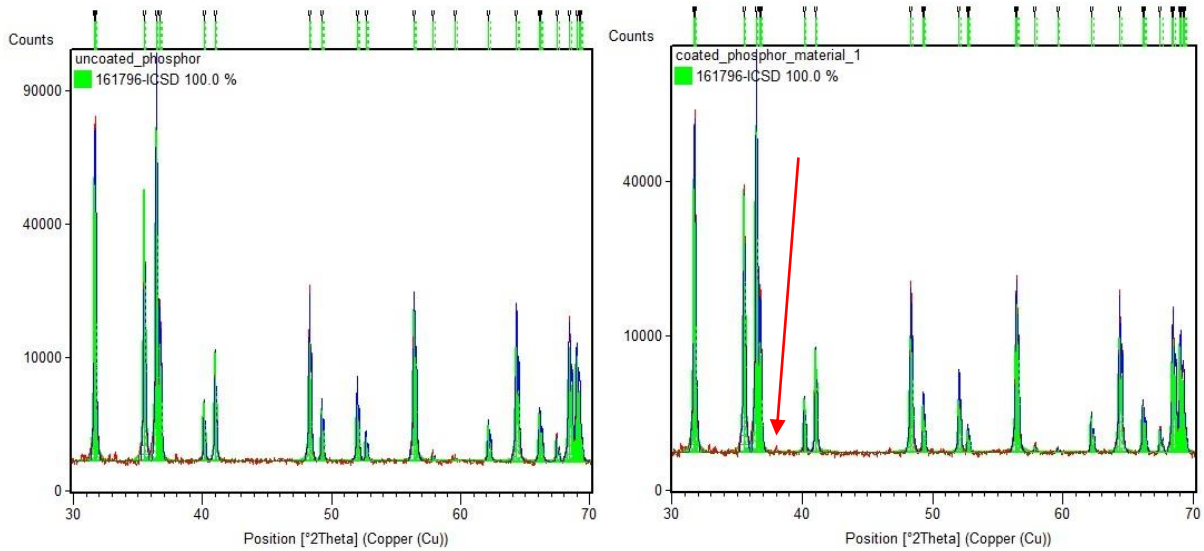

Figure 41: Powder diffractogram of uncoated BR-101H (left) and NM029 after annealing at 400°C (right).

Lattice parameters did not change in general (Table 22). Therefore it can be said that the coating process did not change the host lattice and so educts react with each other, but not with the phosphor.

Table 22: Lattice parameters of uncoated phosphor BR-101H and NM029.

	BR-101H	NM029
space group	$Cmc2_1$	$Cmc2_1$
a [Å]	9.7917	9.7927
b [Å]	5.6461	5.6465
c [Å]	5.0579	5.0588
V [Å3]	279.621	279.726
α=β=γ	90°	90°

The XRD pattern shows no proof for the complete formation of crystalline Al_2O_3 from $Al(OH)_3$ after the annealing process (Figure 41). Only a very small peak at 38° 2θ (see red arrow) indicates the presence of less than 0.5% crystalline Al_2O_3 (ICSD 75479). Therefore it can be concluded that the obtained coating layer is of amorphous nature. Also an increased background indicates amorphous parts, which was taken into account via a background correction.

SEM Al_2O_3 triple coating

Figure 42 reveals a material contrast image of the fabricated cross section of Al_2O_3 coated phosphor NM029, NM032 and NM033, caused by backscattered electrons. Since heavy elements (high atomic number like Ca, Eu) backscatter electrons more strongly than light elements (low atomic number like O or Al), and thus appear brighter in the image. Therefore, the brighter areas in Figure 42 can be ascribed to the $CaAlSiN_3$ phosphor and the darker areas to the Al_2O_3 coating and the dark background to the epoxy resin matrix.

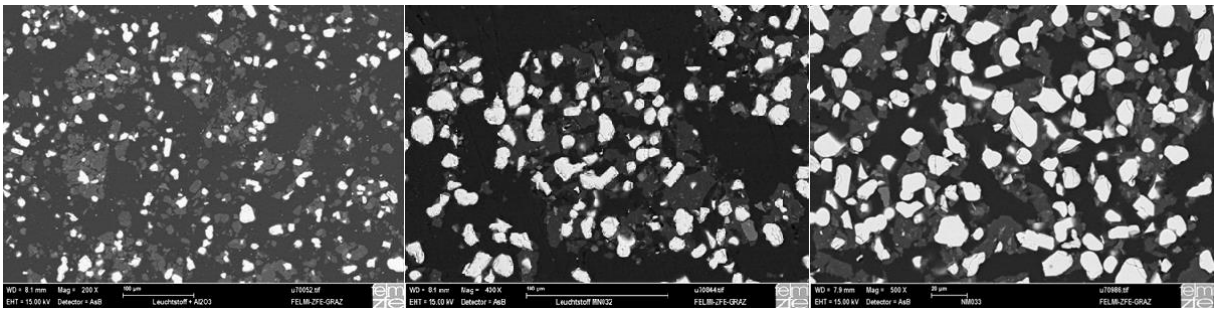

Figure 42: SEM material contrast image (BSE) of cross sections of NM029 (left), NM032 (mid) and NM033 (right).

Figure 43 shows a material contrast image of a single coated phosphor grain of NM029. The determined elements are dyed in different colors and labeled in the upper right corner of the pictures. N (dark green), Al (yellow), Si (magenta) and Ca (green) are found in the brighter areas. O (blue) and Al (yellow) are also found in the darker areas around the brighter areas (phosphor), according to the formation of an Al_2O_3 layer after annealing.

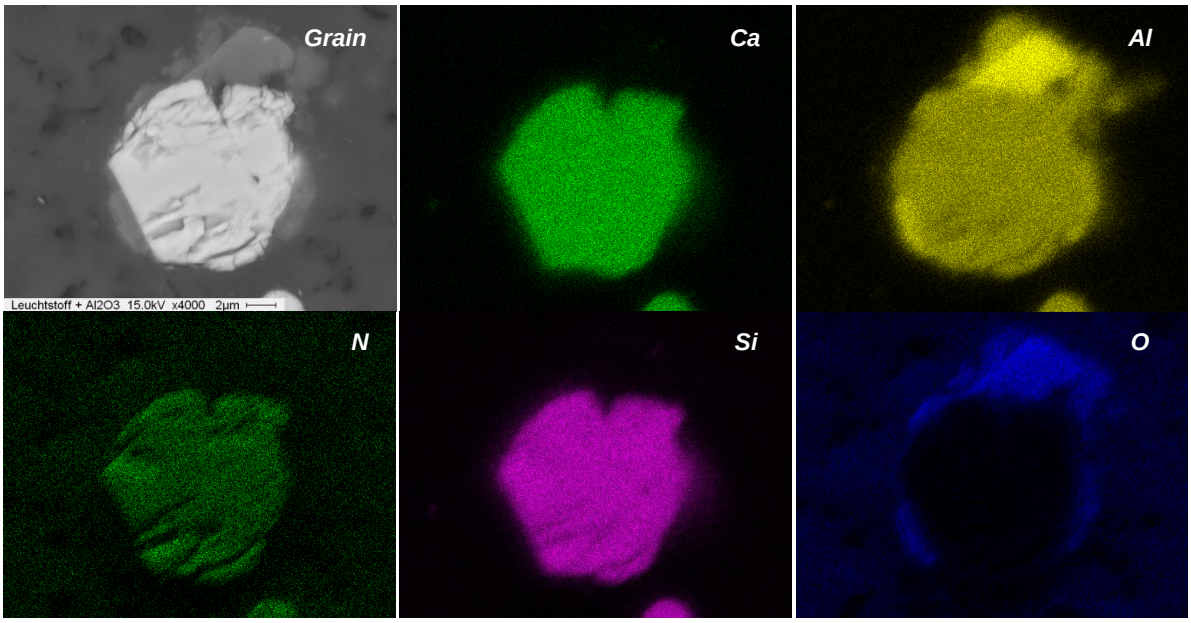

Figure 43: Coated phosphor grain SEM (BSE) image of NM029 with the determined elements highlighted in color.

In contrast to NM029 no completely intact layer of Al_2O_3 was observed on NM032 and NM033 (see Figure 44). The phosphor particles in NM032 and NM033 seem to be embedded in matrix of Al_2O_3, instead of being coated by a thin layer of Al_2O_3.

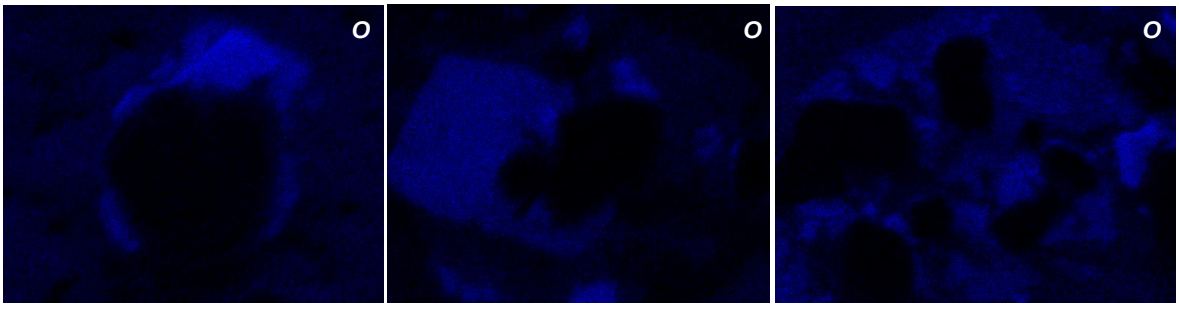

Figure 44: SEM (BSE) image of coated phosphor grains of sample NM029, NM032 and NM033 (blue areas indicate oxygen).

Figure 44 (left) shows an almost intact Al_2O_3 coating layer of a single particle with an irregular layer thickness up to 4µm. The formation of different Al_2O_3 modifications was caused by the reaction conditions. The synthesis of Al_2O_3 coating on the phosphor was done in excess of educts $Al(NO_3)_3 \cdot 9H_2O$ and $NaHCO_3$. Agglomerates are formed when attractive forces overwhelm repulsive forces. The formation of agglomerates can be prevented by changing the reaction conditions of the synthesis like concentration of educts more specifically ion concentration and temperature. In general with larger magnification no homogeneous coating with Al_2O_3 on phosphor particles can be observed (Figure 44). In Figure 45 (NM032, mid) phosphor particles with an inhomogeneous coating can be observed thereby showing two different types of Al_2O_3, one with agglomerates (Area 2) and one with single particles (Area 3). Beside that particles and agglomerates of Al_2O_3 are indicated.

EDX Al_2O_3 triple coating

Figure 45 shows the SEM material contrast images of a cross section of sample NM029, NM032 and NM033. Table 23 shows the obtained EDX spectra of NM029, NM032 and NM033, particular elements of the phosphors host lattice show significant peaks of N, Al, Si and Ca (see Area 1). Coated phosphor particles in NM029 were obtained at high temperatures, high concentration of educts solutions and short reaction time. In NM032 coated phosphor particles were obtained at lower concentrations, longer reaction time and in NM033 at lower concentrations and lower temperatures compared to NM029.

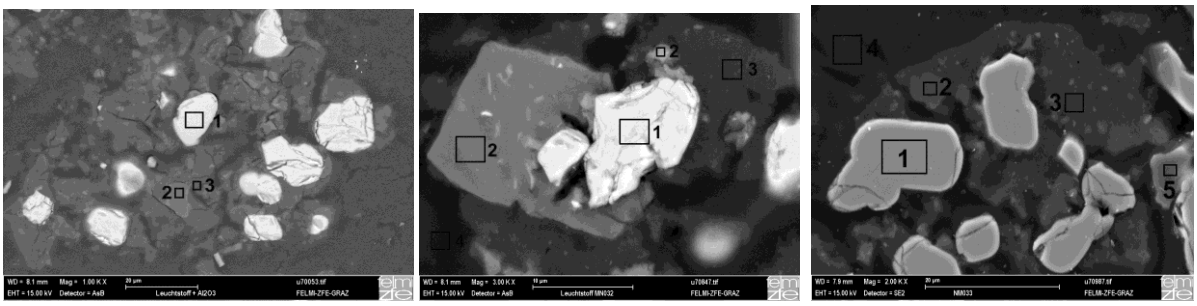

Figure 45: SEM (BSE) material contrast images of NM29, NM032 and NM033.

In general the EDX spectra of NM029, NM032 and NM033 do not differ in their intensities. Peaks of O and C can be assigned to the epoxy resin matrix shown in all 4 areas (see spectra in Table 23). Noticeable changes are observed in peak intensities of the elements like shown in Table 23 of Area 2 and Area 3: The peak for Si and Ca vanishes almost entirely, whereas the peak for O increases due to the formation of Al_2O_3 after the coating and annealing process. In Area 3 both epoxy resin and Al_2O_3 are coexistent. Area 2 and Area 3 have similar spectra: They only differ in agglomeration of Al_2O_3. Area 3 contains more epoxy resin less Al_2O_3, Area 2 more Al_2O_3. Furthermore NM033 shows an abnormal peak for Na (interference with Zn and Pm) and NM029 shows a small peak for S (interference with Mo, Tl and Pb) and Cl (interference with Rh), none of them can be ascribed and clarified.

	Area 1	Area 2	Area 3	Area 4
NM029	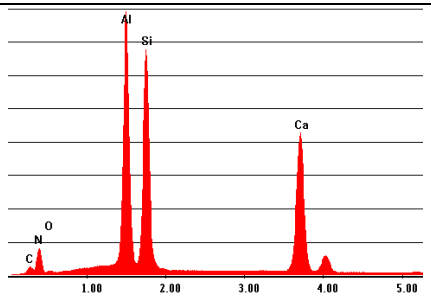	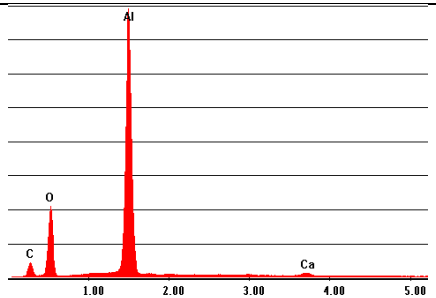	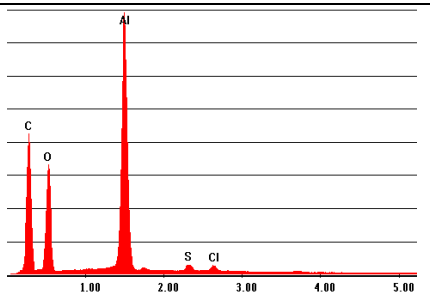	-
NM032	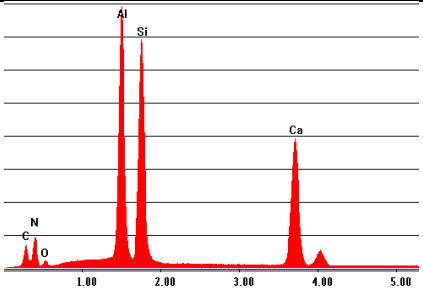	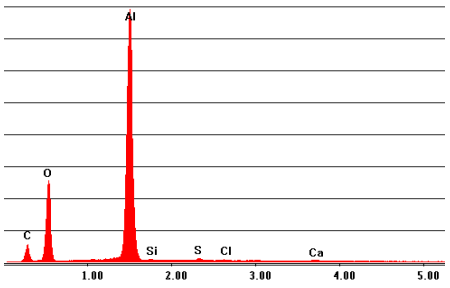	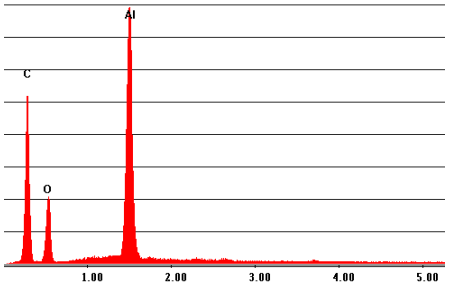	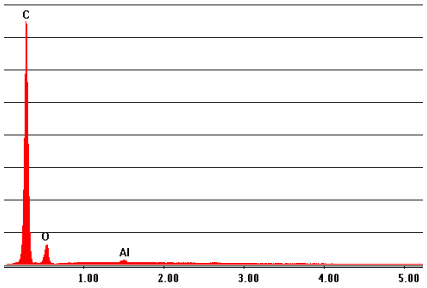
NM033	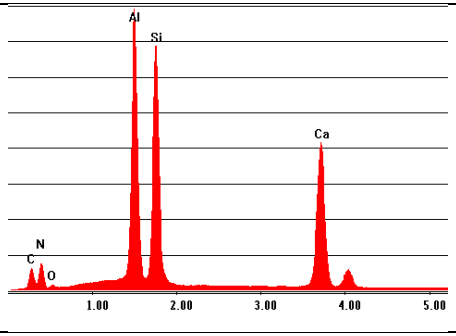	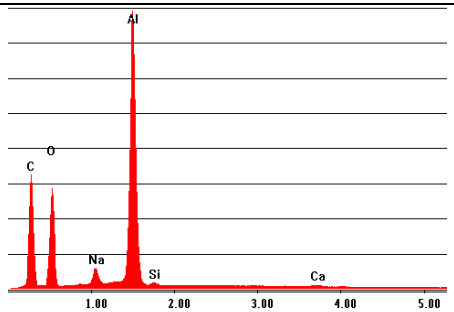	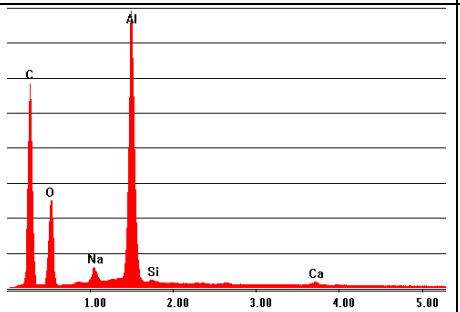	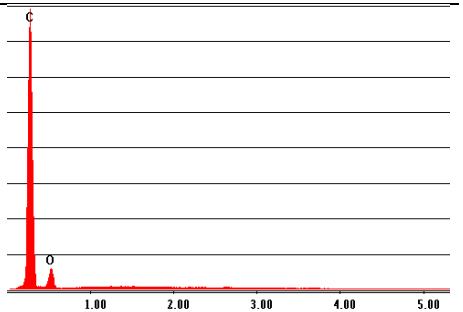

Table 23: EDX spectra of NM029, NM032 and NM033 of the different selected areas (see Figure 45 for location of Area 1,2,3 and 4).

SEM-Focused Ion Beam (FEM) Al_2O_3 triple coating

Images of NM029 and NM032 were recorded via SEM-Focused Ion Beam microscopy, to obtain information about the topography of coated phosphor particles. Figure 46 shows images of NM029 starting in the left upper corner with lowest magnification from left to right and from the top to the bottom with increasing magnification. The images in the first row show particles of irregular particle shape and with a large particle size distribution. With larger magnifications, following details are revealed: The image in the right corner in the last row show the surface of a single particle. It exhibits that the particle is covered by a fine powdery particle fraction.

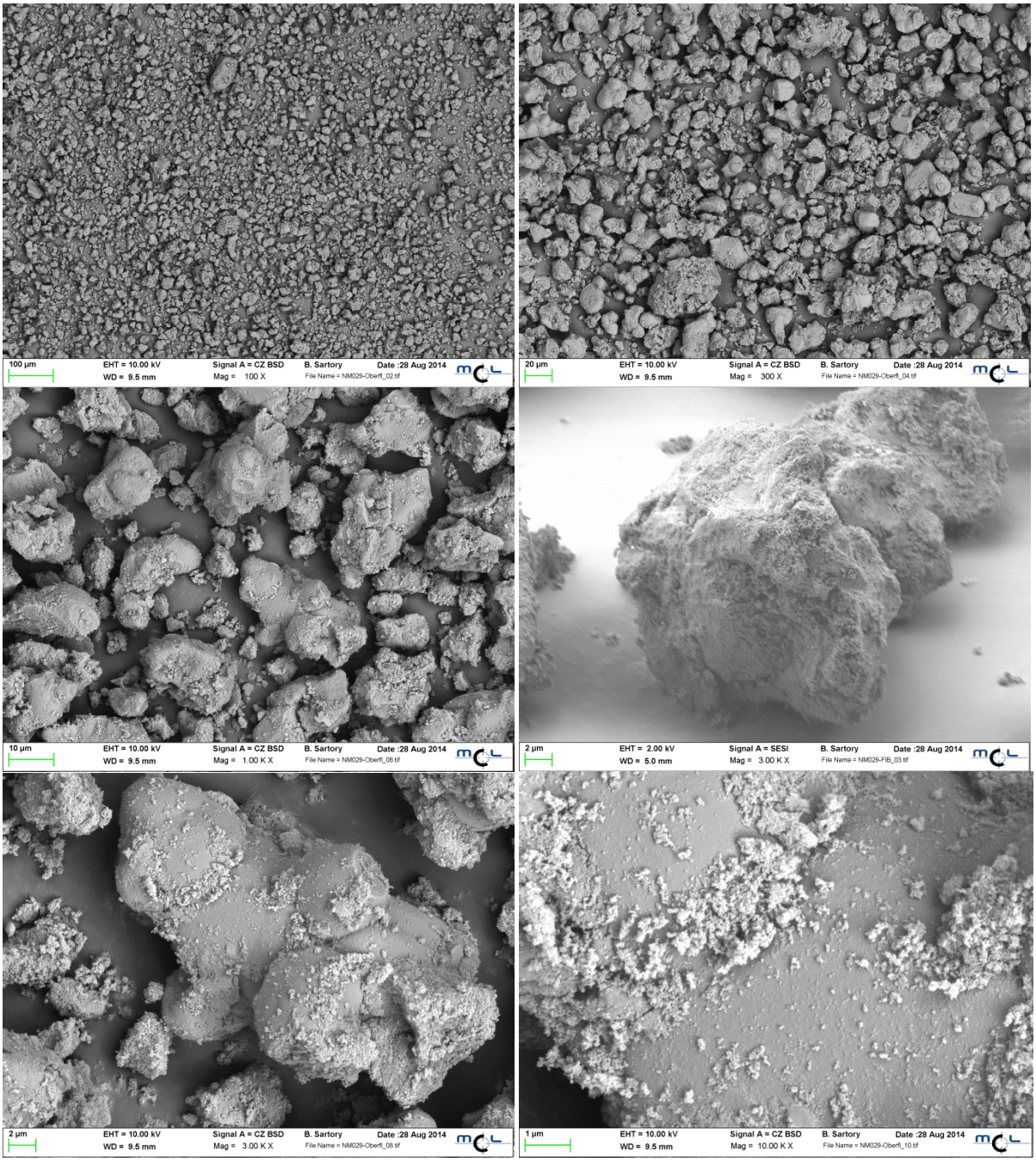

Figure 46: FEM images of NM029 (starting with the left upper corner with lowest magnification).

Also the images of NM032 (see Figure 47) reveal that the particles surface is covered by a fine powdery particle fraction like seen before in NM029, which is in its structure fissured and not smooth nor flat. It can be assumed due to the results of ATR-IR, EDX and XRD (of NM029) analysis, that the fine powdery particle fraction is Al_2O_3.

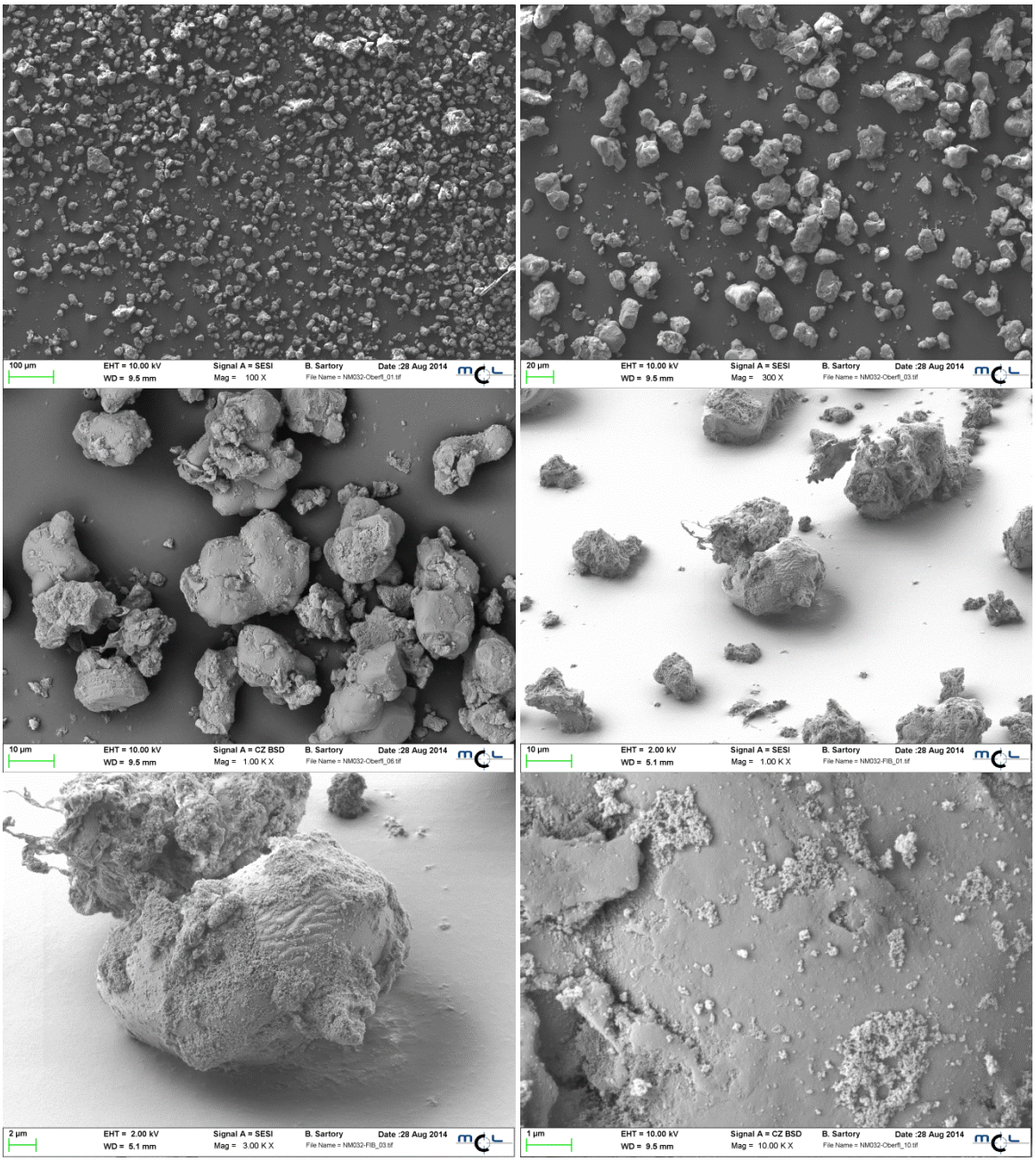

Figure 47: FEM images of NM032 (starting with the left upper corner with lowest magnification).

Due to the higher concentration of educts solutions in experiment NM029 compared to NM032 more Al_2O_3 was formed on phosphor particles. Agglomeration occurred in both experiments, regardless of concentration and reaction time. Figure 48 (left) shows an FEM image of covered phosphor particles and an agglomerate of Al_2O_3 of sample NM032. The enlarged section of Figure 48 (green circle) in Figure 48 (right) reveals a single agglomerate of aluminum oxide. Its structure differs in its shape and its surface structure compared to the surface of phosphor particles. The surface seems to be fissured and neither smooth nor flat.

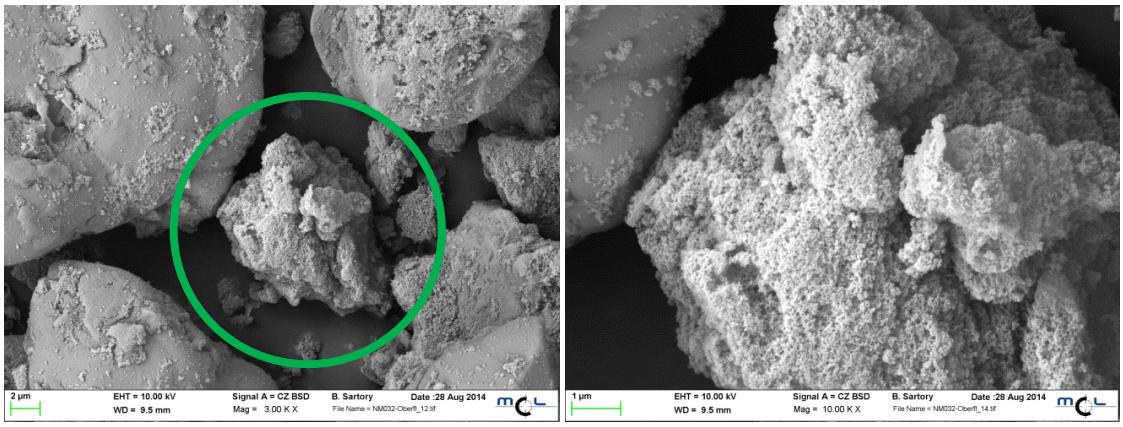

Figure 48: FEM image of NM032 covered phosphor particles and an agglomerate of aluminum oxide (left) and the enlarged section (green circle) of a single aluminum oxide agglomerate (right).

As indicated in the results of XRD analysis the proven product of Al_2O_3 in sample NM029 is not of crystalline but of amorphous structure. To investigate the structure of Al_2O_3 on phosphor particles, a focused gallium ion beam was controlled rastered over the sample NM029 and NM032 for the sample preparation. In the process the sample surface and further the bulk got ablated. Images of the exposed area were taken *via* SEM and are shown in Figure 49 (A, B of NM029 and C, D of NM032). The brighter and compact areas can be assigned to the phosphor and the darker structured areas as Al_2O_3.

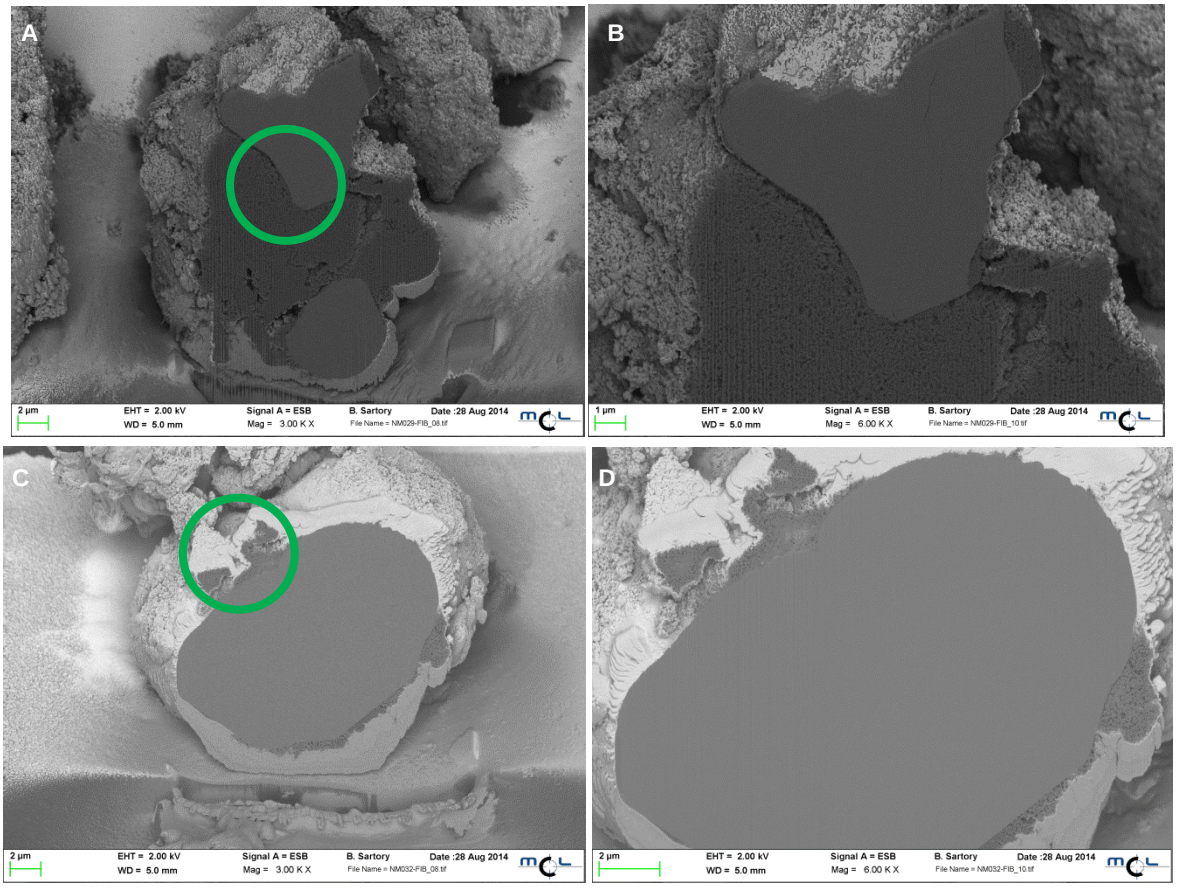

Figure 49: FEM images of ablated area (cross section) of NM029 (above) and NM032 (below) phosphor particles (see enlargement of green circle right).

Image A shows an aluminum oxide matrix in which phosphor particles are embedded, obtained from experiment NM029 (see A and B). Image C and D (see Figure 49) show a single phosphor grain with an almost continuous layer of Al_2O_3 (experiment NM032). In NM032 compared to NM029 the Al_2O_3 layer is thinner and almost covers the whole particle. Sample NM029 was done in large excess of educts, wherein experiment NM032 was carried out in lower concentration. Due to these results it can be said that in higher concentrations agglomerates of $Al(OH)_3$ are preferred formed than a layer of $Al(OH)_3$ on phosphor particles. Thus the probability increases that phosphor particles are embedded in agglomerates of Al_2O_3, coated in a low amount of Al_2O_3 or even not coated with Al_2O_3. Figure 50 shows images of enlarged sections of B and D from Figure 50. The structure of Al_2O_3 seemed to be fissured and neither smooth nor flat. In these images a porous structure of Al_2O_3 is revealed. At the boundary of phosphor grain and Al_2O_3 the difference can be clearly demonstrated. Presumably this structure was formed due to the loss of H_2O in the annealing process. As the annealing process was carried out starting from room temperature and heated up to 400°C with unknown heating rate in a tubular furnace in inert gas atmosphere, the annealing process itself has influence on the resulting product.

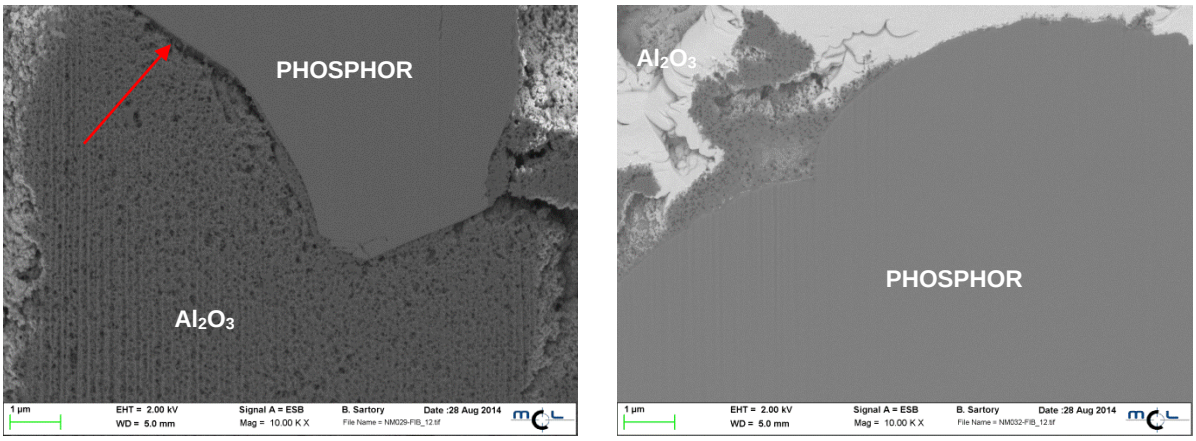

Figure 50: FEM images of cross section of NM029 (left) and NM032 (right) phosphor particles.

Test trials with different heating rates and different inert gas flows should be carried out in future. Moreover in a triple coating experiment heating rates should be varied after coating procedure 1, 2 and 3. From this experiment again FEM images should be made. Probably the structure of Al_2O_3 on the particles will differ and differences at boundaries will appear from coating 1, 2 and 3. The porous structure could disappear or getting actually more porous with bigger holes. Furthermore long term test according the stability of the Al_2O_3 coating on phosphor particles should be carried out.

EDX Al_2O_3 triple coating

Two different detectors were used for EDX analysis and imaging: A SESI which detects secondary electrons or secondary ions and a CZ BSD which is a backscattered electron detector. Following EDX spectra of triple coated phosphor sample NM029 and NM032 are shown, which were recorded via FEM (see Figure 53 and 54). The analysis was carried out using two different kinds of detectors: SESI and CZ BSD. Figure 54 and 55 show the FIB images of the surface of phosphor particles and the corresponding EDX spectra *via* SESI

(see Figure 53) and CZ BSD (see Figure 54) detector of NM029 and NM032. Peaks for N, O, Al, Si, Au and Ca are found. Au stems from the sample preparation. All elements of the phosphors host lattice were detected, except Eu. The formation of the inorganic product Al_2O_3 can be confirmed, due to the small peak for O and the peak for Al. The Al signal is in NM029 higher than in NM032, due to the higher concentration of educts in experiment NM029. Figure 54 shows NM029 (left) and NM032 (right) FIB images of the surface of phosphor particles (above) and the corresponding EDX spectra *via* CZ BSD detector (below). The obtained spectra differ in their signals for O, Si and Ca. Signals for the phosphors elements N, Al, Si and Ca have been detected, except Eu. NM029 show higher peaks for O and a smaller peak for Si compared to NM032. This means that Al_2O_3 is found on the particles in greater amount than in NM032. In NM029 peaks for the phosphors host lattice show high intensities and a smaller peak for O compared to NM029. Because secondary electrons and backscattered electrons are generated in different depths (see Figure 51), other information is obtained *via* a SE and a BSE detector like SESI and CZ BSD and therefore the obtained EDX spectra differ. Figure 51 shows the interaction of a sample with an electron beam like used in SEM. SE give information about the surface of a sample (5nm), whereby BSE give information about the bulk of a sample (400nm). The SESI spectra give information about the morphology and CZ BSE give information about the composition of a sample (material contrast).

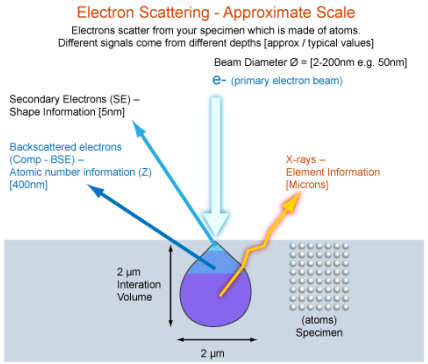

Figure 51: Interaction of a primary electron beam with a sample.

Due to the obtained results, it can be said that the SESI EDX spectra reveal the composition of the coated phosphor surface (see Figure 53) and CZ BSD EDX spectra reveal the composition of the bulk (see sketch Figure 52). In NM029 agglomerates of Al_2O_3 and coated particles were determined *via* FEM. The ratio of Al_2O_3 agglomerates and coated particles in NM029 is bigger than in NM032, due to signals for O and Al are bigger in NM029.

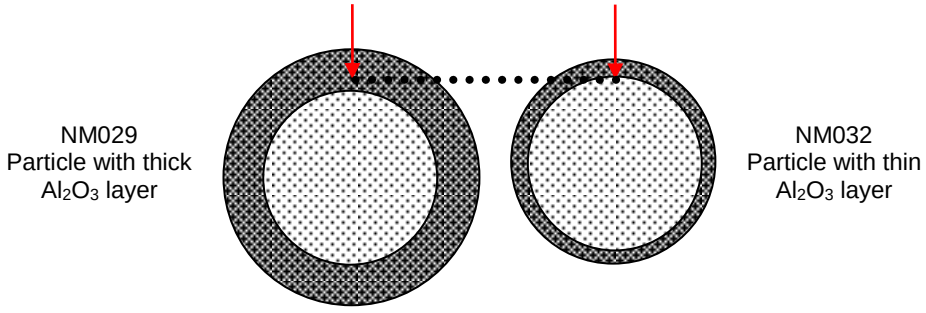

Figure 52: Electron matter interactions (sketch, left) and interaction of electron beam with coated phosphor samples in NM029 and NM032.

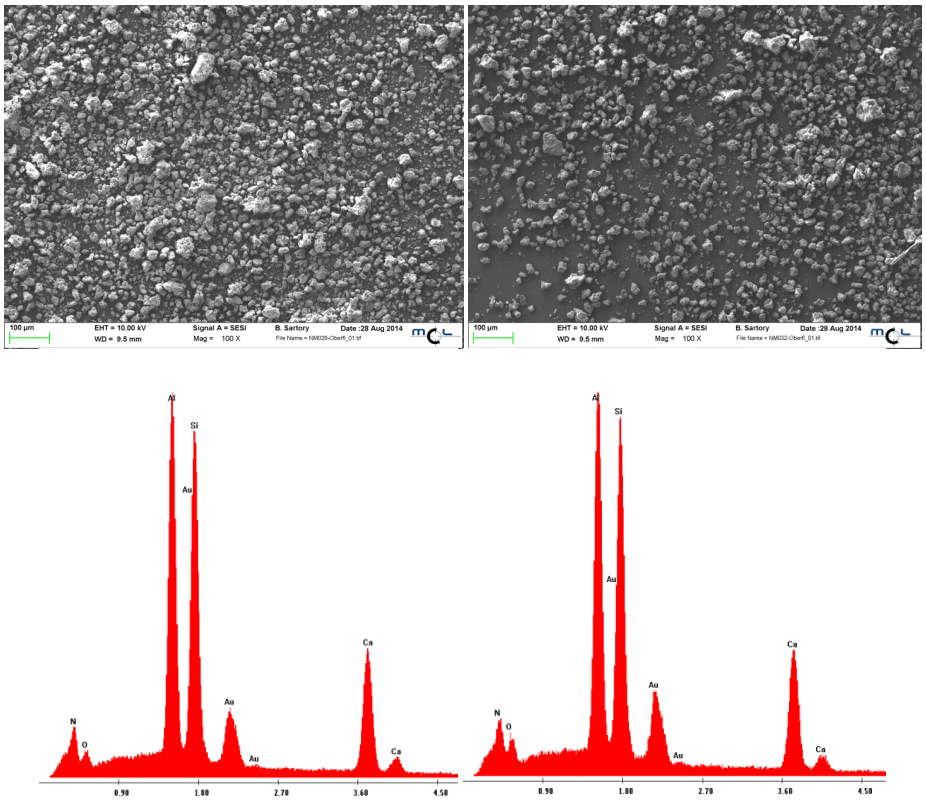

Figure 53: FEM images NM029 (left) and NM032 (right) of the surface of phosphor particles (above) and the corresponding EDX spectra via SESI detector (below)

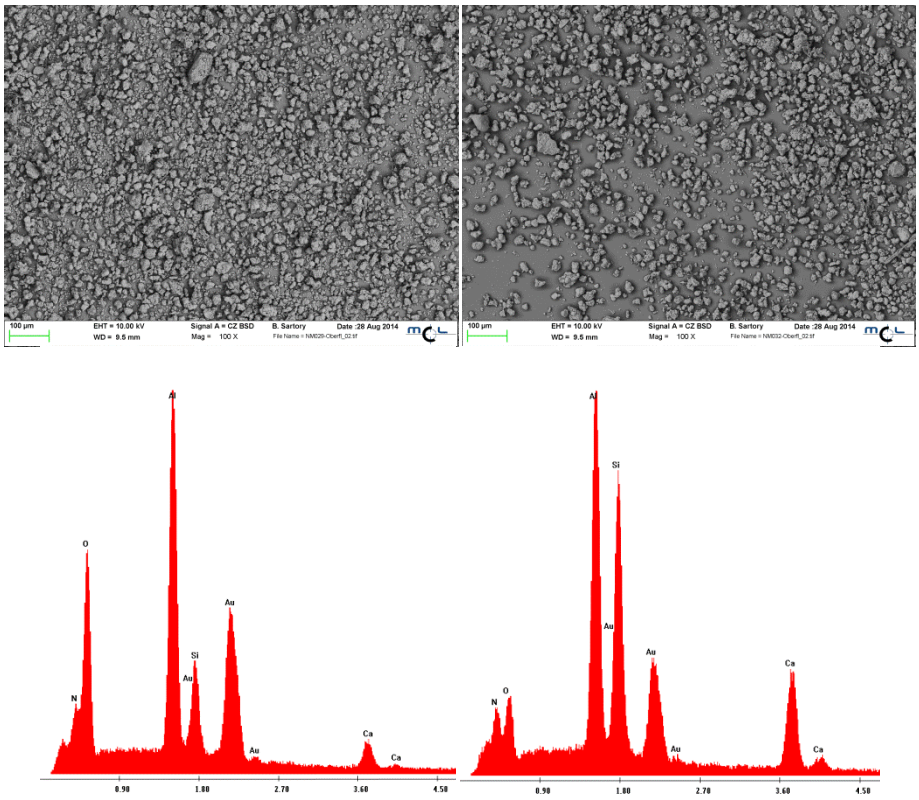

Figure 54: FEM images NM029 (left) and NM032 (right) of the surface of phosphor particles (above) and the corresponding EDX spectra via CZ BSD detector (below).

LUMINESCENCE Al_2O_3 triple coating

Emission spectra of uncoated phosphor and coated phosphor material NM029, NM032, NM033 and NM034 are compared in Figure 55 (left). The shape of the broad single band of the emission of the coated phosphor samples NM029, NM032, NM033 and NM034 compared to uncoated did not change. Also the shape and the width of the emission band did not change after the triple coating process. Affirmative an oxidation of Eu^{2+} to Eu^{3+} was not observed. As a consequence of the high concentrated coating experiment, the shift of the emission maximum of sample NM029 is the largest with 5nm to shorter wavelengths. The minimal shift of 1-5nm of the emission maximum caused a negligible shift of CIE color coordinates (see Table 24 and Figure 55, right).

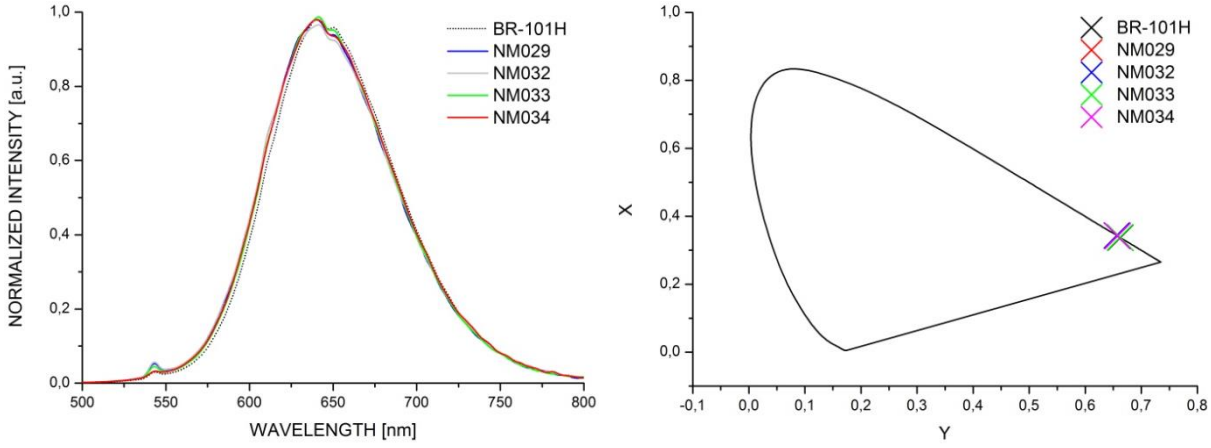

Figure 55: Emission maxima of uncoated and coated phosphor NM029, NM032, NM033 and NM034 (left) and CIE diagram 1931 of uncoated and coated phosphor NM029, NM032, NM033 and NM034.

Furthermore a reduction of the quantum efficiency of all coated phosphor materials compared to untreated phosphor occurred. The quantum efficiency compared to uncoated phosphor decreased for 13% for NM029, 16% for NM032, 13% for NM033 and 29% for NM034. The reduction of the quantum efficiency of coated phosphor material could be caused by the thick layer of Al_2O_3 on the particles. Zhuang et al. reported that the thickness of a coating layer has influence on the luminescence behavior of a coated phosphor.[24] Moreover the images taken with SEM indicate the fact that phosphor particles in NM029 were embedded in a matrix of Al_2O_3 and besides that the XRD analysis determined that the obtained coating is of amorphous nature. Therefore diffuse scattering of light at the Al_2O_3 layer may result in reduced excitation of Eu^{2+} and diminished quantum efficiencies of all coated phosphors.

Table 24: Results of luminescence measurements of triple coating NM029, NM032, NM033 and NM034

Sample	$\lambda_{MAX,\ emission}$ [nm]	Quantum Efficiency [%]	CIE Color Coordinate x	CIE Color Coordinate y
BR-101H	643	75	0.663	0.337
NM029	638	65	0.657	0.343
NM032	643	63	0.656	0.343
NM033	642	65	0.662	0.338
NM034	642	53	0.658	0.342

In general it has to be mentioned that a shift of the emission maxima could be caused by the used sample preparation method for luminescence measurements. Although the samples were made in the same way, the comparability cannot be assured because the layer thickness could vary and hence a diverse concentration in the film may occur.

Al_2O_3 Coating Scale Up experiments

ATR-IR scaleup Al_2O_3 coating

The ATR-IR spectra of scaleup experiments US01, US02 and US03 dried at 100°C and annealed at 400°C are shown in Figure 56. Peak intensities in the finger print area of all spectra decreased compared to uncoated phosphor, except US01 were the peak intensities stayed almost the same. As already mentioned in Chapter 6.1.2 (headline ATR-IR Al_2O_3 triple coating) the absorption peak intensities decrease after the coating process due to hydrolysis of the phosphors surface, compared to uncoated (not hydrolyzed) phosphor. Experiment US01 and US03 were coated once, US02 was coated twice. Furthermore the experiments differ in their reaction time: US01 coating experiment took 75 minutes, US02 and US03 coating experiment took 420 minutes. The ATR-IR spectra show that US01 was hydrolyzed in a low extent, whereby US02 and US03 which were coated for 420 minutes show that they have been hydrolyzed in stronger extent than US01. Therefore signals for US02 and US03 diminish significantly compared to uncoated phosphor.

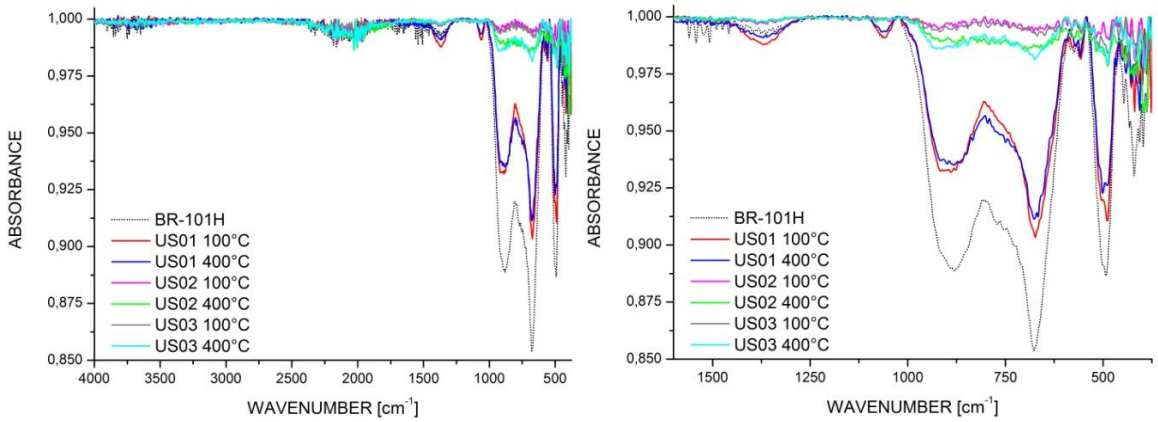

Figure 56: ATR-IR spectra of US01, US02 and US03 dried at 100°C and annealed at 400°C in the range between 4000-375cm^{-1} (left) and in the range of 1600-375cm^{-1}(right).

Following observation was made in the spectra of the dried products: In Figure 57 (left, see red arrow) for sample US01 an increased absorption peak at 1370cm^{-1} is observed, which can be ascribed to the bending vibration of the $\tilde{\upsilon}$[O–H] bond in $Al(OH)_3$, not to residual moisture. Furthermore no broad absorption peak of water is observed at 3400cm^{-1} due to the fact that all samples were dried over night at 100°C and all water was driven off.

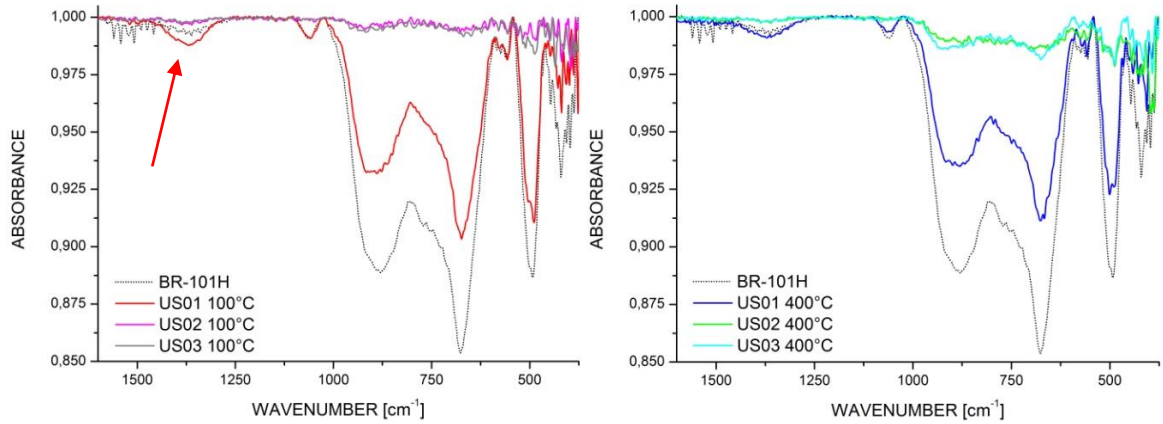

Figure 57: ATR-IR spectra of US01, US02 and US03 dried at 100°C (left) and annealed at 400°C (right) in the range of 1600-375cm^{-1}.

Figure 57 (right) shows the spectra of US01, US02 and US03 after the annealing process. The peak at 1370cm^{-1} decreased slightly after the annealing process due to the formation of Al_2O_3 (see Figure 57, left).

SEM scaleup Al_2O_3 coating

Figure 58 shows SEM images of uncoated phosphor (left), US01 (mid) and US02 (right) at a magnification of 1000x. The electrical conductivity of the phosphor particles decreased due to the coating experiment in some extent, indicated by brighter areas (blurred image). Both experiments led to the formation of agglomerates or to embedding of phosphor particles into a matrix of Al_2O_3 (see green circle). Only a cross section could confirm that.

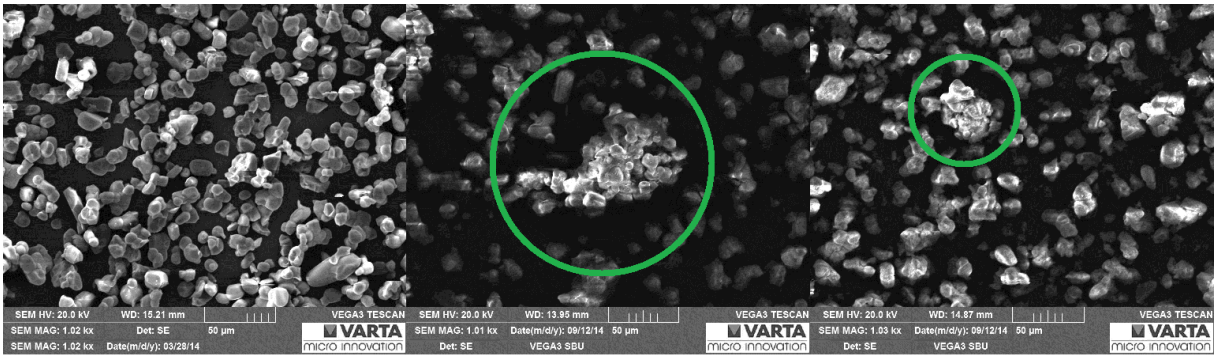

Figure 58: SEM (SE) image of uncoated BR-101H (left), US01 (mid) and US02 (right).

EDX scaleup Al_2O_3 coating

Table 25 (see Figure 59, right) shows the results of EDX analysis in percentage by weight, for elements of the phosphors host lattice and elements of the coating, and the corresponding EDX spectra of US01 (left) and US02 (right). US02 contains a higher percentage by weight of O and Al compared to US01. Also the percentage by weight of N, Si and Ca are lower compared to US01. It can be assumed that more Al_2O_3 was coated on the phosphor particles in US02, due to the double coating of phosphor particles. This also confirms the worse electrical conductivity of coated US02 particles like shown in SEM images (Figure 59, right).

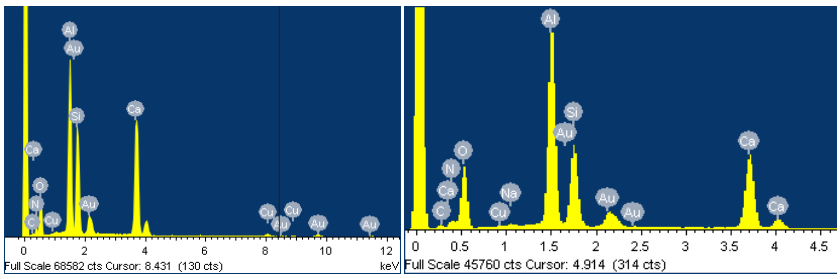

Element [wt%]	US01	US02
N	16	12
O	32	45
Al	18	20
Si	13	10
Ca	21	13
Total	100	100

Figure 59 and Table 25: EDX spectra of US01 (left) and US02 (right) and the corresponding results of elements detected by EDX analysis in percentage by weight.

LUMINESCENCE scaleup Al_2O_3 coating at TRIDONIC Jennersdorf GmbH

TRIDONIC Jennersdorf GmbH performs standardized measurements to obtain information about the luminescence behavior of phosphors like emission spectra, quantum efficiency and CIE color coordinates. The data of tenfold measurement at each excitation wavelength 449nm, 455nm, 460nm and 464nm was evaluated by a provided template by TRIDONIC

Jennersdorf GmbH. The evaluation of the above mentioned results was carried out as followed: The recorded data was imported in the evaluation template, were the maximum efficiency of a phosphor, the efficiency of a phosphor and further on the quantum efficiency was calculated. The efficiency of the phosphor samples in [lm/W] is calculated by division of the light flux [lm] of the phosphor converted light source trough the initial radiant power [mW] (see Equation 8). The maximum efficiency of a phosphor is the theoretical value of lm/W at 100% quantum efficiency, when the number of absorbed photons is equal to the number of emitted photons. It can be calculated by efficiency of the phosphor divided by the quantum efficiency according to Equation 9.[4]

$$Efficiency\ of\ Phosphor = \frac{light\ flux\ phosphor\ converted}{radiant\ power}\left[\frac{lm}{W}\right] \qquad \textit{Equation 8}$$

$$Maximum\ Efficiency\ of\ a\ Phosphor = \frac{light\ flux\ phosphor\ converted}{radiant\ power} \cdot \frac{N\ absorbed\ Photons}{N\ emitted\ Photons}\left[\frac{lm}{W}\right] \qquad \textit{Equation 9}$$

The quantum efficiency of a phosphor is the quotient of the absorbed photons and the emitted photons of a phosphor according Equation 10.

$$Quantum\ Efficiency = \frac{N\ emitted\ Photons}{N\ absorbed\ Photons} \cdot 100 = [\%] \qquad \textit{Equation 10}$$

As the efficiency is dependent on the chromaticity coordinate, a comparison of the value of the efficiency of different phosphors is only useful if it is compared at the same chromaticity coordinate. This chromaticity coordinate also called reference coordinate is located at a x value of 0.44 for red phosphors (internal standard) and was therefore considered while calculations. As a result following quantum efficiencies of phosphor samples BR-101H, US01 and US02 were determined at an excitation wavelength of 449nm, 455nm, 460nm and 464nm shown in Table 26. The results of evaluation are shown in Figure 60 of phosphor BR-101H at an excitation wavelength of 455nm, representative for all measurement of phosphor samples: The blue line (dots) resembles the maximum efficiency (can be theoretical reached) of a phosphor and the black line (squares) resembles the efficiency of a phosphor.

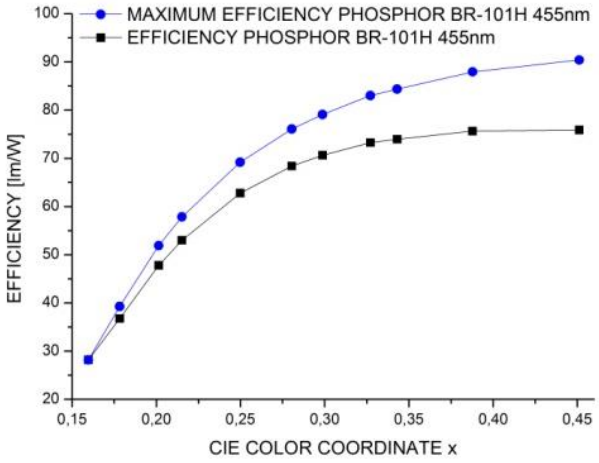

Figure 60: Maximum efficiency of phosphor BR-101H and efficiency of phosphor BR-101H at an excitation wavelength of 455nm.

In general the quantum efficiency decreased slightly with increasing number of coating experiments: It decreased between 0.4% and 3.8% after the coating procedure (with an λ_{EXC} of 449nm by 0.4% and 1.3%, λ_{EXC} of 460nm by 3.1% and 3.8% and at λ_{EXC} of nm by 2.1% and 2.7%). The quantum efficiency of BR-101H at an excitation wavelength of 455nm has to be declared as a measurement error due to the result of 102% quantum efficiency which cannot be higher than 100%.

Table 26: Calculated quantum efficiencies of BR-101H, US01 and US02 at a x value of 0.44.

		Quantum Efficiency [%]		
		BR-101H	US01	US02
$\lambda_{Excitation}$ [nm]	449	84.0	83.7	82.9
	455	-	82.2	82.2
	460	81.7	81.4	80.8
	464	83.1	82.2	81.7

Figure 61 shows the emission spectra of the blue LED, the uncoated and coated phosphor samples at an excitation wavelength of 464nm. The emission maximum of all samples is with 643nm the same. The CIE color coordinate y was calculated from y=1.698x-0.200 (provided template) for x equal 0.440. The calculated CIE color coordinate y for all samples at an excitation wavelength of 464nm is equal 0.545. Table 27 shows the summary of the results from luminescence measurement of BR-101H, US01 and US02 at an excitation wavelength of 464nm and a CIE color coordinate value of x equal 0.44.

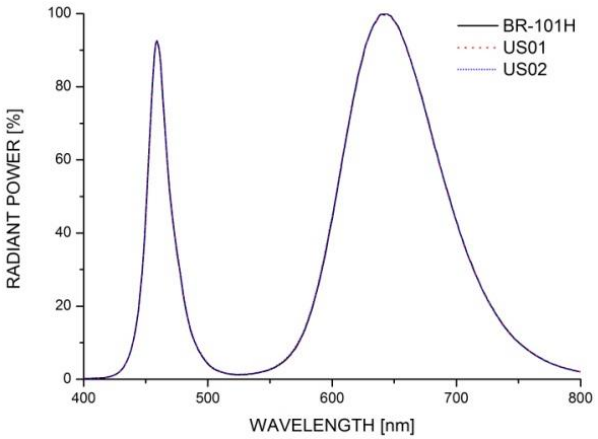

Figure 61: Excitation and emission spectra of BR-101H, US01 and US02 at an excitation wavelength of 464nm.

It is important to note that the results from measurement at ACFC cannot be compared to the results from measurement at TRIDONIC Jennersdorf GmbH as well as from the material data sheet. Compared to the results from luminescence measurement at the ACFC the value of the emission maxima are consistent, but the values of quantum efficiency differ by 10%. Based on experiments at ACFC the determined values of quantum efficiency do differ in ±10%. TRIDONIC Jennersdorf GmbH

Table 27: uncoated Phosphor (results ACFC, MSDS and Tridonic Jennersdorf GmbH).

	$\lambda_{MAX,}$ Emission [nm]	Quantum Efficiency [%]	CIE Color Coordinate x	CIE Color Coordinate y	Method of Determination
ACFC	643	75	0.663	0.337	Absolute
MSDS	-	-	0.652	0.347	-
TRIDONIC	643	83	0.440	0.545	Indirect

6.1.3 Results: MgO Coating

Urea as precipitation agent

According to Equation 11 the precipitation reaction of $MgCl_2$ with urea shall lead to the formation of $Mg(OH)_2$ in sample NM030 and NM031. 1mole of $MgCl_2$ reacts to give 1mole of $Mg(OH)_2$ and after the annealing procedure 1mole of MgO is formed (see Equation 11). For the complete precipitation of $Mg(OH)_2$ a stoichiometric ratio of 1:2 equal $MgCl_2$:urea is necessary.

$$MgCl_2 + 2CO(NH_2)_2 \rightarrow Mg(OH)_2 \downarrow + side\ products \xrightarrow{\Delta T} MgO + 2H_2O \uparrow_{vap}$$

Equation 11: Chemical equation of the precipitation reaction of magnesium hydroxide and further formation of magnesium oxide after annealing.

After annealing at 400°C a decrease of weight due to formation of 2mole is expected. Also an increase of weight of the obtained product (phosphor particles and layer) should be recorded after the coating process in accordance with the calculation shown in Table 28 as shown here for synthesis NM030.

Table 28: Sample weight of precursors for MgO synthesis and weight of products after synthesis as well as after the annealing process based on NM030.

	Material	M [g/mol]	m [mg]	Mole Ratio	n [mmol]
	$CaAlSiN_3$	137.165	0.5098	-	-
Educts	$MgCl_2$	95.211	0.1661	1	1.71
	Urea	60.055	0.2078	2	3.43
Metal Hydroxide	$Mg(OH)_2$	75.327	0.129	-	2.4
Metal Oxide	MgO	40.304	0.069	-	1.2
Product	$CaAlSiN_3$ + MgO	-	0.5167	**-**	**-**

Despite all the above mentioned theory no colloidal $Mg(OH)_2$ was to be seen on the obtained product like in the other coating experiments of Al_2O_3 (see Figure 62). The product was dried and annealed and characterized via ATR-IR and SEM (SE, EDX) to determine whether in fact no MgO was formed.

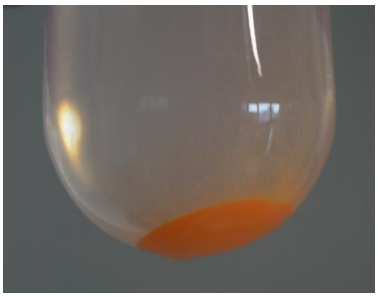

Figure 62: Picture taken after sedimentation of the product after synthesis of the desired MgO coating in sample NM030. No colloidal layer can be seen.

ATR-IR of MgO coating

Figure 63 shows the ATR-IR spectra of uncoated phosphor and coated phosphor NM030 with MgO. No observable additional peak appeared, only peak intensities of NM030 100°C and 400°C decreased compared to uncoated phosphor. Decreased absorption intensities stem from hydrolysis of the phosphors surface. Therefore the formation of MgO cannot be confirmed via ATR-IR. Only hydrolysis in a low extent occurred on phosphor particles, due to the decreased absorption intensities of the coated phosphor.

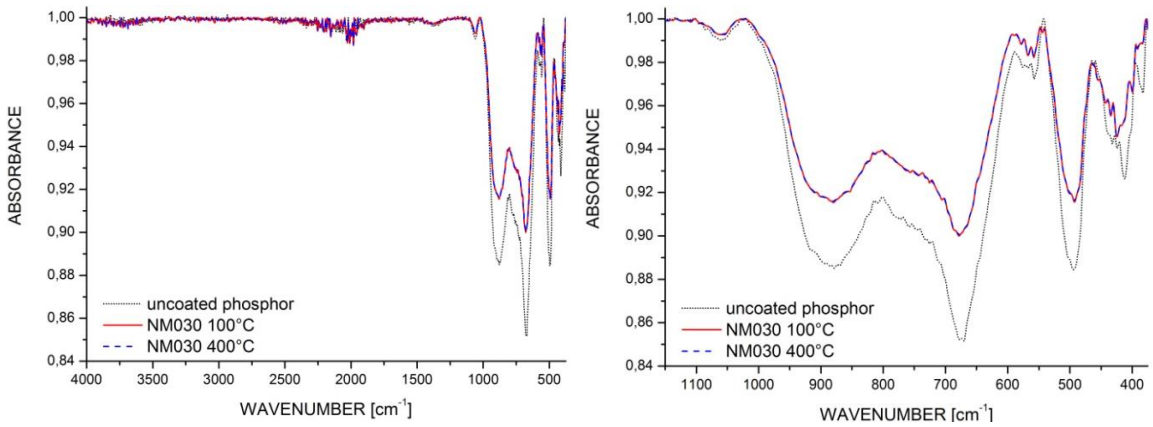

Figure 63: ATR-IR spectra of MgO coating after drying at 100°C and annealing at 400°C of synthesis NM030.

SEM, EDX of MgO coating

An EDX analysis was done to prove the formation of MgO coating. Figure 64 shows the obtained product after MgO coating: No changes on the surface of the phosphor can be seen (see Figure 64 left). Signals for the phosphors host lattice (N, Al, Si and Ca) and from the sample preparation could be detected (C, O, Cu and Au). Furthermore no Mg could be found on phosphor particles determined in mapping mode (see Figure 64, right and the received EDX spectrum). EDX analysis confirmed the suspicion that no MgO was formed. Hence no formation of MgO from $Mg(OH)_2$ after temperature treatment was possible.

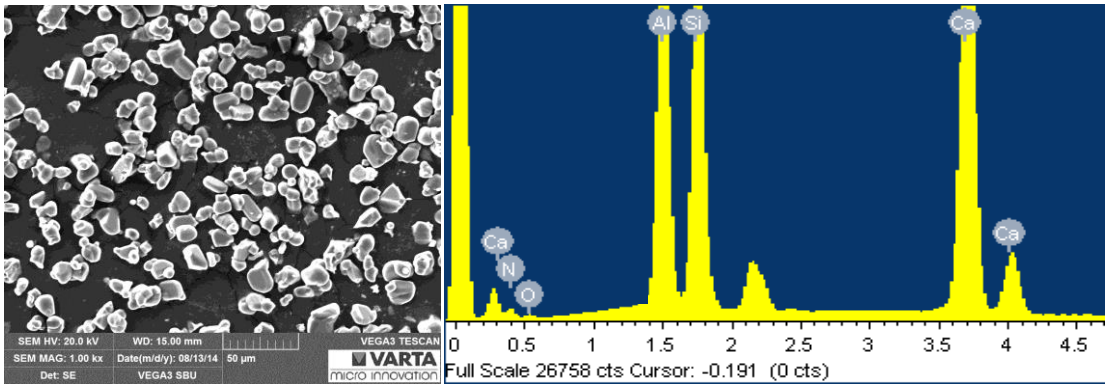

Figure 64: Picture taken with SEM (SE) of MgO coated phosphor NM030 and the obtained EDX spectrum of NM030.

It can be reasonably assumed that the precipitation reaction was not complete or the used base urea is not suitable for the precipitation of $Mg(OH)_2$ and a strong base for example $NaHCO_3$ should be tried as a precipitating agent. Urea is a small, uncharged, non alkaline molecule which is relatively nontoxic. No XRD and Fluorescence Spectroscopy measurements were carried out, due to lack of formation of MgO on phosphor particles confirmed by ATR-IR, SEM and EDX analysis.

$NaHCO_3$ as precipitation agent

Due to the fact that in NM030 no $Mg(OH)_2$ was precipitated and further no MgO was formed, another experiment was carried out with $NaHCO_3$ as a precipitation agent instead of urea.

ATR-IR MgO coating

ATR-IR spectra of coated phosphor NM035 recorded after drying at room temperature, 100°C, 200°C and 400°C compared to uncoated phosphor are shown on Figure 65. Absorption bands of phosphor showed a strong decrease. The strong decreased absorption intensities can be ascribed to hydrolysis of the phosphors surface trough a long reaction time of almost 16h. The peak at 1060cm^{-1} disappeared after temperature treatment (see Figure 66 red arrow). No residual water peak at around 3400cm^{-1} is observed.[32] Two new absorption bands at 1480cm^{-1} and 1420cm^{-1} appeared with increasing temperature, which can be ascribed to the absorption bands of the precipitated $Mg(OH)_2$.[41] After the annealing process of $Mg(OH)_2$ to MgO these bands decrease slightly and form one approximately single peak like shown in spectrum NM035 MgO annealed at 400°C (see Figure 65 red arrow). Compared to the results of NM030, it can be confirmed that $Mg(OH)_2$ was formed after the precipitation reaction and further MgO was formed through the annealing process at 400°C.

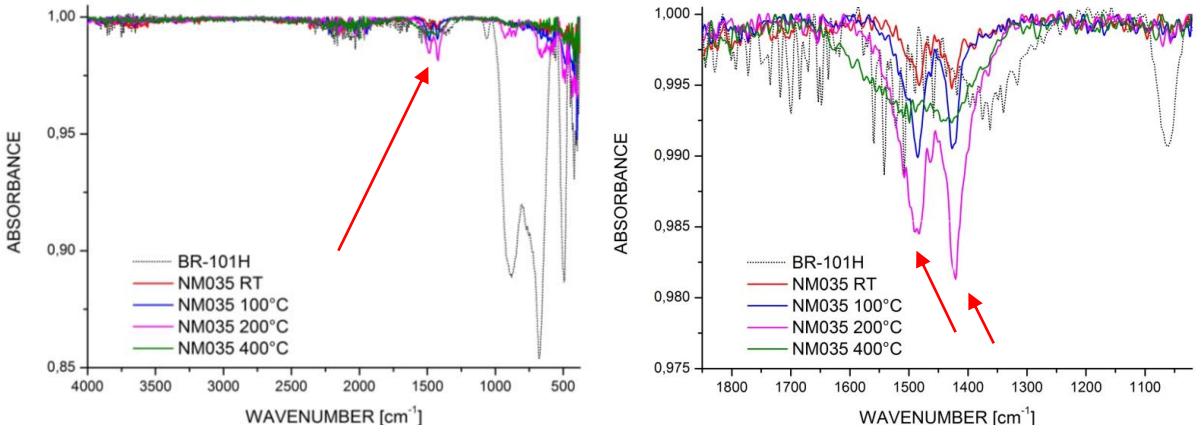

Figure 65: ATR-IR spectra of MgO coating experiment NM035 at RT, 100°C, 200°C and 400°C in the area from 4000-375cm^{-1}.

SEM, EDX MgO coating

Figure 66 (left) shows the SEM picture of coated phosphor NM035. The surface of the phosphor particles has a flaky texture, which can be ascribed to the annealed product of the precipitation reaction. Furthermore separate objects were formed with the same structure presumably small crystalline nuclei of MgO (red circle, see Figure 66).

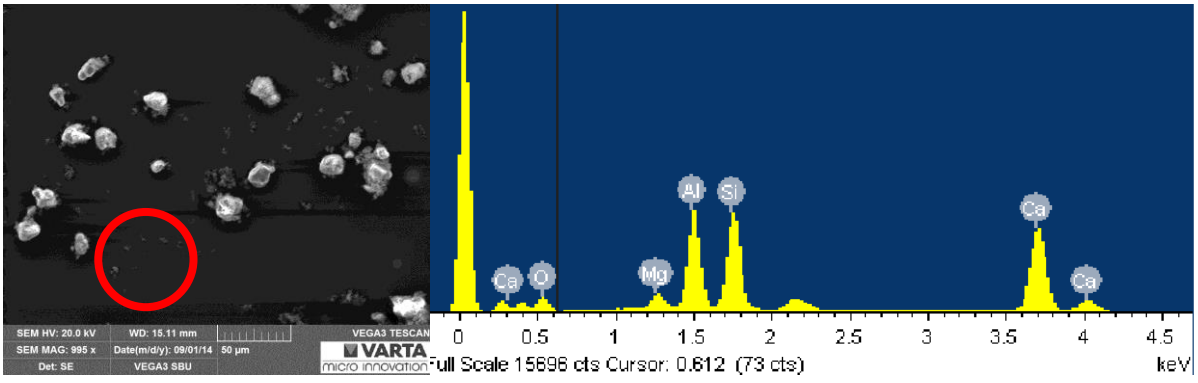

Figure 66: SEM (SE) image of coated phosphor NM035 and an EDX spectrum of a selected phosphor particle coated with MgO.

The EDX analysis recorded in mapping mode on a selected area on a coated phosphor particle revealed following elements in the sample: C, O, Mg, Al, Si, Ca and Au. Signals for C and Au can be ascribed from the sample foil and sample preparation. Cu from the sample foil and N part of the phosphors host lattice were not detected.

SEM cross section MgO

To ensure that the formation of MgO as a layer on phosphor particles was successful SEM and EDX analysis of a cross section were carried out at FELMI. Figure 67 shows material contrast images of the fabricated cross section of MgO coated phosphor NM035. It shows bright areas which can be ascribed to phosphor particles which are surrounded by a halo of darker areas due to MgO. Despite slow addition of educts solutions in drops and long reaction time agglomerates of MgO were formed (see red circle). Furthermore phosphor particles were embedded in a matrix of MgO (see green circle).

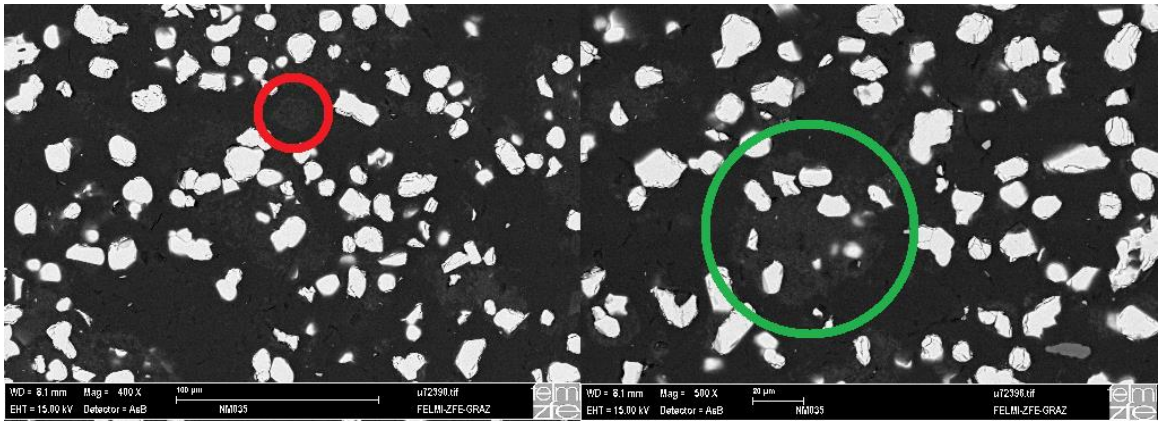

Figure 67: SEM material contrast image (BSE) of cross sections of NM035 (overview of particles).

The elements detected by BSE are dyed in different colors and labeled in the upper right corner of the pictures in Figure 68. Signals for C and O (partly) result from the epoxy matrix, in which the sample was embedded for sample preparation. The elements of the phosphors host lattice N, Al, Si and Ca were detected. Around the phosphor particles a matrix of MgO is indicated trough O and Mg signals (blue and yellow marked). A homogeneous, thin layer of MgO cannot be confirmed through SEM images of phosphor grains. The results are similar to Al_2O_3 coated phosphor in NM033.

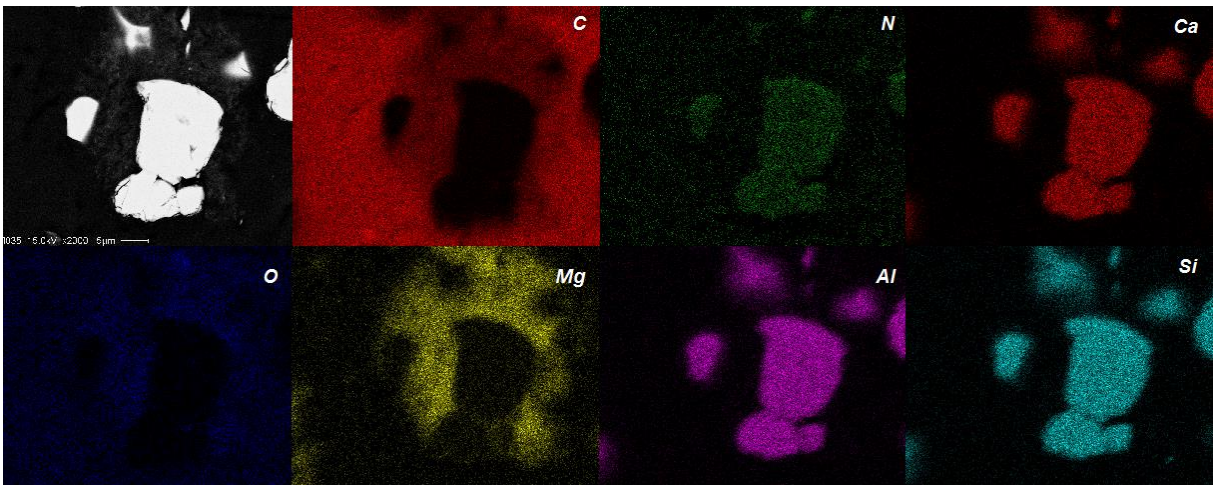

Figure 68: SEM (BSE) image of coated phosphor grains of NM035.

EDX cross section MgO

Figure 69 shows the SEM material contrast images (left) of a cross section of sample NM035 and the corresponding EDX spectra (right). Area 1 show significant peaks of the elements N, Al, Si and Ca and of phosphors host lattice. Signals for C and O can be ascribed to the sample preparation (residual epoxy resin). In Area 2 an even higher peak for C is shown than in Area 1. Area 2 shows peaks for O and Mg, due to the obtained MgO.

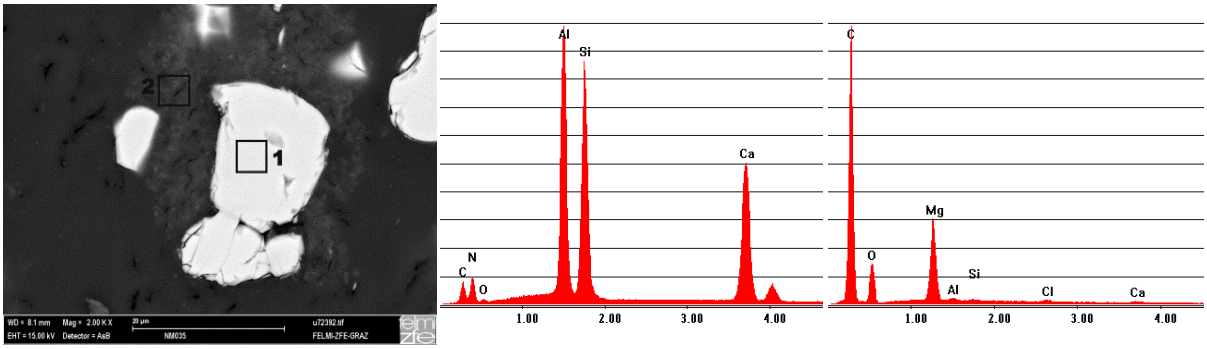

Figure 69: Cross section of coated phosphor particle NM035 (BSE, left), EDX spectra of Area 1 (left) and Area 2 (right).

LUMINESCENCE MgO coating

The emission spectra of uncoated phosphor and coated phosphor are shown in Figure 70. No change was observed: The maximum of emission is 643nm for NM035, same as for BR-101H, the shape of the emission peak did not change and the range of 500-800cm^{-1} also remained unaltered. The coating process via a precipitation reaction in which $Mg(OH)_2$ was formed through $NaHCO_3$ as precipitating agent and further annealing at 400°C does not influence the luminescence behavior of the phosphor. In contrast to the values mentioned before, the CIE color coordinates in Table 29 shift from x 0.663 to 0.662 (-0.2%) and from y 0.337 to 0.338 (+0.3%). Due to a device error the results of quantum efficiency have to be doubted and are therefore here not quoted.

Table 29: Results of luminescence measurements of MgO coating NM035.

Sample	$\lambda_{MAX, emission}$ [nm]	Quantum Efficiency [%]	CIE Color Coordinate x	CIE Color Coordinate y
BR-101H	643	75	0.663	0.337
NM035	643	-	0.662	0.338

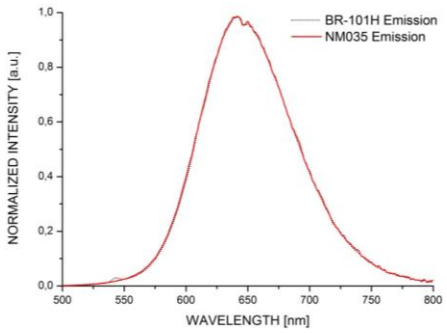

Figure 70: Emission spectra of uncoated and coated phosphor NM035.

COMPARISON Al_2O_3 and MgO coating procedure

Al_2O_3 and MgO coating have been obtained by a solution-coating process via a Brønsted precipitation reaction. They have both in common that they are formed based on the same synthesis route: As the cation source aluminum nitrate and magnesium chloride were used, which were precipitated with $NaHCO_3$ as a precipitation agent to obtain metal hydroxides of formula $M(OH)_x$ with M=Mg,Ca and x=2,3 as proposed by Murphy et al.[20] After the precipitation of metal hydroxides metal oxides were obtained by annealing the metal hydroxides at a temperature of 400°C.

The first step of the two-step-synthesis route can be defined as a Brønsted precipitation reactions. In the Brønsted- Lowry theory acids and bases are defined following characteristic behavior:[42] Brønsted acids act as proton donators (HA) whereby Brønsted bases act as proton acceptors (B). A proton donating and proton accepting system is also called conjugated acid-base system ($HA + B \rightleftarrows A^- + HB^+$). According this definition $Al(OH)_3$ shall be named here as an amphoteric substance. Aluminum hydroxide features special characteristics: As amphoteric hydroxide $Al(OH)_3$ it dissolves in acids as well as in bases.[43] In the former case aluminum salts and in the latter case aluminates are formed according to Equation 12 and Equation 13:

$$Al(OH)_3 + 3H^+ \rightleftarrows Al^{3+} + 3H_2O \qquad \textit{Equation 12}$$

$$Al(OH)_3 + OH^- \rightleftarrows Al(OH)_4 \qquad \textit{Equation 13}$$

In reversal of the balance Equation 12 and 13 aluminum hydroxide is precipitated as colorless precipitate ($L_{Al(OH)_3} = c_{Al^{3+}} \cdot c_{OH^-}^3 = 1.9 \cdot 10^{-33}\, mol/l$) by addition of bases to solutions of aluminum salts and by addition of acids to solutions of aluminates. The nature of the precipitate is dependent on the precipitation itself: A significant dependence upon time is observed. The fresh precipitated aluminum oxide (as amorphous hydroxide $Al(OH)_3 \cdot nH_2O = Al_2O_3 \cdot aq$) has other properties than aged aluminum oxide (as crystalline hydroxide $Al(OH)_3$). The latter is more stable due to acid and base reactions. This can be explained by a reduction in surface and by the degradation of unstable vacancies of the amorphous network during crystallization.[43] It should be mentioned that condensed silicic acid shows these characteristics as well. Based on the characteristic behavior of aluminum hydroxide in presence of acids and bases the pH value while the reaction shall be controlled and hold at around pH 7 by adding of diluted acid or diluted base, if not provided by the sodium bicarbonate in the neutral pH range of 6.2-8.6 (bicarbonate buffering system). Furthermore has to be considered that the solubility is besides temperature also pH dependent.

As magnesium hydroxide show only poor solubility in water it is precipitated when solutions of aluminum salts ($L_{Mg(OH)_2} = c_{Mg^{2+}} \cdot c_{OH^-}^2 = 1.5 \cdot 10^{-12}\, mol/l$) are added with bases according to Equation 14.[44]

$$\mathrm{Mg}^{2+} + OH^- \rightarrow Mg(OH)_2 \qquad \textit{Equation 14}$$

Not every base is suitable for precipitation of Magnesium hydroxide. For example when NH_3 is used as a base the precipitation of $Mg(OH)_2$ is incomplete due to the low hydroxide ion

concentration of the aqueous solution of ammonia. As shown in Chapter 6.1.3 urea as a precipitating agent was not basic enough to precipitate $Mg(OH)_2$.

All generated side products of the Al_2O_3 and MgO coating experiments shall be named at this point (see Equations 15). As hydroxides are hardly soluble, the side products of the Brønsted precipitation reaction CO_2, $NaNO_3$ and NaCl exist as dissolved ions in solution, due to their good solubility in H_2O and IPA). Whereas H_2O get evaporated by the heat generated from the ultrasonic bath.

$$2Al(NO_3)_3 \cdot 9H_2O + 6NaHCO_3 \rightarrow 2Al(OH)_3 + 6NaNO_3 + 6H_2CO_3 + 3H_2O \uparrow_{vap}$$

$$MgCl_2 + 2NaHCO_3 + 2H_2O \rightarrow Mg(OH)_2 + 2NaCl + 2H_2CO_3$$

Equation 15: Chemical equation of the Brønsted precipitation reactions of aluminum and magnesium hydroxide and its side products.

6.2 Grinding Process of BR-101H

As mentioned before, the phosphor may generate ammonia gas by contact with water, acid or moisture. The centrifugal and coriolis forces generated by the planetary mill worked on phosphor particles during the milling process and as anticipated caused the generation of NH_3 gas and led to a pressure release through the safety device. A part of the particles was ejected into the housing of the milling machine by the rotation of the planetary mill. The remaining part was ground until the end of the milling modus. The grinding of particles led to a decreased particle size and accompanied by an increase of the particle surface. The so generated active surface reacted with the milling medium H_2O under a hydrolysis reaction as followed shown in Equation 16.

$$CaAlSiN_3 + H_2O \xrightarrow{shear forces} NH_3 \uparrow + side\ products + \Delta T$$

Equation 16: Hydrolysis reaction of BR-101H phosphors host lattice $CaAlSiN_3$ while grinding process.

The products of the phosphors hydrolysis are NH_3, $Ca(OH)_2$, $Al(OH)_3$, $Si(OH)_4$ and heat. Besides the characteristic odor of ammonia gas and the heated milling bowl, the color change of the ground product was significant. The color of the unexcited uncoated phosphor changed from orange to bright apricot (see Figure 71). Besides the formation of NH_3 and hydrolysis products (indicated by color) the possibility of the oxidation of Eu^{2+} to Eu^{3+} should not be excluded. Should that be the case, serious impacts on the emission band of the phosphor can be expected: Eu^{2+} compounds show broad band emission, whereas Eu^{3+} compounds show a narrow single band (line emitter).[11,45] The visible luminescence behavior of the excited uncoated and ground phosphor changed as well, but has to be further analyzed by luminescence measurements.

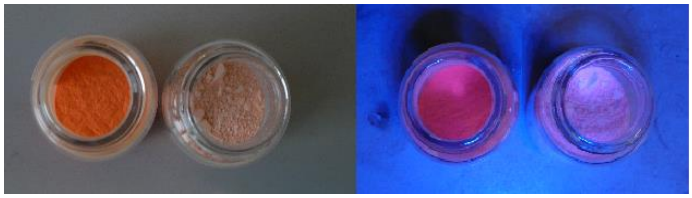

Figure 71: Luminescence behavior of uncoated phosphor and ground uncoated phosphor (unexcited left and excited right).

Despite losses through the milling process milled particles were classified into two fractions on the basis of their milling progress. The milling balls, the milling bowl and particles in fraction mill were rinsed with H_2O, dried over nigh at 100°C, ground and weighed.

SLS of milling fractions

The determination of the particle size distribution was carried out with Statistic Light Scattering in a range between 0.04-500µm (FRITSCH, ANALYSETTE 22 NanoTec plus, measured in duplicates) and calculated via Fraunhofer-theory. The sample was dispersed in a ultrasonic bath in a aqueous solution with potassium pyrophosphate ($K_4P_2O_7$) as dispersant for 10 minutes. The evaluation using Fraunhofer-theory[46] revealed following particle size distribution shown in Figure 72. The unimodal, asymmetric distribution in the range of 0.04-8µm shows a maximum at 0.95µm (see Figure 72, right). The particle size diminished strongly through the grounding process compared to their original size (Figure 72, left) as shown in Table 30.

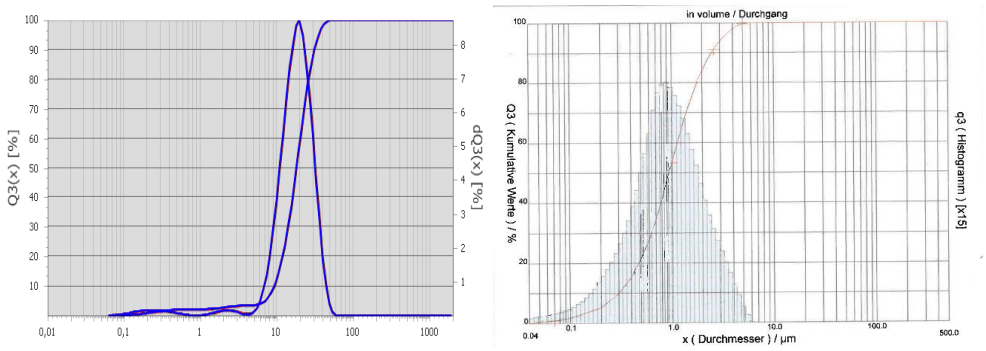

Figure 72: Results of SLS measurement: Particle size distribution of BR-101H (left) and fraction mill (right).

Table 30: Results of particle size determination via SLS.

Particle Size Diameter [%]	BR-101H [µm]	Fraction Mill [µm]
10	9.24	0.30
50	18.1	0.94
90	31.0	2.49

SEM of milling fractions

Figure 73 shows the SEM image of grounded fraction mill with 1.5kx magnification compared to uncoated phosphor with 10kx magnification. The particle size and shape of the particles changed notably. The former single particles with spherical structure show a plate like structure and a large particle size distribution after the grinding process.

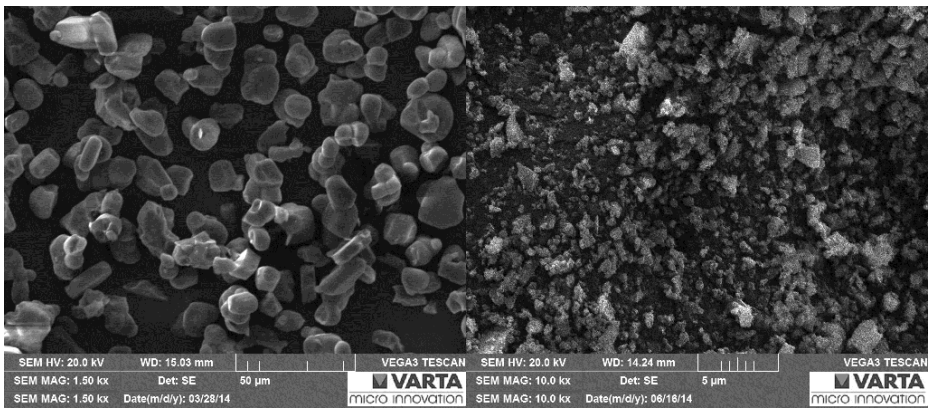

Figure 73: SEM images of BR-101H and fraction mill.

EDX of milling fractions

Figure 74 shows the EDX spectra of the qualitative analysis via EDX of fraction mill (left) and fraction housing (right). The EDX spectra of fraction housing shows peaks of Ca, Al, Si, N (phosphors host lattice), Au (sample preparation), C, O (adhesive tape) and Cu (sample foil) and Pt (interference of Zr and/or Au, see red arrows).

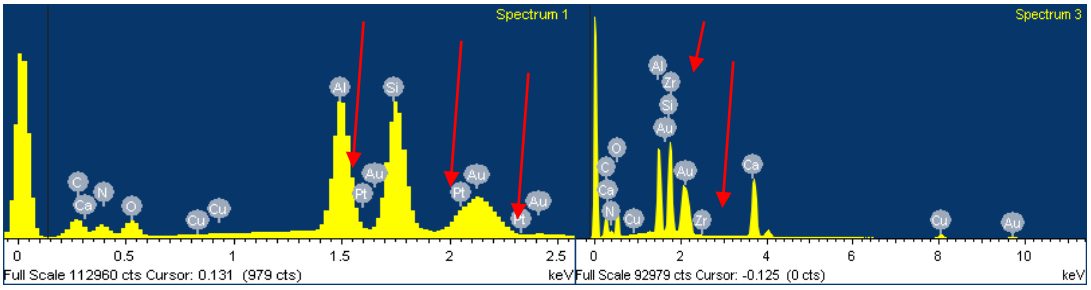

Figure 74: EDX spectra of fraction housing (left) and fraction mill (right)

The spectrum of fraction mill shows the same peaks for the phosphor host lattice, sample holder and preparation, but a sharp peak for Zr. Therefore it can concluded that, the longer the grinding process takes place the higher the amount of abrasion of milling balls (ZrO_2) and of the milling bowl (YSZ) in the product (see red arrows).

ATR-IR of milling fractions

Figure 75 (left) shows the ATR-IR spectra of BR-101H, fraction mill and fraction housing. In spite of drying at 100°C, the products fraction mill and fraction housing show a broad peak at 3600-3000cm^{-1} (see arrows in Figure 75, left), which can be ascribed to the $\tilde{\nu}$[O–H] group of residual water.[32]. The absorption peak intensities of fraction mill increased and even more in fraction housing in the range of 1020-375cm^{-1} compared to uncoated phosphor. The peak intensities of fraction mill and fraction housing increased a lot in the range of 1020-375cm^{-1} compared to uncoated phosphor (see arrows in Figure 75, right),

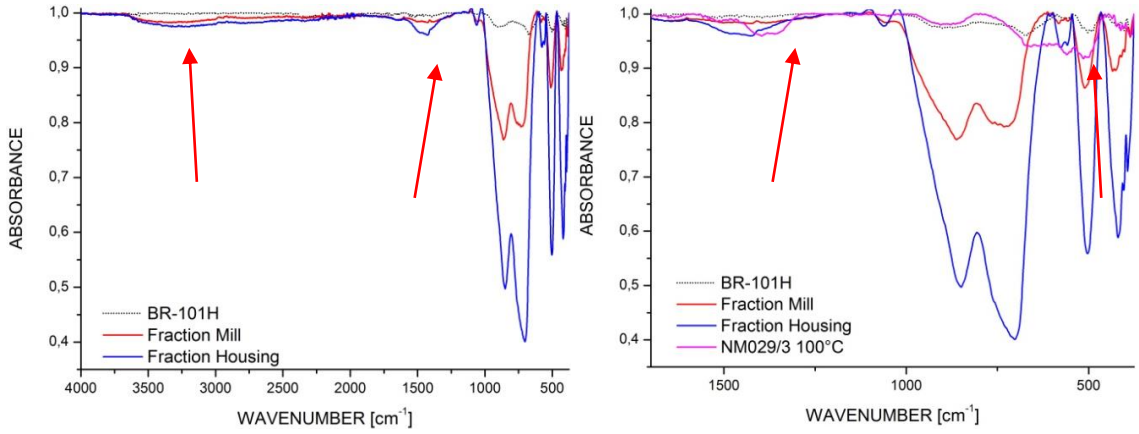

Figure 75: ATR-IR spectra of BR-101H, fraction mill, fraction housing and NM029/3 dried at 100°C.

Due to the fact that hydrolysis of $CaAlSiN_3$ via grinding process led to the formation of $Ca(OH)_2$, $Al(OH)_3$ and $Si(OH)_4$, significant absorption peaks should be found in the recorded spectra: Figure 75 (right) shows the ATR-IR spectra of BR-101H, fraction mill, fraction housing and NM029/3 (Al_2O_3 coating experiment) dried at 100°C. The milling process caused the generation of new absorption peaks (see arrows) in the area around 1600-1020cm^{-1}: One

broad absorption peak at 1430cm^{-1} and one sharp absorption peak at 1060cm^{-1} can be ascribed as the $\tilde{\nu}$[Si–O] stretch.[38]. The ATR-IR spectrum reveals a broad absorption peak around 1380cm^{-1} which can be assigned as a characteristic absorption band of to an aluminum oxide species.[32] Therefore it can be assumed that the milling process led to the formation of hydrolysis product like $Al(OH)_3$ and $Si(OH)_4$ as well as in a small extent to an aluminum oxide species and hydrated silica.

XRD of milling fractions

The XRD analysis revealed that fraction mill contains a considerable amount of the europium-activated calcium aluminum silicon nitride phosphors host lattice (ICSD 161796) shown in Figure 76 (lattice parameters did not changed in general). Therefore it can be said that only the surface of phosphor particles was hydrolyzed (compare to uncoated phosphor), not the bulk of the host lattice. Figure 76 shows big amorphous and crystalline parts which could not be ascribed to characteristic phases (increased background before background correction).

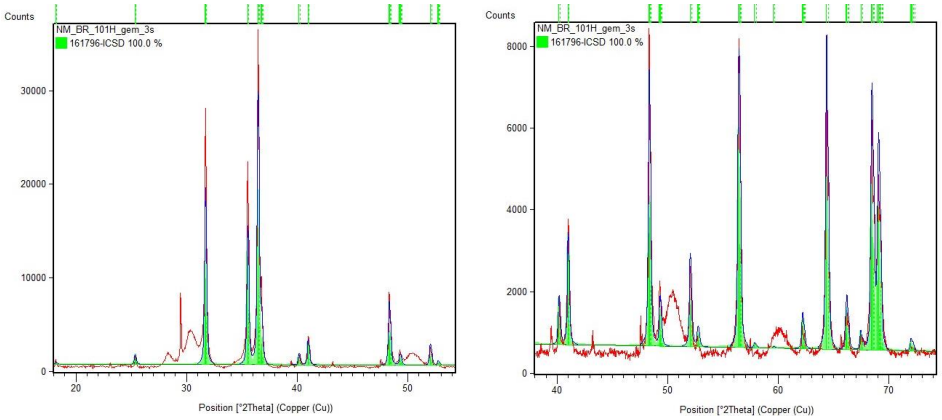

Figure 76: Powder diffractogram of fraction mill in the area between 18-55°2Θ (left) and between 38-75°2Θ (right).

LUMINESCENCE of milling fractions

Table 31 shows the results of luminescence measurement. The quantum yield of fraction mill decreases by a third compared to the untreated phosphor. As mentioned before (see Chapter 5.5) quenching of luminescence of the phosphor may occur while the grinding process, due to traces of Bismuth(III/V)oxide and Titanium oxide on the grounding balls as well as on the interior wall of the grounding bowl. This might be a reason for decreased quantum yield or to a part of the Eu^{2+} was oxidized to Eu^{3+} and therefore lost its typical luminescence behavior in some extent. Color coordinates also changed for the x value of 0.662 to 0.651 (-2%) and for the y value from 0.337 to 0.349 (+3%) (see Figure 77, left). Furthermore the excitation band of BR-101H and fraction mill do not differ in their range, but the shape of the emission band changed. In the area from 525nm to 560nm the small peak at 540nm increased and the emission maxima of fraction mill shifted to shorter wavelengths from 643nm to 634nm (see Figure 77, right).

Table 31: Results of luminescence measurement of fraction mill and BR-101H.

Sample	Quantum Efficiency [%]	x	y	Emission Maxima [nm]
BR-101H	75	0.662	0.337	642
fraction mill	23	0.651	0.346	634

Because of the negative results from luminescence measurement related to decreased quantum efficiency, shift of emission maximum and shift of CIE color coordinates and despite of the fact that grounded particles show a modified surface of Al_2O_3 as well as of SiO_2 (as determined by ATR-IR, SEM and EDX) they are not considered for further coating experiments and for encapsulation into a low melting glass.

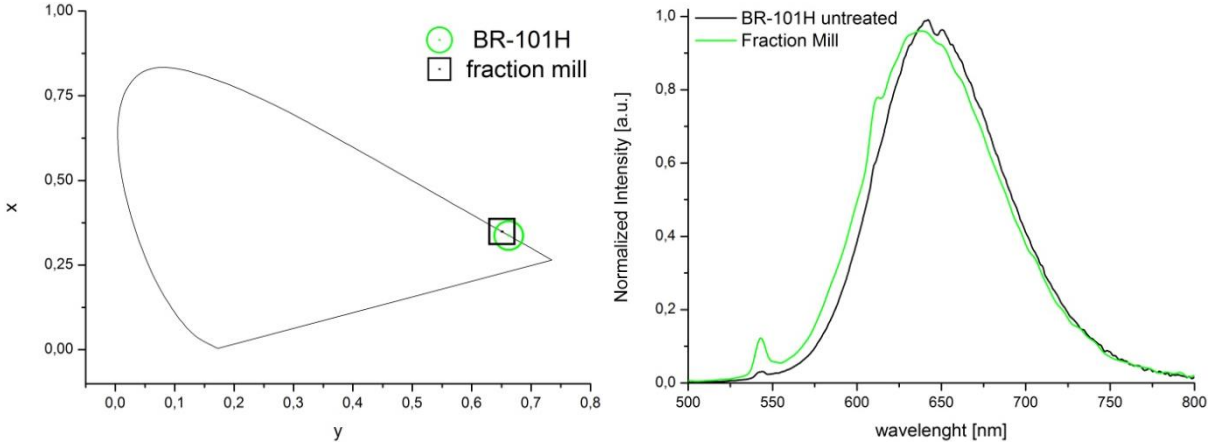

Figure 77: CIE color coordinates and emission and excitation spectra of BR-101H before and after grinding.

6.3 Encapsulation into Glass

6.3.1 Characterization of ZASNP11C

The SEM analysis revealed an irregular particle shape and a large particle size distribution from the nm area till 25µm as shown in Figure 78 (left). Due to the project report[37] ZASNP11C contains 50.0mol% $NH_4H_2PO_4$, Na_2O 16.0mol%, 8.0mol% $ZnSO_4$ and 0.5mol% Al_2O_3. The results of EDX analysis confirmed following elements: O, Al, P and Zn. S was not found and H cannot be detected with EDX and sodium shows interference with Zn. The recorded spectrum of X-ray Fluorescence Spectroscopy carried out with a FISCHERSCOPE® X-RAY XAN-FD from Helmut Fischer GmbH & Co KG showed peaks for Zn and Mo (see Figure 78, right). Mo is not part of the glass matrix and can be assigned as interference from S (see Figure 78 red arrow with K_α 2.5keV).

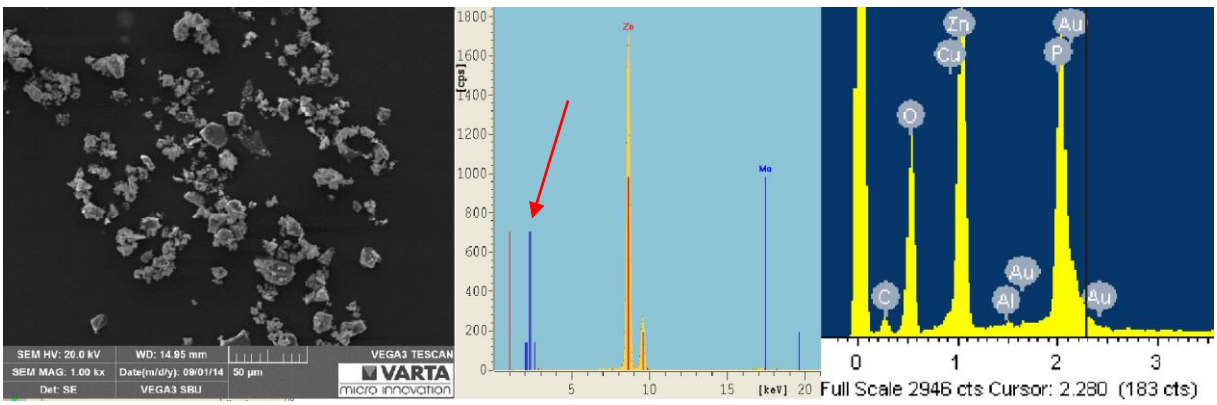

Figure 78: SEM image (left), the XFA spectrum (mid) and the EDX spectrum (right) of ZASNP11C.

6.3.2 Encapsulation into Bullseye Glass

Experiments in a Domed Hot Stage

As the sample was placed on a silicon wafer and not on the supplied sample holders of the Domed Hot Stage oven, the temperature in the oven had to be applied higher, because the heat transfer from the sample holder to the sample was not optimal. Besides that the reaction chamber was flooded with 0.01bar Ar to avoid undesired reactions. Due to this a modified firing schedule with much higher temperatures was used to encapsulate 5wt% BR-101H in Bullseye Glass (see Table 32).

Table 32: Modified firing schedule for encapsulation experiments of Bullseye Glass.

Step	Description	T_{RANGE} [°C]	$Rate_{HEATING}$ [°C/min]	$Rate_{COOLING}$ [°C/min]	T_{HOLD} [min]
1	Initial Process Soak	25-800	6	-	10
2	Rapid Cool Down	800-482	-	9	60
3	Anneal Cool	482-371	-	1	-
4	Final Cool	371-25	-	Natural Cooling	-

Figure 79 (left) shows the reaction chamber and next to it the unexcited and excited phosphor BR101H and NM029 samples before and after the sinter process at 800°C. The color of phosphor material changed as well as the emitted light after excitation. Sample B shows an obvious color change compared to the untreated sample A. Figure 79 right shows the excited phosphor after the sinter process at 800°C. The luminescence of sample D compared to C is nonexistent. Due to the appearance of the product can be concluded, that some reaction occurred (product is not molten but consists of particles). The temperature treated sample appears harder. This can be explained by sintered grains of glass. Grainboundaries migth have been started to be formed. As the powder was loose and not compressed (difussion ways are longer) no compact glass panel was fomed. Furthermore caused the flow of inert gas a lower temperature than given. The same procedure was carried out with 5wt% of coated phosphor NM029 in Bullseye glass as shown in Figure 79 (E and F). Again no luminescence of treated phosphor is to be seen. Due to this results can be said that the uncoated phosphor BR-101H (B and D) and the coated phosphor NM029 (F) are not stable at these high temperatures. For further information about the encapsulation of coated phosphor particles in any glass, test via TG-DSC-MS give important information about the characteristics of the glass.

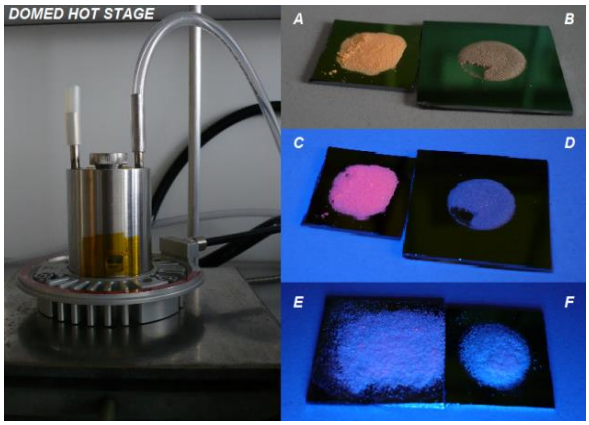

Figure 79: Domed Hot Stage with an extra unit (left). Luminescence of encapsulated phosphor in Bullseye glass. BR-101H before and after sinter process at 800°C unexcited (above A and B) and excited (below C and D, and of 5wt% NM029 in Bullseye Glass before (E) and after sinter process (F) at 800°C, excited by a blue LED.

6.3.3 Encapsulation in ZASNP11C

Experiments in a tubular furnace

After the negative results from encapsulation pretest in Bullseye Glass the behavior of ZASNP11C was investigated at normal pressure: First it was necessary to determine the temperature at which the glass powder starts to show changes in its appearance. A small amount of glass powder was placed on a silicon wafer (see Figure 80, left). The samples were heated up from a starting temperature of 400°C in 10°C steps under inert gas atmosphere of N_2 until softening occurred. At 510°C a transformation occurred: The powder began to liquefy and increased its volume. The colorless powder turned light grey (shown in Figure 80, right). The temperature was held for 30 minutes and naturally cooled down under N_2 flow. After cooling down to room temperature the sintered glass was separated from the silicon wafer.

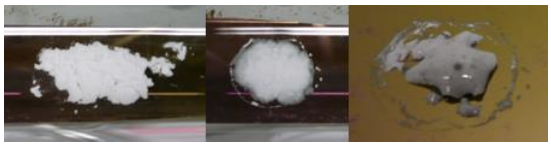

Figure 80: ZASNP11C before sinter process (left), at a temperature of 500°C (mid) and after a sintering temperature of 510 and cooled down to RT (right).

After pretests and determination of a softening range, experiments were carried out in aluminum bowls purchased from NeoLab® and formed to a small bowl with a diameter of 10mm. Aluminum as a sample holder is preferred because of its melting point at 659°C and its suitable thermal conductivity of 204 W/m·K (at 1.013bar and 20°C).[47] Due to the results of SEM, EDX and FIB following samples were chosen to be encapsulated in ZASNP11C. Besides the coated phosphor samples NM029 and NM032, the uncoated phosphor BR-101H should serve as reference. The samples started to melt at 540°C in the aluminum bowls. The temperature was increased up to 560°C to melt the whole sample. The temperature treatment was again too high, because the volume doubled in size and the color of the sample got brownish, except the uncoated phosphor (Figure 81). Hence luminescence is still visible after excitation with a conventional blue LED. The uncoated phosphor shows no loss of luminescence. Besides the loss luminescence of encapsulated samples the volume of the glass sample as well as the encapsulated samples increased: The structure is like foam and the color changed from white to brownish-green. Due to this it might be assumed that a spinel of structure AB_2X_4 presumably $ZnAl_2O_4$ or $ZnAl_2S_4$ was formed (bowls or Al_2O_3 from glass as aluminum source).[48] This has to be proved or disproved via TG-DSC-MS analysis.

Figure 81: ZASNP11C (A), 5gt% of BR-101H in ZASNP11C (B), 5gt% of NM029 in ZASNP11C (C) and 5gt% of NM032 in ZASNP11C (D).

TG-DSC-MS Experiments

Due to the above mentioned changes in shape, volume and color, further experiments were carried out, to observe any changes while encapsulation process. The samples were heated up from room temperature with a heating rate of 10°K/min to an end temperature of 710°C.

The evaluated TG-DSC-MS curves by ICTM can be seen in Appendix 9.4. Figure 82 shows the results of TG-DSC analysis of pure ZASNP11C, 5wt% BR-101H in ZASNP11C and 5wt% NM029 in ZASNP11C. It was decided to analyse the not corrected curves due to signal deterioration of endothermic and exothermic peaks. The obtained not corrected curves of TG analysis (dotted line) show a mass decrease below 100°C due to water evaporation. Besides that all curves show no major changes until 570°C. Above 570°C mass loss of sample 5wt% BR-101H in ZASNP11C and at around 630°C a low mass loss of samples ZASNP11C and 5wt% NM029 in ZASNP11C occurred.

The obtained not corrected curves of DSC analysis (solid line) have one in common: In the range of 35°C to 200°C they show a slope, which results through equilibration of the measurement set up and it is dependent on the atmosphere in the oven (adjustment phase of thermoelectric voltage). After equilibration all curves arise with increasing temperature. After that temperature, they do differ in shape, due to processes in the different samples, which will be following explained. On closer inspection first noticeable changes occur for all samples above 350°C. This change can be ascribed to a change in the glass framework: The glass transition T_g temperature is defined as a transition in amorphous materials from a hard and relatively brittle state into a molten state. Or in other words, the glass transition while heating is a reversible process in which heat is absorbed to accommodate the increase of the heat capacity during the transition.[49] The values for T_g of all samples are shown in Table 33: T_g values for ZASNP11C and 5wt% BR-101H could been determined (see Figure 82 label at symbol+), but not for 5wt% NM029 in ZASNP11C. The determination of the point of inflection was difficult and therefore not possible for sample 5wt% NM029 in ZASNP11C. It can be assumed that no sharp transition (missing step) in the range of 354-390°C occurs. Based on these results, a blend of 5wt% of coated phosphor NM029 in ZASNP11C does influence the characteristics of ZASNP11C due to its changed sintering process (see Figure 82 and compare DSC curve ZASNP11C and 5wt% NM029 in ZASNP11C). Another characteristic temperature is the crystallization temperature T_x, which indicates the beginning of crystallization (T_x, see DSC curves) and occurs after the end of the sintering stage or maximum shrinkage (T_{MS}).[50] Crystallization is a non-reversible exothermic process which releases heat, other than at T_g.[49] ZASNP11C shows two T_g's: First at 350.5°C and the second at 561.9°C. Jena reported a T_g of 380°C. In general ZASNP11C does not behave like a common glass, due to its composition. ZASNP11C can be defined as a material on the border between glasses and ceramics. Besides classic components of glasses like Al_2O_3 and Na_2O, ZNSAP11C contain ingredients like ZnO, $NH_4H_2PO_4$ and $ZnSO_4$, which change the microstructure of the glass and thus its sintering characteristics.

Table 33: Determined T_g and T_x values by TG-DSC-MS analysis of ZASNP11C, encapsulated samples 5wt% BR-101H in ZASNP11C and 5wt% NM029 in ZASNP11C.

T [°C]	pure	5wt% BR-101H	5wt% NM029
$T_{g,1}$	350.5	372.4	-
$T_{x,1}$	415.1	415.0	-
$T_{g,2}$	561.9	-	-
$T_{x,2}$	-	-	-

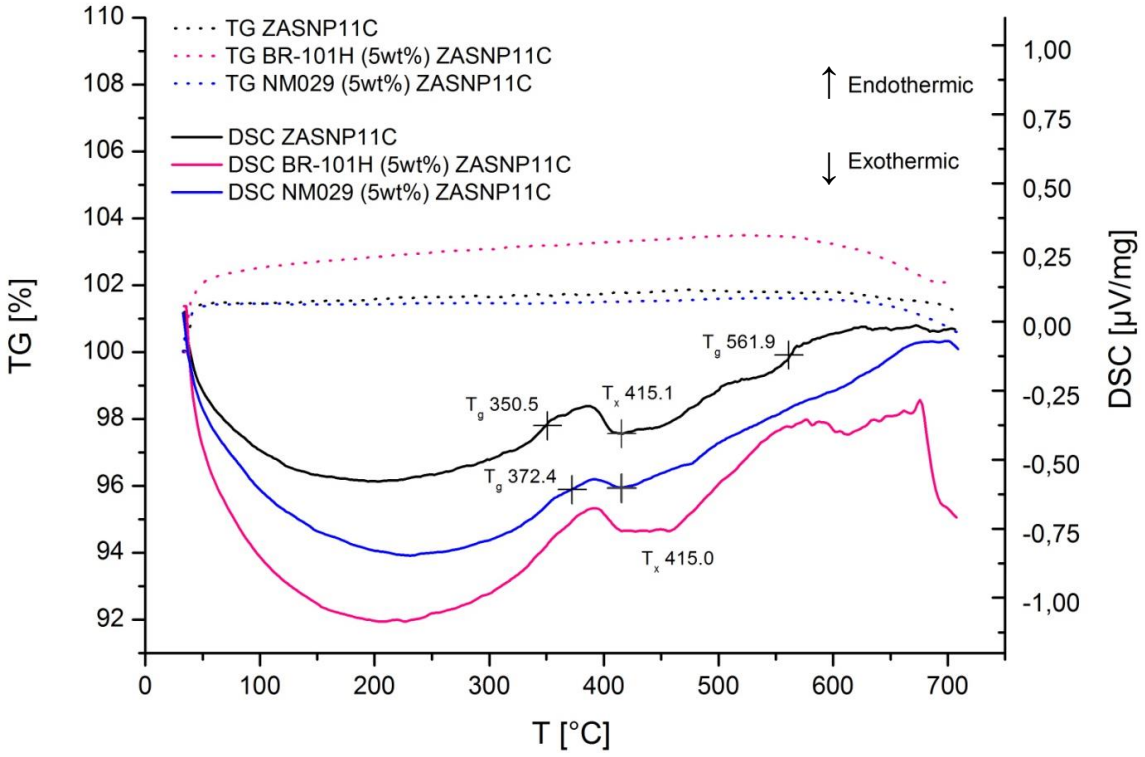

Figure 82: Comparison of TG and DSC curves of ZASNP11C, 5wt% BR-101H in ZASNP11C and 5wt% NM029 in ZASNP11C.

Figure 83 shows the DSC-MS curves of ZASNP11C, 5wt% BR-101H in ZASNP11C and 5wt% NM029 in ZASNP11C in detail. The peaks in the DSC curves (dotted black line) give information about whether a reaction was endothermic (↑) or exothermic (↓). MS curves of ions with molar masses of 12-207 are shown in colored solid lines. Sample ZASNP11C as well as 5wt% NM029 in ZASNP11C show no major changes after T_x, whereby a rash exothermic reaction occurs starting at 560°C in sample 5wt% BR-101H in ZASNP11C (pink line). Several small peaks and a large peak at 675°C indicate decomposition of uncoated phosphor $CaAlSiN_3$ (mass decrease of -1.5%) with increasing temperature. Decomposition of 5wt% BR-101H in ZASNP11C goes along with signals for O_2^+ [36] (brown line), for SO^+ [48] (cyan line) and S_2, SO_2 [64] (purple line) detected via coupled MS. As $ZnSO_4$ is a part of ZASNP11C it decomposes into ZnO, SO_2 and O_2 at temperatures above 680°C.[51] ZASNP11C show decomposition in low extent starting at 630.0°C (mass decrease of -0.2%). This decomposition goes along with a signals for S_2, SO_2 [64] (blue line) due to decomposition of $ZnSO_4$. These results correspond to the mass loss shown in the TG curves at a temperature around 570°C. The endothermic signals at around 380°C for CO_2^+ [44] (green line) can be ascribed to adherent CO_2, since it is not part of the composition of the glass powder nor of the phosphor. 5wt% NM029 in ZASNP11C show no prove of decomposition until 700°C. It show a small endothermic peak due to the formation of S_2, SO_2 [64] from decomposition of $ZnSO_4$.

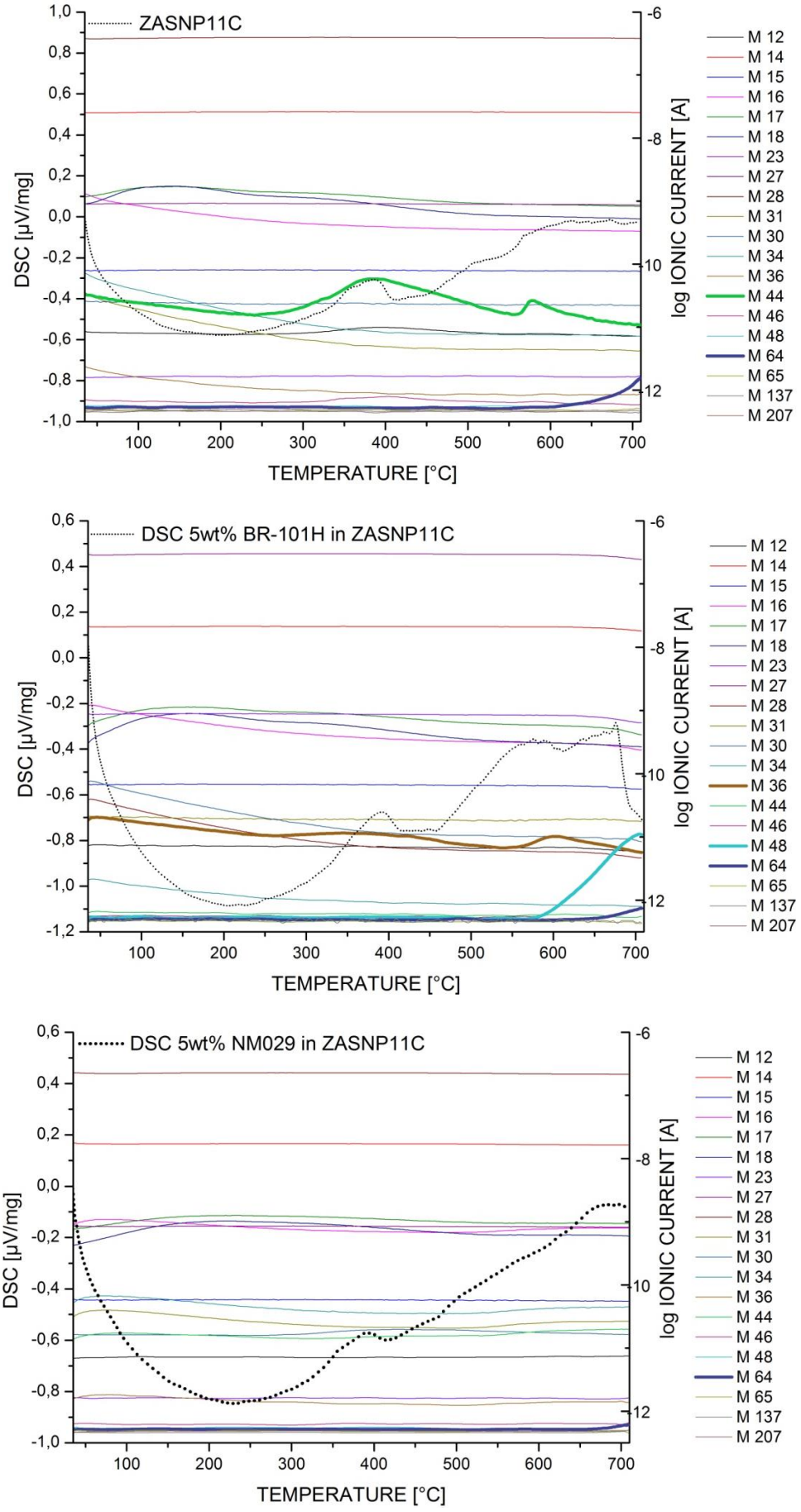

Figure 83: DSC-MS curves of ZASNP11C, 5wt% BR-101H in ZASNP11C and 5wt% NM029 in ZASNP11C in the range of 35°C-710°C with MS results of molar masses M=12-207.

Figure 84 shows the obtained products after TG-DSC-MS analysis. The colors of the obtained products changed like in the pretest from Chapter 6.3.3 in Figure 81. No luminescence after temperature treatment is seen, because the glass was blended with only 5wt% phosphor. Besides that is the obtained product not transparent for light.

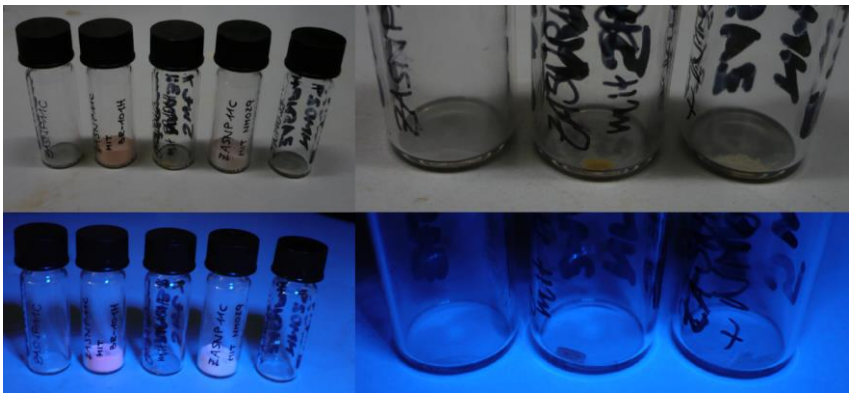

Figure 84: Luminescence behavior of samples characterized by TG-DSC before and after temperature treatment (710°C) unexcited (above) and excited (below). The enlarged picture shows pure ZASNP11C (left), 5wt% BR-101H in ZASNP11C (mid) and 5wt% NM029 in ZASNP11C (right).

As a consequence of the results of TG-DSC-MS analysis following conclusion can be drawn: The obtained Al_2O_3 coating determined by SEM, EDX, FIB, XRD and ATR-IR has improved the phosphors properties according to its stability against temperatures above 550°C. No decomposition occurs. Thus our proposed Al_2O_3 coated phosphor particles can be encapsulated into ZASNP11C and therefore it can be presumed that our coated phosphor particles can be also encapsulated into other glass types with even higher T_g's. The glass ZASNP11C is not well suited for melting and processing at atmospheric pressure. As it is already described in the Jena report a processing at higher pressure , like pressure sintering would be preferable.

7 CONCLUSION

Experiments in this work were carried out in order to obtain SiO_2, Al_2O_3 and MgO coated silicon nitride phosphor particles to improve their thermal stability, as they tend to be degraded by atmospheric moisture and elevated temperatures under operation.

Unfortunately no SiO_2 coated phosphor particle *via* a modified Stöber synthesis were confirmed. All efforts already failed due to the conditional sensitivity of used barium silicon nitride phosphor LP-N620. Since acids and bases are needed as catalysts in the hydrolysis of TEOS, to form a SiO_2 layer on the phosphor particles, the phosphors host lattice was hydrolyzed by water. This occurred in a certain extent, which was observable by the phosphors luminescence behavior after the coating procedure. Almost all emission maxima shifted from 621nm to shorter wavelengths. NM001-NM003 show shifts of even 20nm to shorter wavelengths. Due to unsatisfying results SiO_2 coating experiments were stopped.

Al_2O_3 or MgO coated phosphor particles were obtained by a two-step-synthesis: *Via* a Brønsted precipitation reaction from a mixture of aluminum nitrate as well as magnesium chloride with a base metal hydroxides were formed and further annealed by an appropriate temperature treatment of 400°C to form a metal oxide layer of Al_2O_3 and MgO on phosphor particles. ATR-IR indicated the formation of metal hydroxide after coating process on the coated samples by characteristic absorption bands of $\tilde{\upsilon}$[O-H], which vanished after temperature treatment at 400°C. Absorption peaks for $\tilde{\upsilon}$[Al-O] and $\tilde{\upsilon}$[Al-O-Al] as well as $\tilde{\upsilon}$[Mg-O] indicated the formation of Al_2O_3 and MgO. Furthermore SEM (SE, BSE, FIB) images of cross sections illustrated that the obtained layer of metal oxide covers the whole phosphor grain. XRD measurements exhibit that the coating and the annealing process did not damage the phosphors host lattice. Only the surface of phosphor particles gets hydrolyzed by the coating procedure not the bulk. Luminescence properties of the coated phosphor samples did not changed in general, only negligible shifts of emission maxima and CIE color coordinates occurred. Due to the obtained layer of metal oxide on phosphor particles, the quantum yield decreased caused by diffuse scattering of light on the amorphous oxide layer. Moreover an oxidation of the activator ion Eu^{2+} to Eu^{3+} did not occur.

We have demonstrated a route to coat an europium activated $CaAlSiN_3$ phosphor with metal oxide layers of Al_2O_3 and MgO for further use in Chip-On-Board Technology. TG-DSC-MS measurements on pure ZASNP11, 5wt% BR-101H in ZASNP11 and 5wt% NM029 in ZASNP11C have proved unambiguously that the thermal stability of coated phosphor has improved compared to uncoated phosphor. Therefore Al_2O_3 coated phosphor particles are suitable for the encapsulation into the glass ZASNP11C.

8 FUTURE PROSPECTS

We describe a possible sample preparation, a design layout of the annealing body, a firing schedule and characterization methods for the inspection of the successful implementation of encapsulation of coated phosphor particles in ZASNP11C as followed.

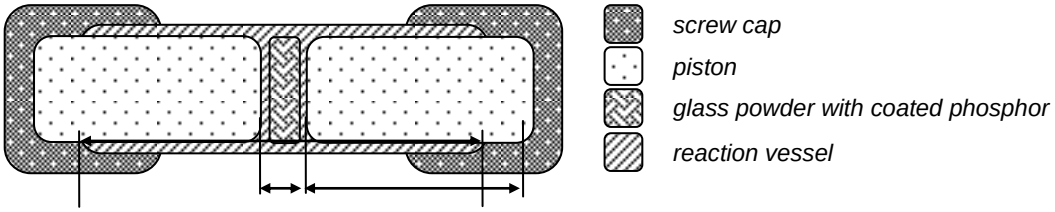

Figure 85: Sketch of the annealing body for encapsulation of coated phosphor particles in glass ZASNP1C.

The assembling of the sample should be carried out in a glove box containing N_2 or Ar. The glass powder should be mixed with maximum 5% by weight, in order to keep the properties of the glass material and not to modify its structural conditions. We suggest using a reaction vessel shown in Figure 28 made out of steel, and pistons made out of aluminum to generate the needed pressure by use of different coefficients of linear expansion. On the assumption of the linear expansion Δl of steel to be equal with the linear expansion Δl of aluminum and Δl of glass, the following calculation for the linear expansion of aluminum $\Delta l_{Al} = l_0 \cdot \alpha \cdot \Delta T$ in due consideration of the pressure margin can be formulated as followed:[52]

$$\Delta l_{steel} = \Delta l_{Al} + \Delta l_{glass}$$

$$l_1 \cdot \alpha_{steel} \cdot \Delta T = \left(l_2 \cdot 2 \cdot \alpha_{aluminum} + l_3 \cdot \alpha_{glass}\right) \cdot \Delta T$$

$$l_2 = \frac{l_1 \cdot \alpha_{steel} - l_3 \cdot \alpha_{glass}}{2 \cdot \alpha_{aluminum}}$$

Table 10 shows the coefficients of linear expansion α of steel, aluminum and glass. Aluminum has a larger coefficients of linear expansion α than steel, thus aluminum is going to expand in length under thermal treatment according to the last equation.

Table 34: Coefficients of thermal expansion α of steel, aluminum and glass and the legend for the pattern of Figure 86.[47]

Material	Coefficient of Thermal Expansion α $[1/K]$	Pattern Legend
Steel	$1.15 \cdot 10^{-5}$	
Aluminum	$2.38 \cdot 10^{-5}$	
Glass (flint, SiO_2)	$8.0 \cdot 10^{-6}$	

We recommend adhering to the following firing schedule: The sintering process should be carried out at 400°C for duration of at least 15 minutes.[37] The cooling should be naturally carried out. The product should be grounded and characterized by Fluorescence Spectroscopy in order to proof the luminescence properties after encapsulation. To compare the results the same procedure should be done with uncoated phosphor BR-101H. Furthermore a long-term-testing in a saturated humid atmosphere under working conditions should be carried out to see if an encapsulation into glass is better than an encapsulation in silicone like it is state of the art.

9 REFERENCES

[1] *http://dictionary.reference.com/browse/led*, 05.08.**2014**, *12:28*

[2] Brown, T.L.; LeMay, H.E., Bursten, B.E.: *Chemie: Die zentrale Wissenschaft*, Pearson **2007**, 10. Edition, p.593

[3] Schubert, E.F.: *Light-Emitting Diodes*, Cambridge University Press **2005**, Chapter 4, p.55

[4] Jüstel, T.; Nikol, H.; Ronda, C.: *Angew. Chem.* Int. Ed. **1998**, 37, p.3084-3103

[5] *http://en.wikipedia.org/wiki/Light-emitting_diode*, 05.08.**2014**, 12:40

[6] Litfin, G.: *Technische Optik in der Praxis*, Springer **2005**, 3.Edition, Chapter 7, p.179-183

[7] Hur, S.; Song, H.J.; Roh, S.-S.; Kim D.-W.; Hong, K.S.: *Mater. Chem. and Phys.* **2013**, 139, p.350-354

[8] Piao, X.; Machida, K.-I.; Horikawa, T.; Hanzawa, H.; Shimomura, Y.; Kijama, N.: *Chem. Mater.* **2007**, 19, p.4592-4599

[9] *http://ec.europa.eu/energy/lumen/index_en.htm*, 05.08.**2014**, 13:02

[10] *http://www.lumitech.at*: *Die hohe Kunst: Weißes Licht, Farbkonversion*, p.1-6

[11] Jüstel, T.; www.fh-muenster.de/juestel: *Leuchtstoffe für LED-Applikationen* **2014**, p.1-34

[12] Poynton, C.; *Computer Graphics, Algorithms and Interfaces*, Chapter 25: The CIE system of colorimetry, Morgan Kaufmann Series **2012**, 2.Edition, p.265–286

[13] Godman, T.M.: *Colour Design: Theories and Applications*, *International standards for color,* Woodhead Publishing **2012**, Chapter 7, p.177-218

[14] Song, J.-M.; Park, J.-S.; Nahm, S.: *Ceram. Int.* **2013**, 39, p.2845-2850

[15] Kim, H.S.; Horikawa, T.; Hanzawa, H.; *Machida, K.: J. Phys. Conf. Ser.* **2012**, 379, p.1-4

[16] Uheda, K.; Hirosaki, N.; Yamamoto, Y.; Naito, A.; Nakajima, T.; Xamamoto, H.: *Electrochem. Solid St.* **2006**, 9 (4), H22-H25

[17] Yamamoto, H.: *Nitride Semiconductor Light-Emitting Diodes (LEDs): Materials, Technologies and Applications,* **2014**, p.144–180

[18] Yang, L.; Zhang, Na; Zhang, R.; Wen, Bo; Li, H.; Bian, X.: *Mater. Lett.* **2014**, p.134-136

[19] Wen, H.; Wang, F.: *Nanocrystalline Materials* **2014**, Second Edition, p.121-123

[20] Murphy et al.: *US Patent Application Publication* **2011**, 0279011/A1, p.1-9

[21] *http://www.lumitech.at: Maximale Energieefizienz, COB LED-Module*

[22] Luo, X.; Hu, R.: *Nitride Semiconductor Light-Emitting Diodes (LEDs) Materials, Technologies and Applications* **2014**, Chapter 15, p.441-462

[23] Sun, J.; Sun, R.; Du, H.: *Appl. Surf. Sci.* **2012**, 258, p.4569-4573

[24] Zhuang, J.; Xia, Z.; Liu, H.; Zhang, Z.; Lia, L.: *Appl. Surf. Sci.* **2011**, 257, p.4350-4353

[25] Stöber, W; Fink, A.; Bohn, E.: *J. Colloid Interface Sci.* **1968,** 26, p.62-69

[26] Azuma, Y.; Nogami, K.; Ohshima N.: *J. Ceram. Soc. JPN,* **2006**, Int. Edition, Vol.100, p.639-644

[27] Büchner, W.; Schliebs, R.; Winter, K.H.; Büchel, G.: *Industrielle Anorganische Chemie, Verlag Chemie GmbH* **1984**, Chapter 4, p.299-317

[28] Schrank, F.; Pachler, P.; Reil, F.: *Lebensdauer und Zuverlässigkeit in der LED-Beleuchtung: Systemstabilität Konverter; LED-Modul Untersuchung des Einflusses von Ripple und Temperatur, Presentation at VDI –Konferenz* **2014**, p.1-21

[29] *http://echa.europa.eu/documents/10162/49bc364c-db7a-45c5-9d58-8cf3d69ae72a*, 07.08.**2014**, 20:46

[30] Zhang, Z.;Delsing, A.C.A.; Notten, P.H.L.; Zhao, J.; Dorenbos, P.; Hintzen, H.T.: *ESC J. Solid State Sci. Technol.* **2013**, 2 (4), R70-R75

[31] Hollemann, A.F.; Wiberg, E.: Wiberg, N. *Lehrbuch der Anorganischen Chemie* **2007**,102.Edition, p.1838-1841

[32] Ghezelbash, Z.; Ashouri, D.; Mousavian, S.; Ghandi, A., H.; Rahnama, Y.: *Bull. Mater. Sci.* **2012**, 35, p.925-931

[33] Hofmann, H.; Renken, A.; Baerns, M.: *Chemische Reaktionstechnik - Lehrbuch der Technischen Chemie Band 1* **1992**, 2.Edition, p.241

[34] *http://www.duran-group.com/de/ueber-duran/duran-eigenschaften.html,* 25.08.**2014**,14:16

[35] *http://www.corninggorillaglass.com/products-with-gorilla*, 12.08.**2014**, 09:16

[36] *http://www.corning.com/docs/specialtymaterials/pisheets/PI2317.pdf*, 12.08.**2014**, 9:32

[37] Hermann, A.: Projektbericht zu Einbettung und Beschichtung verschiedener Chromophore zur Erzielung einer verbesserten Langzeitstabilität gegenüber Feuchtigkeit, Temperatur und Strahlung-Phase I, Friedrich-Schiller-Universität Jena, Otto-Schott-Institut für Glaschemie **2011**, p.1-11

[38] Rubio, F.; Rubio, J.; Oteo, J.L.: *Spectrosc.Int. J.* **1998**, p.199-219

[39] *http://webbook.nist.gov/cgi/cbook.cgi?ID=C78104&Mask=80*, 01.09.**2014**, 09:03

[40] Hollemann, A.F.; Wiberg, E.; Wiberg, N.: *Lehrbuch der Anorganischen Chemie* **1995**,102.Edition, S.1081

[41] Rinoud, H.: *J. Am. Ceram. Soc.* **1964**, Vol.48, No.7, p.376-380

[42] Hollemann, A.F.; Wiberg, E.; Wiberg, *N.*: *Lehrbuch der Anorganischen Chemie* **2007**,102.Edition, p.241-242

[43] Hollemann, A.F.; Wiberg, E.; Wiberg, N.: *Lehrbuch der Anorganischen Chemie* **1995**,102. Edition, S.1077-1078

[44] Hollemann, A.F.; Wiberg, E.; Wiberg, N.: *Lehrbuch der Anorganischen Chemie* **1995**,102. Edition, S.1120

[45] Zhang, J.; Chen, B.; Liang, Z.; Li, X.; Sun, J.; Cheng, L.; Zhong, H.: *J. Alloy. Comp.* **2014**, p.204-209

[46] FRITSCH, Germany, *http://www.fritsch.de/produkte/mahlen/planetenmuehlen/,* 09.04.**2014**, 16:02

[47] *Tabellenbuch Metall* **1999**, 41. Neubearbeitete und erweiterte Auflage, p.112-113

[48] Hollemann, A.F.; Wiberg, E.; Wiberg, N.: *Lehrbuch der Anorganischen Chemie* **2007**,102. Edition, S.1162

[49] Sahoo, K.L.; Sahu, R.: *J. Non-Cryst. Solids* **2013**, 365, p.33-36

[50] Lara, C; Pascual, M.J.; Duran, A.: *J. Non-Cryst. Solids* **2004**, 348, p.149-155

[51] *https://roempp.thieme.de/roempp4.0/do/data/RD-26-00409*, Georg Thieme Verlag KG, 16.09.**2014**, 16:45

[52] Fischer, R.; Stadlbauer, S.: *Institute of Inorganic Chemistry, Graz University of Technology* **2014**

10 APPENDIX

10.1 List of Figures

All Figures, except Figure 1, 2, 3, 4, 5, 6, 7, 8, 10, 24 and 51 has been obtained via the program OriginPro 8.5, were drawn in Microsoft WORD, pictures of experiments were taken by Nika Mahne or are labeled in the right corner of the image (FELMI, MCL and VARTA MICRO INOVATION).

Figure 1	http://spectrum.ieee.org/semiconductors/optoelectronics/the-leds-dark-secret, 28.07.**2014**, 22:36
Figure 2	http://dangerousprototypes.com/docs/File:PN_junction.png, 28.07.**2014**, 18:34
Figure 3	http://de.wikipedia.org/wiki/Leuchtdiode#mediaviewer/Datei:Bandmodellkrp.png, 28.07.**2014** 21:15
Figure 4	http://www.gluehbirne.ist.org/led.php, 05.08.**2014**, 13:25
Figure 5	www.fh-muenster.de/juestel: *Leuchtstoffe für LED-Applikationen* **2014**, p.5-6
Figure 6 (r)	http://upload.wikimedia.org/wikipedia/commons/5/5f/CIE-1931_diagram_in_LAB_space.svg, 24.09.**2014**, 22:10 Poynton, C.; Computer Graphics, Algorithms and Interfaces, Chapter 25: The CIE system of colorimetry, Morgan Kaufmann Series **2012**, 2.Edition, p.265–286
Figure 6 (l)	Poynton, C.; Computer Graphics, Algorithms and Interfaces, Chapter 25: The CIE system of colorimetry, Morgan Kaufmann Series **2012**, 2.Edition, p.265–286
Figure 7	www.fh-muenster.de/juestel: *Leuchtstoffe für LED-Applikationen* **2014**, p.27
Figure 8	TRIDONIC Jennersdorf GmbH, **2014**
Figure 10	Murphy et al.: *US Patent Application Publication* **2011**, 0279011/A1, Front Page
Figure 24	*http://webbook.nist.gov/cgi/cbook.cgi?ID=C78104&Mask=80*, 24.09.**2014**, 14:17
Figure 51	*http://li155-94.members.linode.com/myscope/analysis/eds/xraygeneration/* 10.09.**2014**, 16:58

10.2 List of Abbreviations

AFAP	As Fast As Possible
ATR-IR	Attenuated Total Reflection Infrared Spectroscopy
BSE	Backscattered Electrons
CIE	Commission Internationale de l'Éclairage
COB	Chip-On-Board
DSC	Differential Scanning Calorimetry
EDX	Energy-dispersive X-ray Spectroscopy
ESD	Electrostatic Discharge
FIB	Focused Ion Beam
LED	Light Emitting Diode
MS	Mass Spectroscopy
MSDS	Material Safety Data Sheet
SE	Secondary Electrons
SEM	Scanning Electron Microscopy
SLS	Static Light Scattering
TEOS	Tetraethyl Orthosilicate
TG	Thermogravimetry
UV	Ultraviolet
VIS	Visible Light
XRD	X-ray Diffraction
XRF	X-ray Fluorescence Spectroscopy

10.3 Table of Synthesis Parameters

Table 35: Preparation and amount of educts for SiO_2 coating experiments and parameters with europium activated $Ba_2Si_5N_8$ phosphor after Azuma et al.[26]

Number	m [g] $Ba_2Si_5N_8$	V [ml] EtOH	V [ml] NH_3	V [ml] HCl	V [ml] H_2O	t_{adding} [min] TEOS	V [ml] TEOS in H_2O	Treaction time [h:min]	Separation Method	V [ml] Dispersant
NM001-1	0.1481	2.7	12.1, 1M	-	0.36	10	0.17 in 40	3:00	Filtration	none
NM001-2	0.1527	2.7	12.1, 2M	-	0.36	10	0.17 in 40	3:00	Filtration	none
NM002-1	0.5020	5.0	47.3, 1M	-	1.4	10	0.7 in 50	3:00	Centrifugation	none
				-		90	0.3 in 5			
NM002-2	0.5121	5.0	47.3, 2M	-	1.4	10	0.7 in 50	3:00	Centrifugation	none
				-		90	0.3 in 5			
NM003-1	0.5004	10	47.3, 1M	-	1.4	10	0.53 in 5	3:00	Centrifugation	none
				-		45	0.53 in 5			
				-		90	0.53 in 5			
				-		120	0.53 in 5			
				-		125	0.53 in 5			
NM003-2	0.4909	10	47.3, 2M	-	1.4	10	0.53 in 5	3:00	Centrifugation	none
				-		45	0.53 in 5			
				-		90	0.53 in 5			
				-		120	0.53 in 5			
				-		125	0.53 in 5			
NM004-1	0.4940	10	47.3, 1M	-	1.4	10	0.53 in 5	3:00	Centrifugation	none
NM004-3	0.4816	10	-	47.3, 1M	1.4	10	0.53 in 5	3:00	Centrifugation	none

Table 36: Preparation and amount of educts for SiO_2 coating experiments and parameters with europium activated $Ba_2Si_5N_8$ phosphor after Murphy et al.[20]

Number	m [g] $Ba_2Si_5N_8$	V [ml] EtOH	V [ml] TEOS	V [ml] H_2O	t_{adding} [min] TEOS	V [ml] TEOS in H_2O	pH-value	$T_{reaction}$ [h:min]	Separation Method	T_{Bath} [°C]	V [ml] Dispersant
NM005-1	0.4954	2.74	0.27	0.5	-	-	3	1:30	Filtration	40	none
NM005-2	0.4955	2.74	0.27	0.5	20	0.27 in 2	3	1:30	Centrifugation	18	none
					40	0.27 in 2					
					60	0.27 in 2					
					80	0.27 in 2					
NM005-3	0.4849	5	0.27	0.5	20	0.27 in 2	3	1:30	Centrifugation	40	none
					40	0.27 in 2					
					60	0.27 in 2					

Table 37: Preparation and amount of educts for SiO_2 coating experiments and parameters with europium activated $Ba_2Si_5N_8$ phosphor after Sun et al.[23]

Number	m [g] $Ba_2Si_5N_8$	V [ml] EtOH	V [ml] H_2O	V [ml] NH_3	V [ml] HCl	t_{adding} [min] TEOS	V [ml] TEOS in EtOH	Dispersion Method	T_{Bath} [°C]	$T_{reaction}$ [h:min]	Separation Method	V [ml] Dispersant
NM006-1	0.4790	30	-	80, 0.13M	-	-	3ml in 23	Stirrer, US	42	1:30	Centrifugation	none
NM006-2	0.4978	30	-	-	80, 0.1M	-	3ml in 23	Stirrer, US	42	1:30	Centrifugation	none
NM007-1	0.4955	10	1.4	47.3, 0.1M	-	15	0.53 in 5	Stirrer, no US	42	1:30	Centrifugation	none
						30	0.53 in 5					
						60	0.53 in 5					
						90	0.53 in 5					
						120	0.53 in 5					
NM007-2	0.4884	10	1.4	47.3, 0.1M	-	15	0.53 in 5	No stirrer, US	18	1:30	Centrifugation	none
						30	0.53 in 5					
						60	0.53 in 5					
						90	0.53 in 5					
						120	0.53 in 5					

Table 38: Preparation and amount of educts for Al_2O_3 coating experiments and parameters with europium activated $Ba_2Si_5N_8$ phosphor after Murphy et al.[20]

Number	Educt	m [g]	n_{Ratio} [ ]	n [mmol]	c [mol/l]	Drip Rate [ml/min]	t_{adding} [min] $Al(NO_3)_3 \cdot 9H_2O$	V [ml] $Al(NO_3)_3 \cdot 9H_2O$	V [ml] $NaHCO_3$	$t_{Reaction}$ [h:min]	US	Dispersant ml	$T_{US\text{-}Bath}$ [°C]	Separation Method	$T_{Annealing}$ [°C]
NM012-1	$Ba_2Si_5N_8$	0.3060	-	-	-	added manually via syringe	10	1.5, 0.60M	-	90	yes	0.2ml, 22µM $Na_4P_2O_8 \cdot 9H_2O$	18	Centrifugation	200
	$Al(NO_3)_3 \cdot 9H_2O$	0.3376	1	0.9	0.60		15-60	-	20, 0.26M						
	$NaHCO_3$	0.4368	5.8	5.2	0.26										
NM012-2	$Ba_2Si_5N_8$	0.3142				added manually via syringe	10	1.5, 0.60M	-	90	yes	2ml, 22µM $Na_4P_2O_8 \cdot 9H_2O$	18	Centrifugation	200
	$Al(NO_3)_3 \cdot 9H_2O$	0.3378	1	0.9	0.60		15-60	-	20, 0.26M						
	$NaHCO_3$	0.4365	5.8	5.2	0.26										
NM012-3	$Ba_2Si_5N_8$	0.2985	-	-	-	added manually via syringe	10	1.5, 0.60M	-	120	yes	0.2ml, 22µM $Na_4P_2O_8 \cdot 9H_2O$	18	Centrifugation	200
	$Al(NO_3)_3 \cdot 9H_2O$	0.3369	1	0.9	0.60		15-75	-	20, 0.26M						
	$NaHCO_3$	0.4370	5.8	5.2	0.26										
NM012-4	$Ba_2Si_5N_8$	0.2990	-	-	-	added manually via syringe	10	1.5, 0.60M	-	120	yes	2ml, 22µM $Na_4P_2O_8 \cdot 9H_2O$	18	Centrifugation	200
	$Al(NO_3)_3 \cdot 9H_2O$	0.3372	1	0.9	0.60		15-75	-	20, 0.26M						
	$NaHCO_3$	0.4374	5.8	5.2	0.26										

Table 39: Preparation and amount of educts for Al_2O_3 coating experiments and parameters with europium activated $Ba_2Si_5N_8$ phosphor after Murphy et al.[18]

Number	Educt	m [g]	n_{Ratio} [ ]	n [mmol]	c [mol/l]	Drip Rate [ml/min]	t_{adding} [min] $Al(NO_3)_3 \cdot 9H_2O$	V [ml] $Al(NO_3)_3 \cdot 9H_2O$	V [ml] $NAHCO_3$	$t_{Reaction}$ [h:min]	US	Dispersant ml	$T_{US\text{-}Bath}$ [°C]	Separation Method	$T_{Annealing}$ [°C]
NM009-4 Al_2O_3	$Al(NO_3)_3 \cdot 9H_2O$	1.6684	1	0.45	0.3 in H_2O	added manually via syringe	10 15,20,25,30	1.5, 0.3M 0.2, 0.3M	--	1:30	no	0.2 Octanol 0.3 Octanol	18	Centrifugation	200
	$NaHCO_3$	0.2182	5.8	2.60	0.13 in H_2O										
NM009-3	$Ba_2Si_5N_8$	0.4966	-	-	-	added manually via syringe	10 15,20,25,30	1.5, 0.3M 0.2, 0.3M	-	1:30	yes	0.2 Octanol 0.3 Octanol	23	Centrifugation	200
	$Al(NO_3)_3 \cdot 9H_2O$	1.6679	1	0.45	0.3 in H_2O										
	$NaHCO_3$	0.2180	5.8	2.60	0.13 in H_2O										
NM010-1	$Ba_2Si_5N_8$	0.5030	-	-	-	added manually via syringe	10 15,20,25,30	1.5, 0.53M 0.2, 0.53M	-	1:30	yes	0.2 Octanol 0.3 Octanol	58	Centrifugation	200
	$Al(NO_3)_3 \cdot 9H_2O$	1.9737	1	5.26	0.53 in H_2O										
	$NaHCO_3$	0.9661	2.2	11.5	0.23 in H_2O										
NM010-2 Al_2O_3	$Al(NO_3)_3 \cdot 9H_2O$	1.9729	1	5.26	0.53 in H_2O	added manually via syringe	10 15,20,25,30	1.5, 0.53M 0.2, 0.53M	-	1:30	no	0.2 Octanol 0.3 Octanol	58	Centrifugation	200
	$NaHCO_3$	0.9660	2.2	11.5	0.23 in H_2O										
NM010-4	$Ba_2Si_5N_8$ 50µm ≥ x	0.5183	-	-	-	added manually via syringe	10 15,20,25,30	1.5, 0.53M -	- 0.2, 0.23M	1:30	yes	0.2 Octanol	58	Centrifugation	200
	$Al(NO_3)_3 \cdot 9H_2O$	1.9732	1	5.26	0.53 in H_2O										
	$NaHCO_3$	0.9655	2.2	11.5	0.23 in H_2O										

Table 40: Preparation and amount of educts for Al_2O_3 coating experiments and parameters with europium activated $Ba_2Si_5N_8$ phosphor after Murphy et al.[20]

Number	***Educt***	***m [g]***	***n_{Ratio} [ ]***	***n [mmol]***	***c [mol/l]***	***Drip Rate [ml/min]***	***$t_{Reaction}$ [h:min]***	***US***	***Dispersant ml***	***$T_{US-Bath}$ [°C]***	***Separation Method***	***$T_{Annealing}$ [°C]***
NM029 Al_2O_3	$Al(NO_3)_3 \cdot 9H_2O$	*0.8307*	*1.5*	*2.2*	*0.1* in H_2O	0.34 automatic syringe pump	*1:15*	*yes*	none	42	Filtration	400
	$NaHCO_3$	*0.5528*	*1*	*6.6*	*0.33* in H_2O							
NM011	$CaAlSiN_3$	0.5770	-	-	-	added manually via syringe	1:15	yes	0.2 Octanol	18	Centrifugation	200
	$Al(NO_3)_3 \cdot 9H_2O$	0.3376	1	0,90	0.60 in H_2O							
	$NaHCO_3$	0.4368	5.8	5,20	0.26 in H_2O							
NM013	$CaAlSiN_3$	0.4944	-	-	-	added manually via syringe	1:15	yes	1.0 $Na_4P_2O_7 \cdot 10H_2O$	42	Centrifugation	200 - 700
	$Al(NO_3)_3 \cdot 9H_2O$	1.6684	1.7	4.45	0.30 in H_2O							
	$NaHCO_3$	0.2182	1	2.60	0.13 in H_2O							
NM029/1	$CaAlSiN_3$	1.0036	-	-	-	0.34 automatic syringe pump	1:15	yes	none	42	Filtration	400
	$Al(NO_3)_3 \cdot 9H_2O$	0.8278	1	2.21	0.09 in H_2O							
	$NaHCO_3$	0.5547	6.60	6.60	0.33 in H_2O							
NM029/2	$CaAlSiN_3$	0.9796	-	-	-							
	$Al(NO_3)_3 \cdot 9H_2O$	0.8835	1	2.36	0.09 in H_2O							
	$NaHCO_3$	0.5550	2.8	6.61	0.33 in H_2O							
NM029/3	$CaAlSiN_3$	0.9673	-	-	-							
	$Al(NO_3)_3 \cdot 9H_2O$	0.8877	1	2.37	0.09 in H_2O							
	$NaHCO_3$	0.5577	2.8	6.64	0.33 in H_2O							
NM032/1	$CaAlSiN_3$	1.0101	-	-	-	0.05 automatic syringe pump	7:00	yes	none	42	Filtration	400
	$Al(NO_3)_3 \cdot 9H_2O$	0.3235	1	0.86	0.03 in H_2O							
	$NaHCO_3$	0.1829	2.5	2.18	0.11 in H_2O							
NM032/2	$CaAlSiN_3$	0.7355	-	-	-							
	$Al(NO_3)_3 \cdot 9H_2O$	0.3286	1	0.88	0.04 in H_2O							
	$NaHCO_3$	0.1848	2.5	2.18	0.11 in H_2O							
NM032/3	$CaAlSiN_3$	0.6125	-	-	-							
	$Al(NO_3)_3 \cdot 9H_2O$	0.3227	1	0.86	0.03 in H_2O							
	$NaHCO_3$	0.1864	2.6	2.22	0.11 in H_2O							

Table 41: Preparation and amount of educts for Al_2O_3 coating experiments and parameters with europium activated $CaAlSiN_3$ phosphor after Murphy et al.[20]

Number	Material	m [mg]	n_{Ratio} [ ]	n [mmol]	c [mol/l]	Drip Rate [ml/min]	$t_{Reaction}$ [h:min]	US	Dispersant ml	$T_{US-Bath}$ [°C]	Separation Method	$T_{Annealing}$ [°C]
NM033/1	$CaAlSiN_3$	1.0018	-	-	-	0.05 automatic syringe pump	7:00	yes	none	18	Filtration	400
	$Al(NO_3)_3 \cdot 9H_2O$	0.2818	1	0.75	0.03 in H_2O							
	$NaHCO_3$	0.2055	3.3	2.45	0.12 in H_2O							
NM033/2	$CaAlSiN_3$	0.9397	-	-	-							
	$Al(NO_3)_3 \cdot 9H_2O$	0.2829	1	0.75	0.03 in H_2O							
	$NaHCO_3$	0.2052	3.2	2.44	0.12 in H_2O							
NM033/3	$CaAlSiN_3$	0.8012	-	-								
	$Al(NO_3)_3 \cdot 9H_2O$	0.2773	1	0.74	0.03 in H_2O							
	$NaHCO_3$	0.2131	3.4	2.54	0.13 in H_2O							
NM034/1	$CaAlSiN_3$	1.0011	-	-	-	0.05 automatic syringe pump	7:00	none	none	18	Filtration	400
	$Al(NO_3)_3 \cdot 9H_2O$	0.2936	1	0.78	0.03 in H_2O							
	$NaHCO_3$	0.1844	2.8	2.20	0.11 in H_2O							
NM034/2	$CaAlSiN_3$	0.8857	-	-	-							
	$Al(NO_3)_3 \cdot 9H_2O$	0.2948	1	0.78	0.03 in H_2O							
	$NaHCO_3$	0.1860	2.8	2.20	0.11 in H_2O							
NM034/3	$CaAlSiN_3$	0.7962	-	-	-							
	$Al(NO_3)_3 \cdot 9H_2O$	0.2924	1	0.78	0.03 in H_2O							
	$NaHCO_3$	0.1840	2.8	2.19	0.11 in H_2O							
US01	$CaAlSiN_3$	6.0015	-	-	-	0.34 automatic syringe pump	1:15	yes	none	42	Filtration	400
	$Al(NO_3)_3 \cdot 9H_2O$	1.7621	1	4.70	0.09 in IPA							
	$NaHCO_3$	1.1047	2.8	13.2	0.29 in H_2O							
US02/1	$CaAlSiN_3$	6.0005	-	-	-	0.112 automatic syringe pump	7:00	yes	none	42	Filtration	400
	$Al(NO_3)_3 \cdot 9H_2O$	1.7665	1	4.71	0.09 in IPA							
	$NaHCO_3$	1.1061	2.8	13.2	0.29 in H_2O							
US02/2	$CaAlSiN_3$	6.1109	-	-	-							
	$Al(NO_3)_3 \cdot 9H_2O$	1.7631	1	4.70	0.09 in IPA							
	$NaHCO_3$	1.1056	2.8	13.2	0.29 in H_2O							
US03	$CaAlSiN_3$	6.0055	-	-	-	0.112 automatic syringe pump	7:00	yes	none	42	Filtration	400
	$Al(NO_3)_3 \cdot 9H_2O$	1.7651	1	4.71	0.09 in IPA							
	$NaHCO_3$	1.1131	2.8	13.3	0.29 in H_2O							

Table 42: Preparation of precursor solutions for the MgO coating experiments and parameters with europium activated $CaAlSiN_3$ phosphor after Murphy et al.[20]

Number	*Material*	*m [mg]*	n_{Ratio} *[ ]*	*n [mmol]*	*c [mol/ml]*	$t_{Reaction}$ *[min]*	*US*	*Dispersant ml*	$T_{US\text{-}Bath}$ *[°C]*
NM030	$CaAlSiN_3$	0.5098	-	-	-	210	yes	none	42
	$MgCl_2$	0.1661	1	1.71	0.04				
	Urea	0.2078	2.0	3.43	0.09				
NM031 MgO	$CaAlSiN_3$	-	-	-	-	210	yes	none	42
	$MgCl_2$	0.1648	1	1.73	0.04				
	Urea	0.2055	2.0	3.42	0.09				
NM035	$CaAlSiN_3$	5.01	-			945	yes	none	18
	$MgCl_2$	1.1902	1	12.5	0.31				
	$NaHCO_3$	1.5009	1.7	20.9	0.42				

10.4 TG-DSC-MS Curves (ICTM)

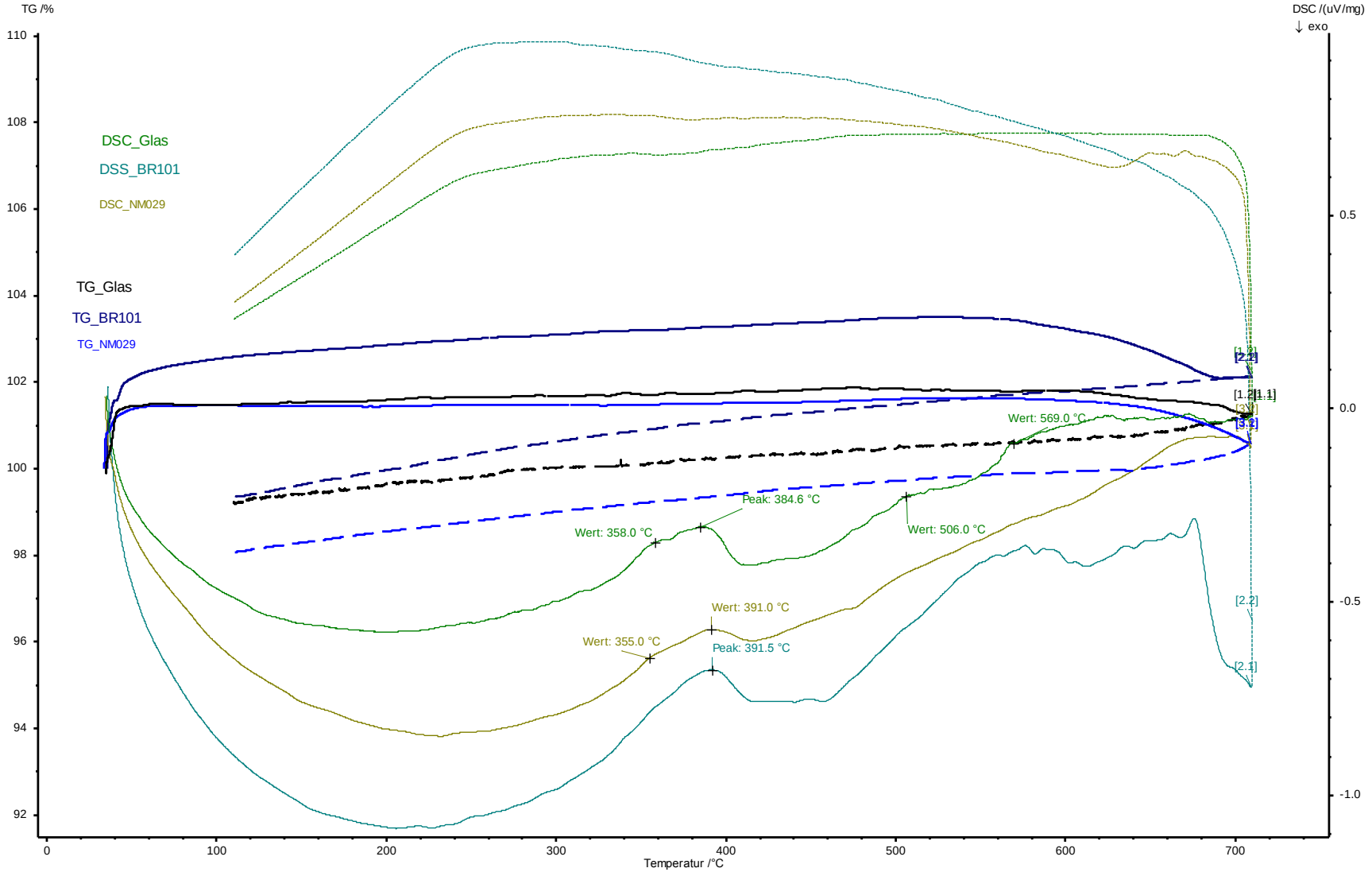

Figure 87: Comparison of evaluated TG and DSC curves of ZASNP11C, 5wt% BR-101H in ZASNP11C and 5wt% NM029 in ZASNP11C.

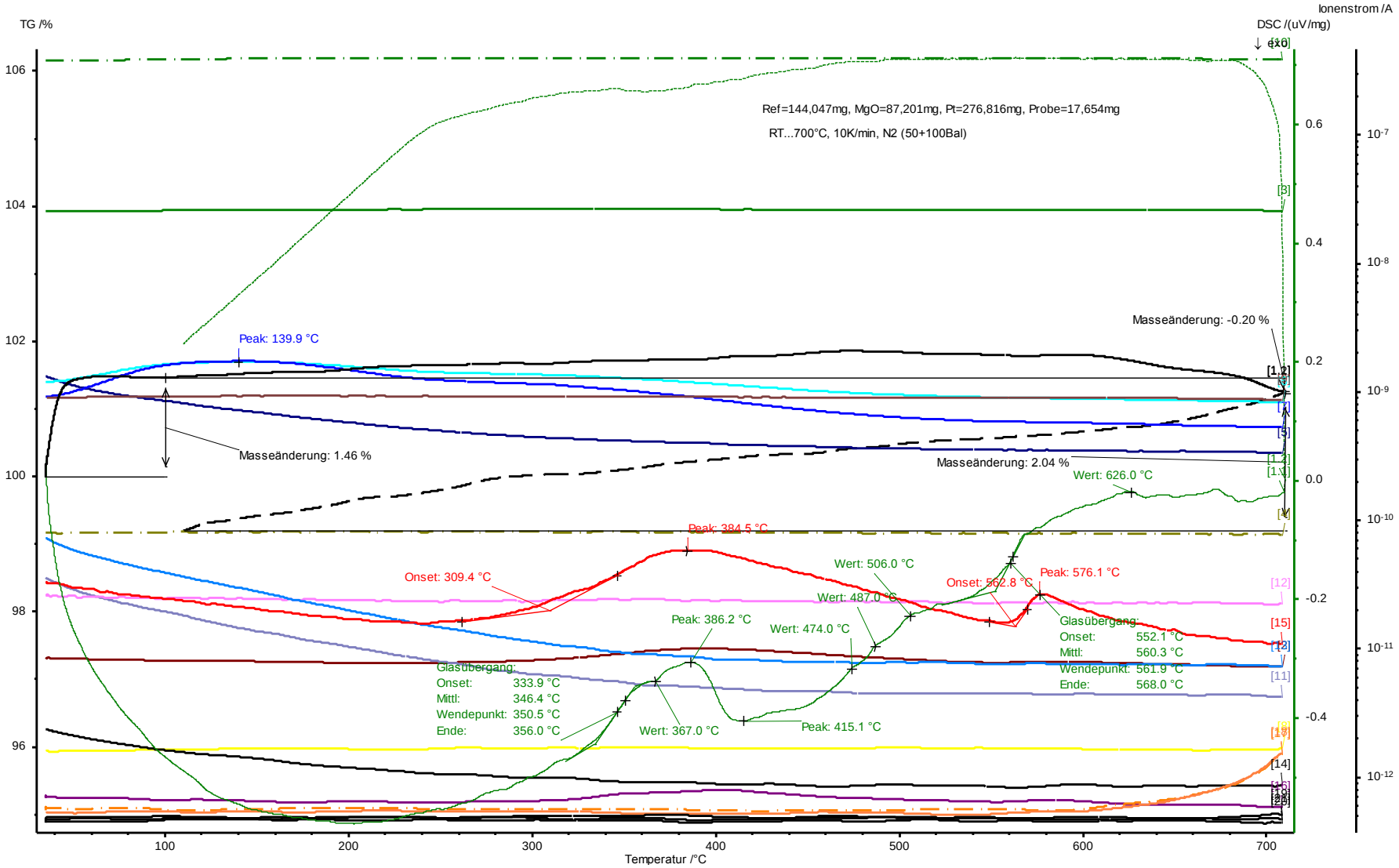

Figure 88: Comparison of evaluated TG-DSC-MS curves of ZASNP11C.

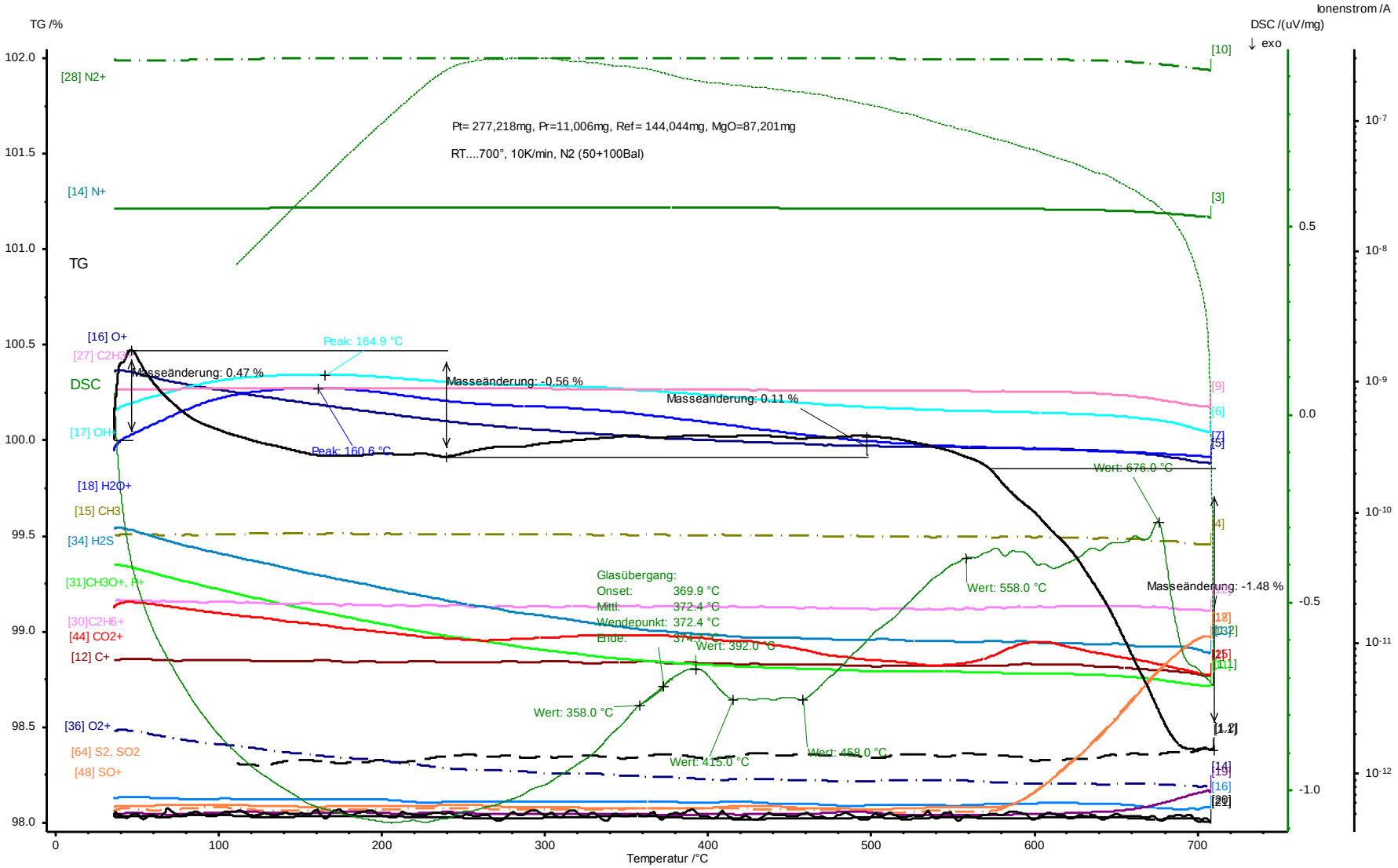

Figure 89: Comparison of evaluated TG-DSC-MS curves of 5wt% BR-101H in ZASNP11C.

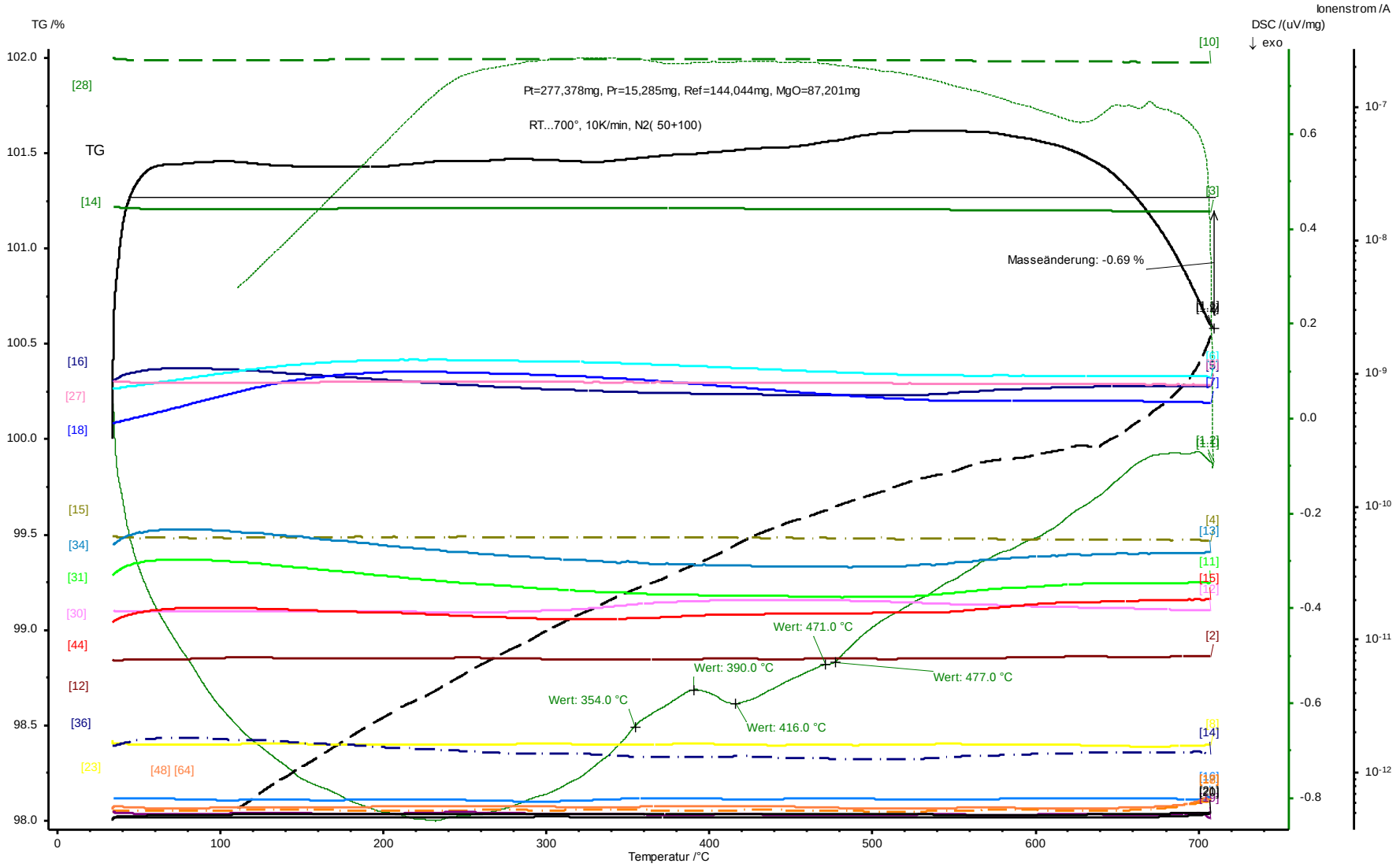

Figure 90: Comparison of evaluated TG-DSC-MS curves of 5wt% NM029 in ZASNP11C.